The Role of Ocean-Atmosphere Interaction over the Gulf Stream SST-front in North Atlantic Sector Climate

Dissertation
zur Erlangung des Doktorgrades
der Mathematisch-Naturwissenschaftlichen Fakultät
der Christian-Albrechts-Universität zu Kiel

vorgelegt von
Ralf Hand

Kiel, 2015

GEOMAR
Helmholtz-Zentrum für Ozeanforschung Kiel

C A U
Christian-Albrechts-Universität zu Kiel
Mathematisch-
Naturwissenschaftliche Fakultät

Erster Gutachter:	Prof. Dr. Noel S. Keenlyside
Zweiter Gutachter:	Prof. Dr. Richard J. Greatbatch
Tag der mündlichen Prüfung:	25.11.2014
Zum Druck genehmigt:	02.02.2015

gez. Prof. Dr. Wolfgang J. Duschl, Dekan

Contents

Zusammenfassung

In der vorliegenden Arbeit wird der Einfluss von Fronten der Meeresoberflächentemperatur (engl. Sea Surface Temperature, SST) der mittleren Breiten auf die Atmosphäre aus verschiedenen Blickwinkeln am Beispiel der Golfstromregion betrachtet. Die Arbeit ist in drei Teile gegliedert:

Im ersten Teil wird der Einfluss der Modellauflösung auf die korrekte Darstellung von in der in der Frontregion relevanten Prozessen diskutiert. Hierzu wurde eine Serie von Experimenten mit dem allgemeinen atmosphärischen Zirkulationsmodell ECHAM5 ausgewertet. Der Niederschlag weist im Atmosphärenmodell eine deutliche Sensitivität gegenüber der Auflösung auf; auf die anderen untersuchten Größen ist der Einfluss der Modellauflösung hingegen gering. Dies deutet darauf hin, dass die Unterschiede zwischen den Läufen unterschiedlicher Auflösung im Wesentlichen aus den Niederschlagsparametrisierungen resultieren. Im Winter scheint eine sehr hohe Modellauflösung zudem die Wiedergabe der Zugbahn extratropischer Stürme (des sog. North Atlantic storm track) zu verbessern.

Der zweite Teil beschäftigt sich mit der Frage, inwiefern die Variabilität der Meeresoberflächentemperatur in der Golfstromregion generell einen Einfluss auf die mit der SST-Front verbundenen atmosphärischen Prozesse hat. Ein transienter ECHAM5-Ensemblelauf belegt eine hohe Sensitivität des konvektiven Niederschlags im Bereich der SST-Front bezüglich der Randbedingungen des Modells; zudem weisen konvektiver Niederschlag und SST im Bereich der Front eine hohe Korrelation auf. Im Sommer kommt es zu einer Verstärkung des aus der Literatur als “pressure adjustment” bekannten Mechanismus, der auch den klimatologisch gemittelten Zustand der Atmosphäre in dieser Region beschreibt. Im Winter ist der erhöhte Niederschlag sehr wahrscheinlich mit atmosphärischen Kalt- und Warmfronten verknüpft.

Im letzten Teil werden schließlich Ozean-Atmosphäre-Wechselwirkungen im Kontext der Klimaerwärmung am Beispiel einer Langzeitsimulation mit dem Erdsystemmodell MPI-ESM betrachtet. Ziel war es herauszufinden, welchen Einfluss Veränderungen des lokalen Temperaturmusters an der Ozeanoberfläche auf die sich erwärmende Atmosphäre haben - sowohl lokal als auch auf größeren räumlichen Skalen. Im Bereich der historischen Golfstromfront, der Region in der im heutigen Klima ein deutliches lokales Niederschlagsmaximum zu finden ist, projiziert das Klimamodell für die Zukunft eine Abnahme des Niederschlags. Dies kann eindeutig mit einer Abschwächung des SST-Gradienten in dieser Region in Verbindung gebracht werden. Die großskaligen atmosphärischen Veränderungen stellen hingegen eine direkte Reaktion auf den veränderten Strahlungsantrieb und die großskaligen Veränderungen der SST dar; der Einfluss lokaler Veränderungen der SST-Muster in der Golfstromregion beschränkt sich im analysierten Modell somit auf den lokalen Einfluss.

Abstract

This work deals with various aspects of the atmospheric response to mid-latitude SST fronts, in particular in the Gulf Stream region. It consists of three parts:

In the first part the effect of enhanced model resolution on the correct representation of the processes in the frontal region is discussed, based on analysis of a set of experiments using the atmospheric general circulation model ECHAM5. Precipitation shows sensitivity to resolution, but most other quantities that we analysed do not. Therefore, this sensitivity is likely caused by the parameterisation of atmospheric convection. In winter, also the representation of the North Atlantic storm track seems to benefit from higher model resolution.

The second part focuses on the question of whether or not SST variability in the Gulf Stream region in general has an influence on the atmospheric processes related to the SST front. A transient ECHAM5 ensemble run, shows that convective precipitation has a high sensitivity to atmospheric boundary conditions in the region of the SST front and that local SSTs and convective precipitation are highly correlated there. In summer the so-called pressure adjustment mechanism, which has been identified in the climatological mean state, is enhanced when warm SST anomalies occur. In winter the enhanced precipitation is likely related to atmospheric fronts. Their frequency is not enhanced significantly, but the amount of precipitation per front is effected.

The last part of this work deals with ocean-atmosphere interactions in a warming climate, based on a long-term integration with the Earth System Model MPI-ESM. The objective was to assess to what extend SST changes in the North Atlantic contribute to the global warming signal in the atmosphere, locally as well as on larger spatial scales. For the region of the historical Gulf Stream SST-front - a region were the historical run shows a local maximum in precipitation - the model projection shows a decrease in winter-time precipitation that is connected to a weakening of the SST gradients there. The large-scale atmospheric response in contrast was found to be mainly a direct response to the changed radiative forcings and the large scale SST increase and shows only little evidence of an impact from changes in the SST patterns in the Gulf Stream region.

1 Introduction

The Gulf Stream region is a key-region for ocean-atmosphere interaction in the North Atlantic sector. It was shown that the sharp SST gradients in this region cause a narrow precipitation band on the southern side of the front, which is connected to a local minimum in sea level pressure, low-level wind convergence and deep upward motion (Minobe et al., 2008).

The objective of this work is to improve the understanding of the atmospheric processes associated with changes of the Gulf Stream SST-front on different time scales - from the atmosphere's response to multi-annual sea surface temperature (SST) variability to (simulated) long-term changes associated with a global warming scenario. A main focus is on precipitation, as it shows a high sensitivty to SST. But also, the large scale atmospheric circulation is considered. While on inter-annual and shorter time scales the SST is mainly controlled by the short-term atmospheric variability, on decadal and longer time scales ocean dynamics begin to be the controlling factor (Gulev et al., 2013). It is a caveat for the understanding of many processes that both, the marine atmosphere and the ocean, are poorly covered by detailed observations. Relying on satellite data, which are available on a global domain, is only possible for the period since ∼1980, which is too short to analyse processes on decadal and longer time scales. Therefore, this study heavily relies on numerical models. However, in terms of the climatology, the models represent the currently observed patterns of the atmospheric circulation quite well. They also exhibit realistic variability of the large scale atmospheric circulation on decadal time scales (e.g. IPCC, 2013).

A crucial advantage of using models is that they allow us to isolate certain characteristic SST patterns observed in connection with certain processes of long-term atmospheric or ocean variability and to make statistically robust conclusions about the atmospheric response to these patterns. The setup with prescribed SSTs cannot reproduce the feedbacks to the ocean. However, this simplification can also be seen as an advantage, since the complexity is reduced and the one-way interaction from the ocean to the atmosphere can be studied in detail.

This work starts with an analysis of the role of model resolution on the processes related to mid-latitude SST fronts. Previous studies discussed how far the resolution of atmosphere models and the related SST forcing are relevant for the ability of the model to reproduce the observed patterns of mid-latitude ocean-atmosphere interaction (Minobe et al., 2008), and how enhanced resolution in coupled models could improve predictive skill on inter-annual timescales. In this context, attention should be paid to the reduction of the SST bias in the North Atlantic, a common problem of most state-of-the art coupled models that is known to impact the atmospheric circulation (e.g. Keeley et al., 2012; Scaife et al., 2011). Recently, it was shown that the atmosphere's response to mid-latitude SST anomalies changes with enhanced resolution (Scaife et al., 2014, Guidi Zhou, pers. communication)

While it was shown that the climatological precipitation is strongly influenced by the presence of the Gulf Stream SST front (Minobe et al., 2008), only little attention has been paid to the question, to what extent precipitation and SST variability are linked in this region. Motivation to investigate the latter issue is invigorated by a study of Gulev et al. (2013), who showed in an analysis of turbulent heat fluxes that at least on longer (decadal) timescales the ocean drives the atmosphere in the mid-latitude North Atlantic. Therefore, in the second part of this thesis a transient run with an atmospheric general circulation is analyzed with focus on the relationship between rainfall and SST on multi-annual to decadal timescales. The results from this analysis motivated a sensitivity experiment with the same model, to verify that local SST anomalies can be the cause for the correlation that was found in the transient run.

Numerical simulations with state-of-the-art coupled ocean-atmosphere models imply, that climate change will also involve huge changes in the ocean circulation (e.g. IPCC, 2013). For the North Atlantic, many models simulate a slowdown of the Atlantic Meridional Overturning Circulation (AMOC) in the future in response to warmer temperatures in the regions where extremely cold temperatures are a driving factor for the thermohaline circulation in present day. Also freshwater input from enhanced precipitation and melting ice play a role in changing the water density in the high latitudes. Furthermore, changes in the North Atlantic wind patterns are likely to influence the wind-driven ocean circulation. The Gulf Stream is part of the thermohaline driven AMOC as well as of the wind driven North Atlantic subtropical gyre. The objective of the last part of this work is to understand the feedback of this ocean changes on the atmosphere, with a focus on the impact on the processes in the Gulf Stream region. A series of sensitivity experiments were performed using SST simulated by the MPI model, following the RCP8.5 scenario, for the CMIP5.

The coupled model shows a strong warming of the North Atlantic in connection with a northward shift of the boundary between the subtropical and the subpolar gyre (Matthias Fischer, pers. communication). The motivation for these experiments was to get a better understanding of how the atmospheric part of the model responds to generally warmer SSTs on the one hand, and a shift of the SST fronts on the other, since especially the position of the storm track could be sensitive to the position of the SST front (Ogawa et al., 2012; Nakamura et al., 2004; Brayshaw et al., 2008).

2 The role of model resolution in the simulated response to the Gulf Stream SST front

2.1 Introduction

Model resolution is a major factor controlling the computational costs of climate model integrations. While coarse resolution integrations are cheap to run, they suffer from the fact that physical and dynamical processes, with spatial scales similar or smaller than the resolution of the model, might not be realistically represented. Hence, a compromise between available computational resources and resolution of the processes, relevant for the purpose of a model study, has to be found.

Early studies already suggested that enhanced model resolution leads to major improvements in terms of global model performance (Boville, 1991). Recent studies show that further enhancements of model resolution can lead to improvements in NAO prediction on seasonal time scales (Scaife et al., 2014). It was shown that enhancements in model resolution can lead to a better reproduction of blocking frequency in the HADGEM3, through a reduction of the ocean model's mean state SST bias (Scaife et al., 2011). For ECHAM5 it was shown that the representation of the climate mean state in general benefits from higher horizontal resolution, but at higher horizontal resolutions also an appropriate vertical resolution is required to get this enhancements (Roeckner et al., 2006; Hagemann et al., 2006).

Jung et al. (2006) combined an analysis of cyclone statistics from the ERA40 reanalysis and seasonal model integrations with the ECMWF model, both at various horizontal truncations. They showed that the representation of intense extra-tropical cyclones becomes much more realistic in very high resolution integrations (i.e. TL255) and that at least for the intense cyclones, this improvement can be connected to improvements in the physical and dynamical processes in the model, and not just to the pure effect of better resolving small scale features (so-called "truncation effect"). In contrast, for shallow cyclones, the benefits concerning shallow cyclones are basically limited to the effects of the truncation effect.

It was shown that the occurrence of extreme precipitation events shows a strong dependence on model resolution (Volosciuk et al., 2015). Extreme events often cause very small scale precipitation maxima with spatial scales smaller than the model resolution. Therefore, the maximum precipitation is partly smoothed out, when looking on the spatially averaged values for an entire grid box (the so-called "averaging effect", Chen and Knutson (2008)). The coarser the model resolution, the more this effects influences the precipitation maxima computed by the model. Volosciuk et al. (2015) show that the resolution dependent change of extreme precipitation goes beyond this pure smoothing effect, but also includes effects arising from changes in the physical processes itself (the so-called "scale interaction effect"). The latter changes are also persistent, when running the model in a higher resolution and smoothing the output data to a coarser grid in postprocessing. A major improvement in terms of representation of physical processes due to model resolution is made when enhancing resolution from T63 to T106. The benefit is larger in convective regions than in regions where the precipitation is to large extent linked to large-scale weather systems.

Beyond horizontal resolution, vertical resolution can play a role (e.g. Pope et al., 2001; Volosciuk et al., 2015). Recent studies show, that the stratosphere can modulate the atmospheric signal arising from mid-latitude ocean-atmosphere interaction in the North Atlantic sector (Omrani et al., 2014).

This chapter focuses on the effect of resolution on the mean state by comparing seasonal climatologies for summer and winter from satellite SST-forced ECHAM5 ensembles, in different horizontal and vertical resolutions, to NCEP-NCAR reanalysis data. The objective is, to investigate which resolution (if any of the resolutions considered) is sufficient to reproduce the observed processes connected to mid-latitude SST fronts in the North Atlantic sector correctly.

2.2 Model & Data

In this chapter a set of model runs performed with ECHAM5 (Röckner et al., 2003) is used. The model was driven by weekly varying SST and sea ice conditions from the NOAA-OI dataset (Reynolds et al., 2002). The dataset provides daily SST data at a resolution of 0.25°, so that SST fronts can be resolved in some detail. A set of experiments with different horizontal resolutions, i.e. T31, T42, T63, T106 and T213 is considered. The two lowest resolutions were performed at a vertical resolution of 19 levels, the three others at 31 levels. The model top in all cases is at 10 hPa. For all resolutions an ensemble of three members,

covering the period from 1982 to 2009, was analysed.

For verification of the modelled precipitation, the climatological means from two observational data sets (fig. 2.1) are compared to that simulated by ECHAM5 (figs. 2.2 & 2.3). The first dataset, TRMM 3B43, is a merged product from the Tropical Rainfall Measuring Mission, combining high resolution satellite measurements with rain gauge data. It has the advantage of a very high resolution (0.25°x0.25°), but the limitation to be only available for part of the period of the model integrations (1998 to 2009). The second dataset, CMAP, combines satellite estimates, gauge observations, and numerical model outputs (Xie and Arkin, 1997). It is available for the whole period of the model integrations, but has a coarse resolution (2.5°x2.5°, corresponds approximately to T42). For low-level convergence and vertical winds the modelled fields are compared to the NCEP-NCAR reanalysis (Kalnay et al., 1996), which is available at 2.5° spatial resolution since 1948 onwards.

2.3 Results

In general ECHAM5 is able to reproduce well the main features of the precipitation patterns in the North Atlantic, but shows the tendency to overestimate total precipitation (figs. 2.1, 2.2 & 2.3 & table 2.1). The amplitude of the signal strongly depends on the resolution, since neither the low-resolution model runs nor the low-resolution observational product is capable to resolve the small-scale precipitation maxima in the region of the SST front. We start our comparison of the differently resolved runs with an analysis of the seasonal mean patterns of total and convective precipitation (fig. 2.2 and fig. 2.3). The figures show the deficiencies of the coarser resolution cases to resolve details of the precipitation pattern. fig. A.1 and A.2 in the Appendix additionally shows the same figures, but with all data interpolated to the coarsest resolution to allow a direct quantitative comparison between the different runs without being misled by extreme maxima on small spatial scales, which would not change the integral over a coarser grid box. The maps in fig. A.3 to A.5 in the Appendix further show the spatial distribution of the changes for the different precipitation types with all data. For getting a quantitative estimate of differen in precipitation, box means for the region of the precipitation maximum were computed (table 2.1, see boxes in fig. 2.2 and fig. 2.3 for definition of these regions).

In summer, at coarse resolution the model shows a maximum of total precipitation northwest of Florida, mainly caused by a local maximum of convective precipitation there (fig. 2.2). This maximum vanishes when switching to a higher model resolution. In gen-

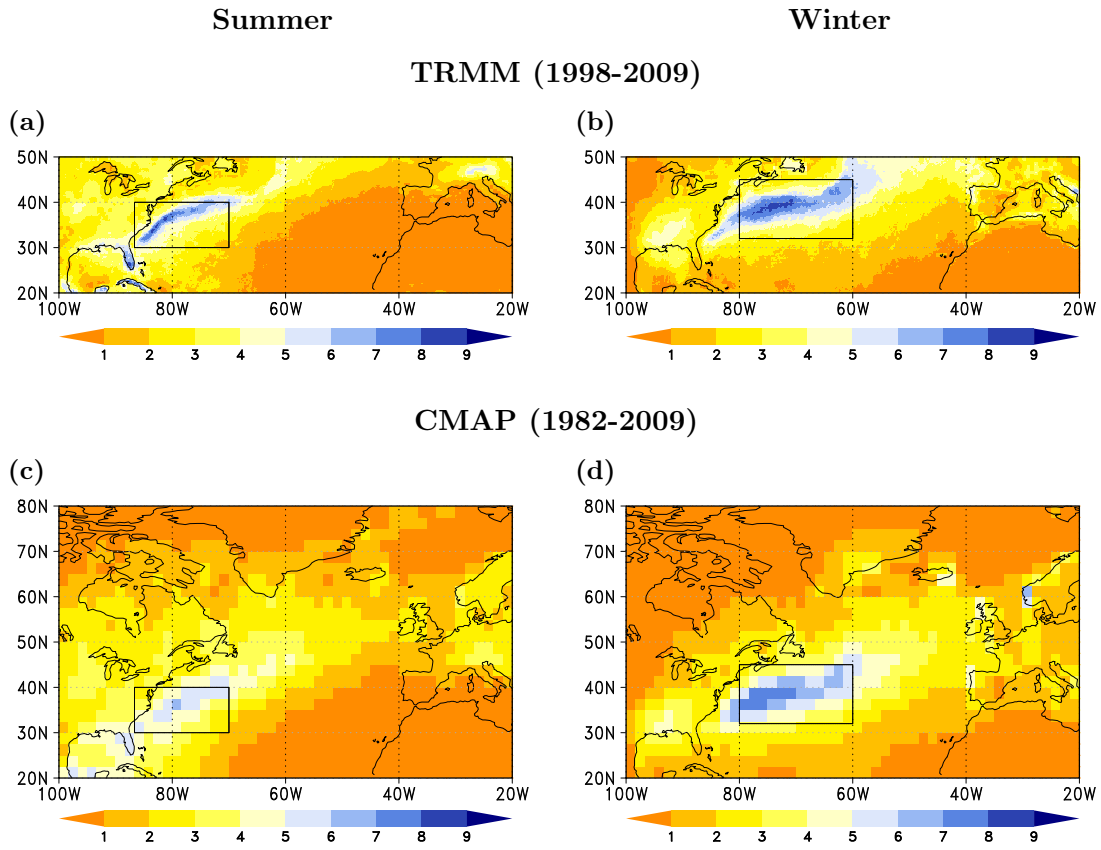

Figure 2.1: Seasonal Climatologies of total precipitation (in mm/day) in the TRMM 3B43 dataset (a & b, 1998 to 2009) and the CMAP dataset (c & d, 1982 to 2009) for summer (JJA, left column) and winter (DJF, right column). The boxes indicate the region used for the boxmeans shown in table 2.1.

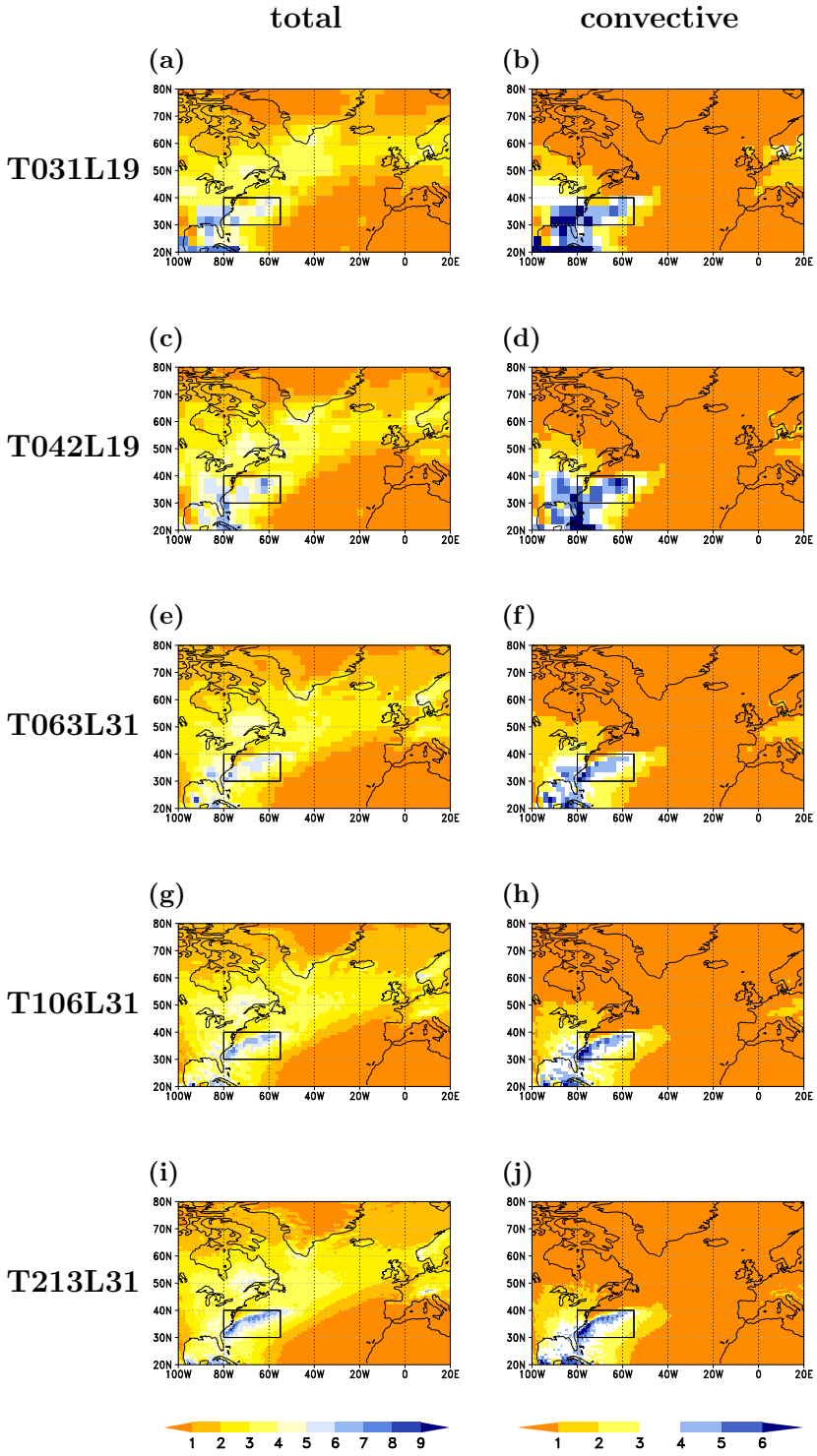

Figure 2.2: Climatological summer-time (JJA) precipitation in a set of AGCM runs at different resolutions. Total (left) and convective (right) precipitation (in mm/d, averaged over three ensemble members per run, covering the period 1982-2009) from ECHAM5 runs at T031L19 (a and b), T42L19 (c and d), T063L31 (e and f), T106L31 (g and h) and T213L31 (i and j) resolution. Note that the colorbars differ for total and convective precipitation! The boxes indicate the region used for the boxmeans shown in table 2.1.

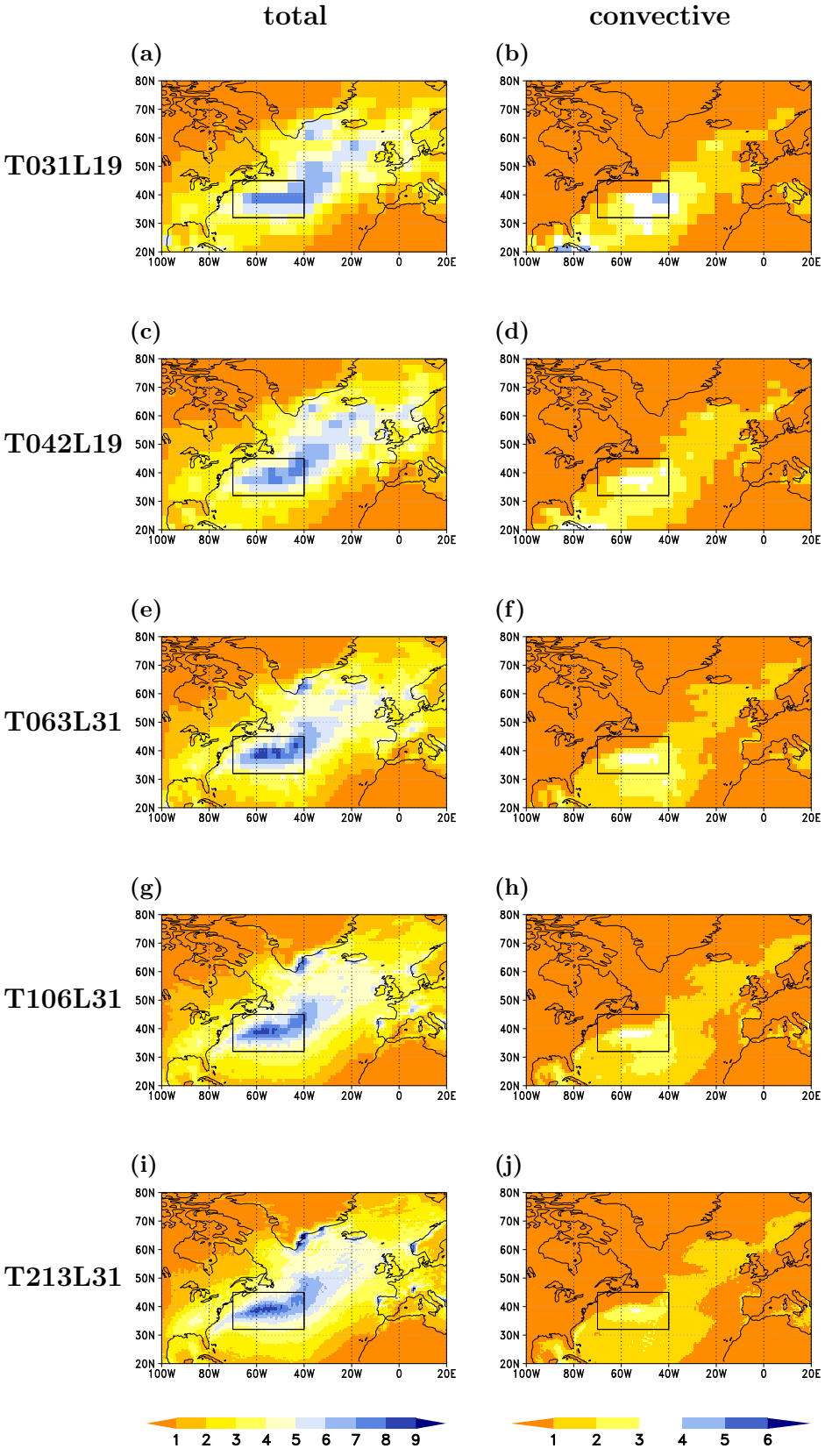

Figure 2.3: Same as 2.2, but for winter.

	summer 70°W-40°W/32°N-45°N			**winter** 80°W-55°W/30°N-40°N		
	convective	large-scale	total	convective	large-scale	total
T31L19	3.646	0.341	3.986	2.334	3.290	5.624
T42L19	4.102	0.279	4.381	2.067	3.052	5.119
T63L31	3.635	0.631	4.266	1.980	3.704	5.684
T106L31	3.384	0.949	4.333	1.725	3.970	5.695
T213L31	3.388	1.198	4.586	1.527	4.110	5.638
CMAP			3.704			4.910

Table 2.1: Climatological boxmeans of different precipitation types for the boxes indicated in Figs. 2.2 and 2.3.

eral, the convective precipitation shows a tendency to decrease over land, while there is only modest change in convective precipitation over the oceans. The precipitation band following the southern flank of the Gulf Stream SST front is only poorly reproduced in coarse resolution, even though there is a local maximum in convective precipitation. Enhancing the resolution slightly reduces this convective precipitation, but the total precipitation is enhanced anyway, due to an increase in large-scale precipitation (table 2.1). The detailed structure of the narrow precipitation band is only distinct when running the model in T213 resolution.

In winter, also a decrease in convective precipitation and an increase in large-scale precipitation can be found with increasing resolution. However, in contrast to summer, this does not lead to qualitative changes in total precipitation in the Gulf Stream region, since the response of large-scale and convective precipitation nearly compensate each other (table 2.1). Local patches of enhanced precipitation in regions with strong orography (e.g. along the Norwegian coast, in the Alps and around the north-eastern corner of the Iberian peninsula) are not resolved in the coarse resolutions, but also do not cause quantitative precipitation changes when interpolating them to a coarser grid.

It has been shown that rainfall in the Gulf Stream region goes along with low-level wind convergence and deep upward motion (Minobe et al., 2008). Therefore, the dependence of low- and mid-level upward wind and low-level wind convergence on model resolution

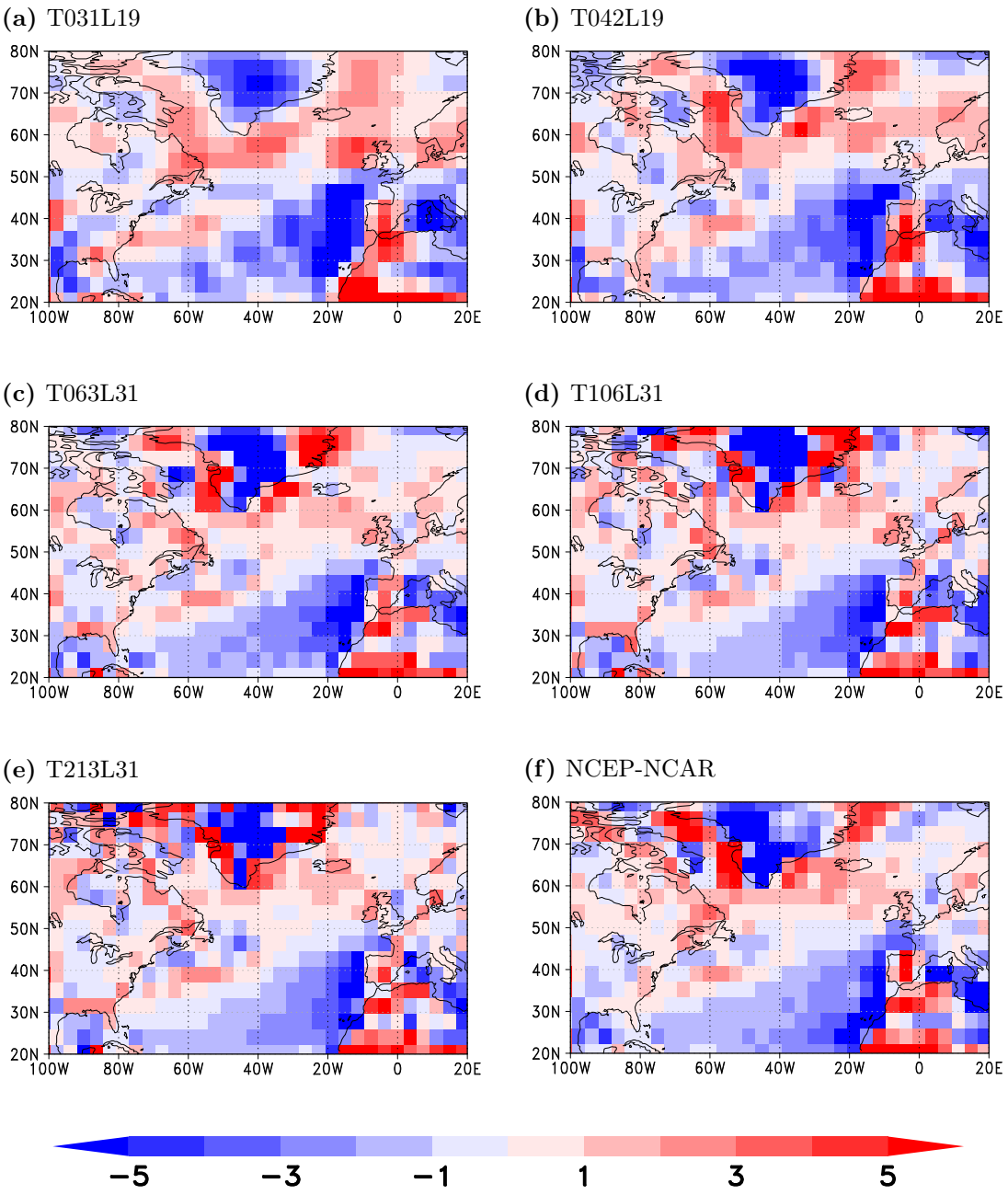

Figure 2.4: Summer-time means of the 10m-wind convergence (in 10^{-6}/s) from ECHAM5 at different resolutions ((a) to (e)) and from NCEP-NCAR reanalysis data (f). For better comparability, all data were interpolated to the same horizontal grid, i.e. T31.

were analyzed. In summer large parts of the subtropical Atlantic show large-scale wind-divergence, as usual for the regions of the descending branch of the Hadley cell. In contrast, the region around the Gulf Stream shows wind convergence in the region between 80°W to 50 °W and 30°N to 45 °N (fig. 2.4). The model shows only very little depencence of the summer-time low-level convergence to model resolution.

Resulting summer-time upward motion also shows little sensitivity to resolution in the low levels (fig. 2.5). However, mid-tropospheric upward motion shows a slightly higher dependence on resolution (fig. 2.6). While all resolutions match the NCEP-NCAR reanalysis (fig. 2.6f) qualitatively well, low resolutions show a quantitative overestimation, while intermediate and high resolutions reproduce the maxima from the reanalysis also quantitatively (fig. 2.6d to 2.6e). However, it has to be considered, that NCEP-NCAR is a low resolution product based on model output, and results might differ when comparing to a higher resolution product.

In winter the low-level convergence pattern shows a dipole pattern with divergence along the North American east coast and convergence south-east of it (fig. 2.7). The absolute values are enhanced with respect to summer. For the low resolutions, a maximum is found around 40°N/40°W. For the resolutions beyond T063L31, the pattern turns more zonal (fig. 2.7c to 2.7e). The associated pattern of low-level upward wind shows a westward shift of its local maximum with enhanced resolution. However, similar to summer, not much improvement with respect to NCEP-NCAR can be found beyond T063L31 resolution. The mid-troposphere uplift (fig. 2.9) shows a much wider pattern than found in the low levels. Similar to summer, the low resolutions quantitatively overestimate the strength of the lifting, while this overestimation vanishes in the finer resolution runs.

As we will show later in chapter 3 the precipitation-generating mechanisms in ECHAM5 differ between summer and winter. Winter-time precipitation in the model can be connected to atmospheric fronts associated with the through-passing cyclones in the North Atlantic storm-track. It has been shown, that bandpass-filtered variances can give a good estimator for the mean state of storm tracks (Chang, 2009). Therefore an analysis of the standard deviation of 2 to 8 day bandpass-filtered 850 hPa potentiality height anomaly as proxy for the intensity and the position of the winter-time storm-track was performed (fig. 2.10). In comparison to the NCEP-NCAR reanalysis, the model in general produces a too strong potentiality height variability on these time scales and the orientation of the storm track is too zonal in the coarse runs. The tilt of the storm track becomes slightly more North-eastward with refinement of the model resolution, but the intensity of the

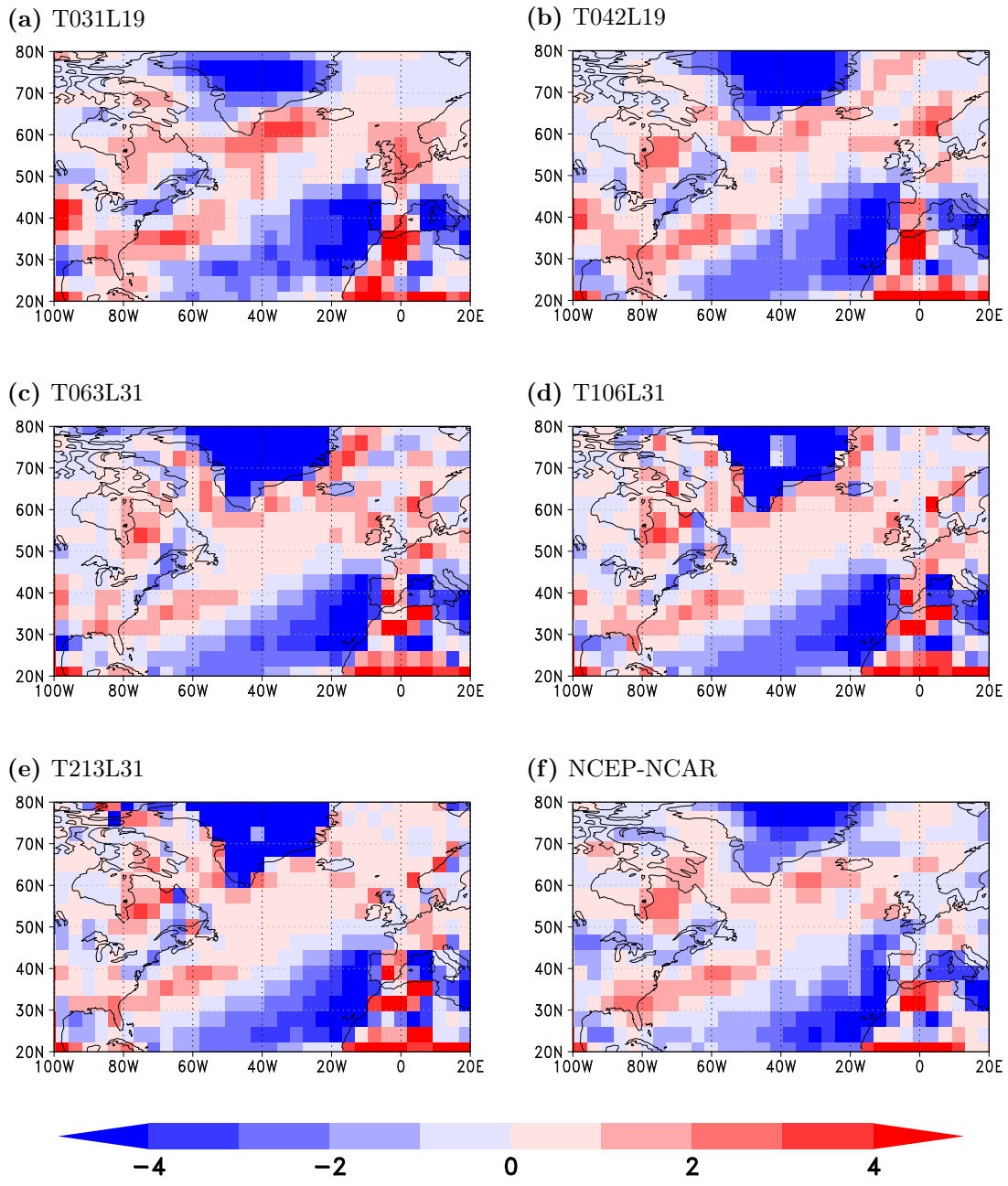

Figure 2.5: Summer-time means of 850 hPa upward wind (in Pa/s) for ECHAM5 at different resolutions (a to e) and from NCEP-NCAR reanalysis data (f). For better comparability, all data were interpolated to the same horizontal grid, i.e. T31.

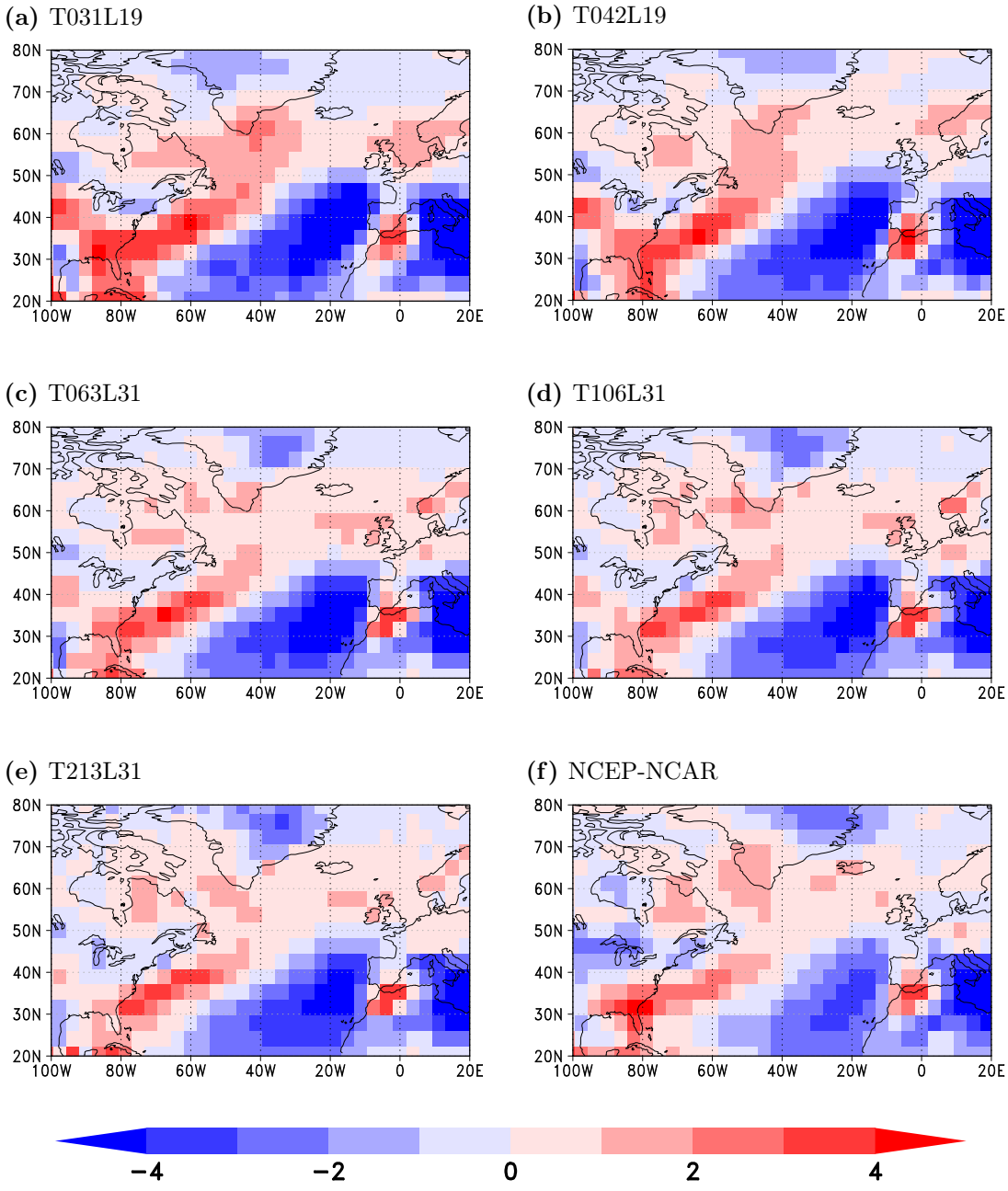

Figure 2.6: Summer-time means of 500 hPa upward wind (in Pa/s) for ECHAM5 at different resolutions (a to e) and from NCEP-NCAR reanalysis data (f). For better comparability, all data were interpolatet to the same horizontal grid, i.e. T31.

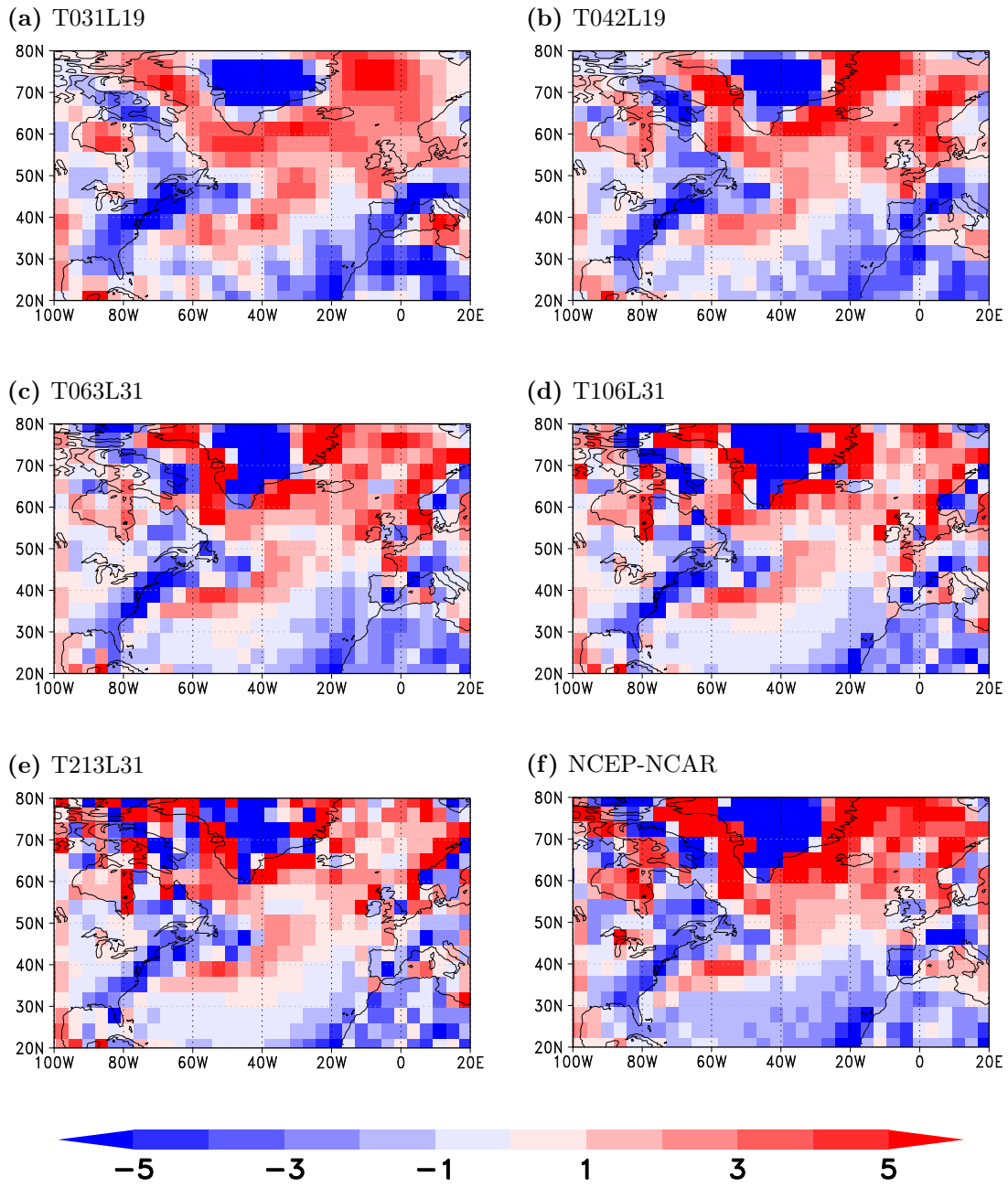

Figure 2.7: Winter-time means of the 10m-wind convergence (in 10^{-6}/s) for ECHAM5 at different resolutions (a to e) and from NCEP-NCAR reanalysis data (f). For better comparability, all data were interpolated to the same horizontal grid, i.e. T31.

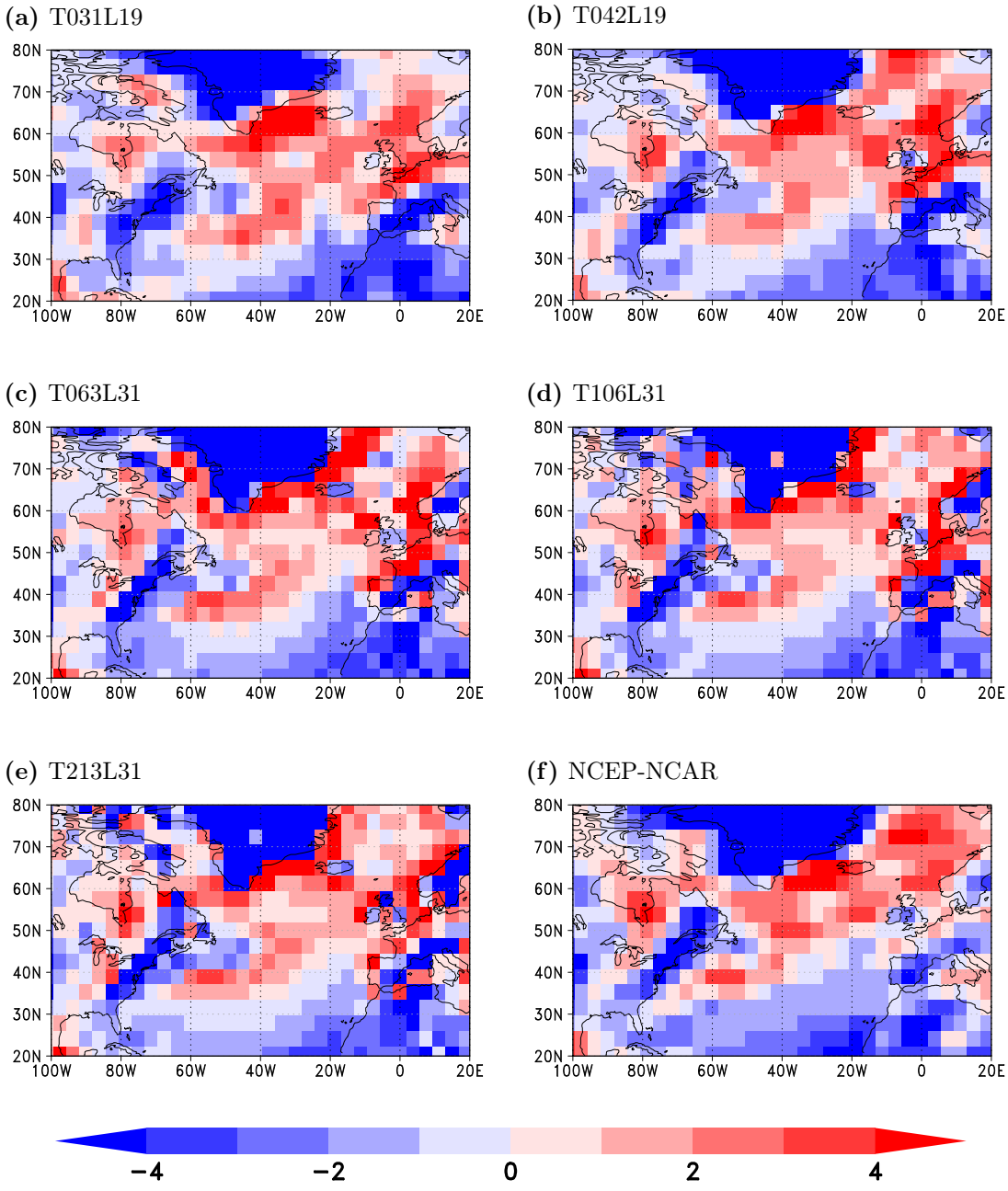

Figure 2.8: Winter-time means of 850 hPa upward wind (in Pa/s) for ECHAM5 at different resolutions (a to e) and from NCEP-NCAR reanalysis data (f). For better comparability, all data were interpolated to the same horizontal grid, i.e. T31.

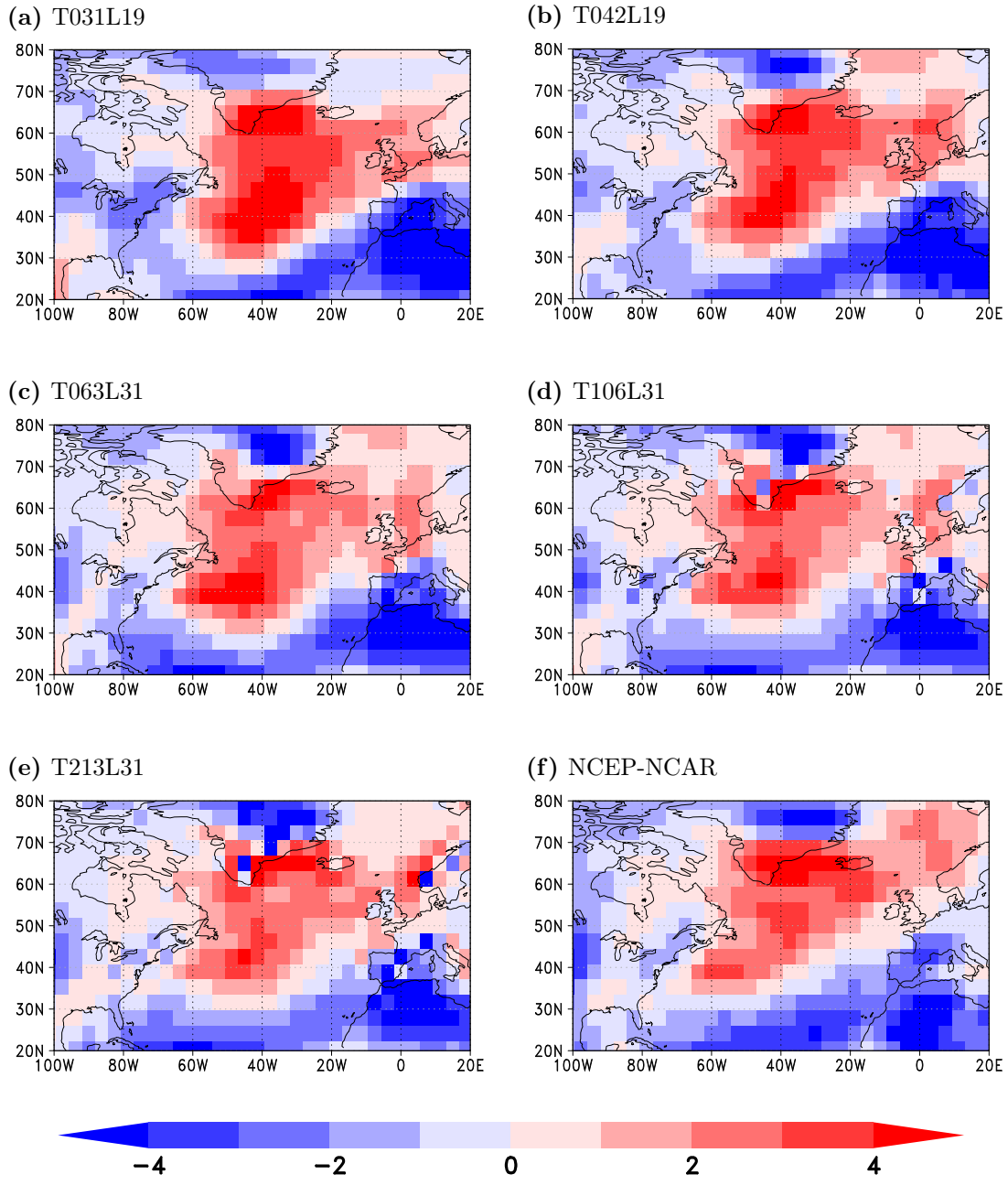

Figure 2.9: Winter-time means of 500 hPa upward wind (in Pa/s) for ECHAM5 at different resolutions (a to e) and from NCEP-NCAR reanalysis data (f). For better comparability, all data were interpolated to the same horizontal grid, i.e. T31.

variability is even increased, especially in the region around Newfoundland, where the variability has its maximum. With increased resolution, the modeled storm track splits up into two separated maxima, one at the coast of Newfoundland and one slightly west of Iceland. This split structure is also found in the reanalysis data. Contrarily, enhanced vertical resolution seems to dampen the variability, as it can be seen by comparing fig. 2.10b and fig. 2.10c.

Resolving small-scale features in the region of the SST front can have an important effect on the modeled latent and sensible heat fluxes at the ocean surface with potential impacts on large-scale processes, e.g. the North Atlantic storm track (Piazza et al., to be submitted). Therefore, the resolution dependence of latent and sensible heat fluxes were analysed (Figs. 2.11 and 2.12). Since fluxes strongly depend on the temperature difference between the ocean and the atmosphere, they are very small in summer. For this reason, this analysis is restricted to winter. The patterns for both quantities fit well with that from the NCEP-NCAR reanalysis, while the amplitude for both is slightly underestimated. Again it has to be considered, that fluxes are also a modeled quantity in the coarse resolution reanalysis product. Both quantities only show very little resolution dependence in ECHAM5.

Quantitative differences of the finer resolutions with respect to T31L19 are shown in the appendix, including significance tests based on a bootstrapping algorithm (fig. A.11 to A.13).

2.4 Summary & Discussion

Model resolution in ECHAM5 has an effect, exceeding that of pure smoothing of local structures. The most distinct differences occur for precipitation. Convective precipitation in general shows a decrease in the region of the Gulf Stream SST front for both seasons as resolution is increased. In winter total precipitation only shows little dependence on model resolution. This indicates that the reduction in convective precipitation is nearly compensated by an increase in large scale precipitation.

The other quantities that were analyzed show less resolution dependency than precipitation. This can be seen as an indication, that the effects seen in precipitation are mainly caused by a resolution dependency of the parameterisation that are involved in generating precipitation in the model, rather than in changes in the physical processes. However, there are moderate changes also in some other quantities that were discussed.

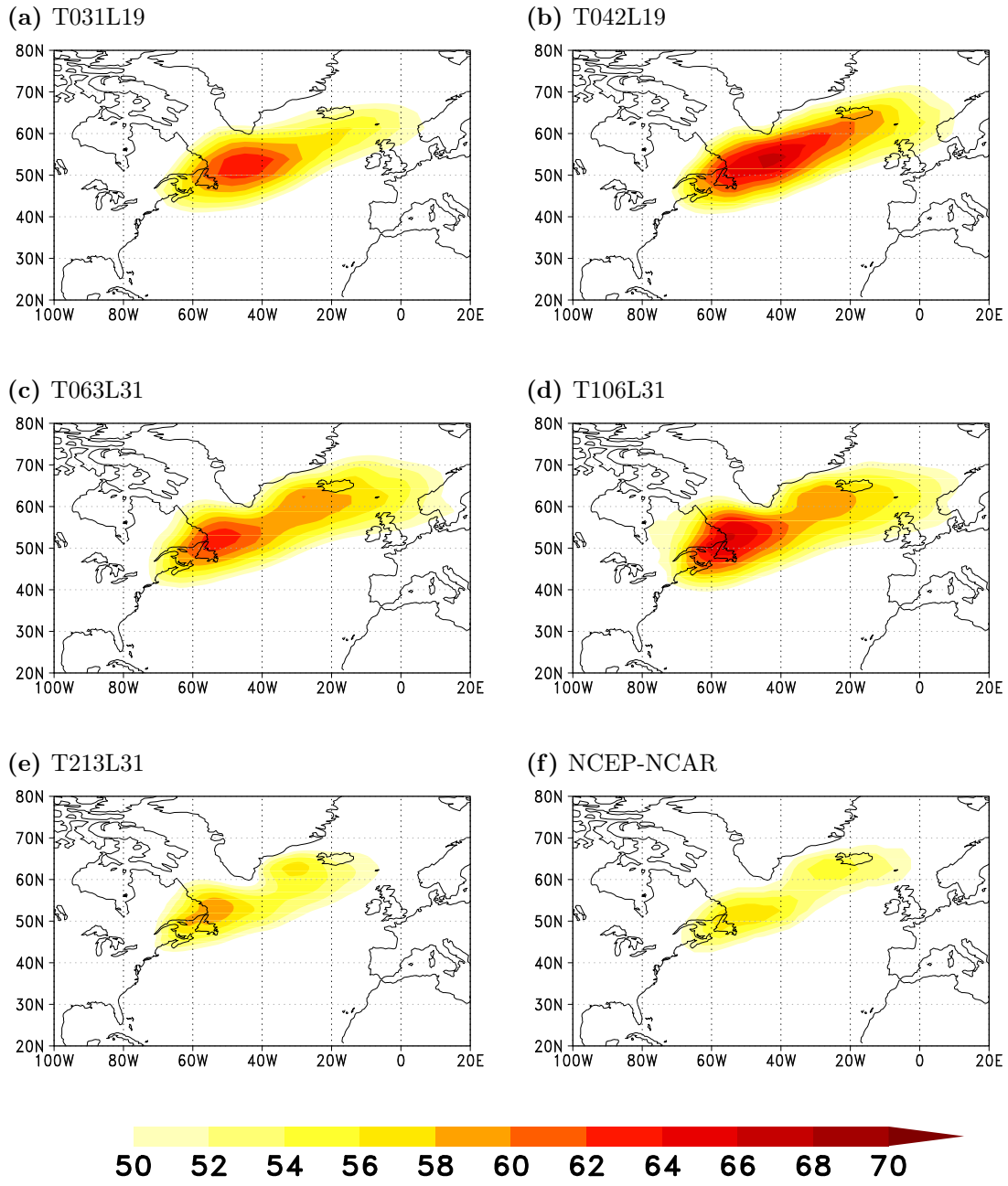

Figure 2.10: The winter-time storm track in ECHAM5. Shown is the standard deviation of the 2 to 8-day bandpass-filtered 850 hPa geopotential height (in m) over the 3 ensemble members of each resolution.

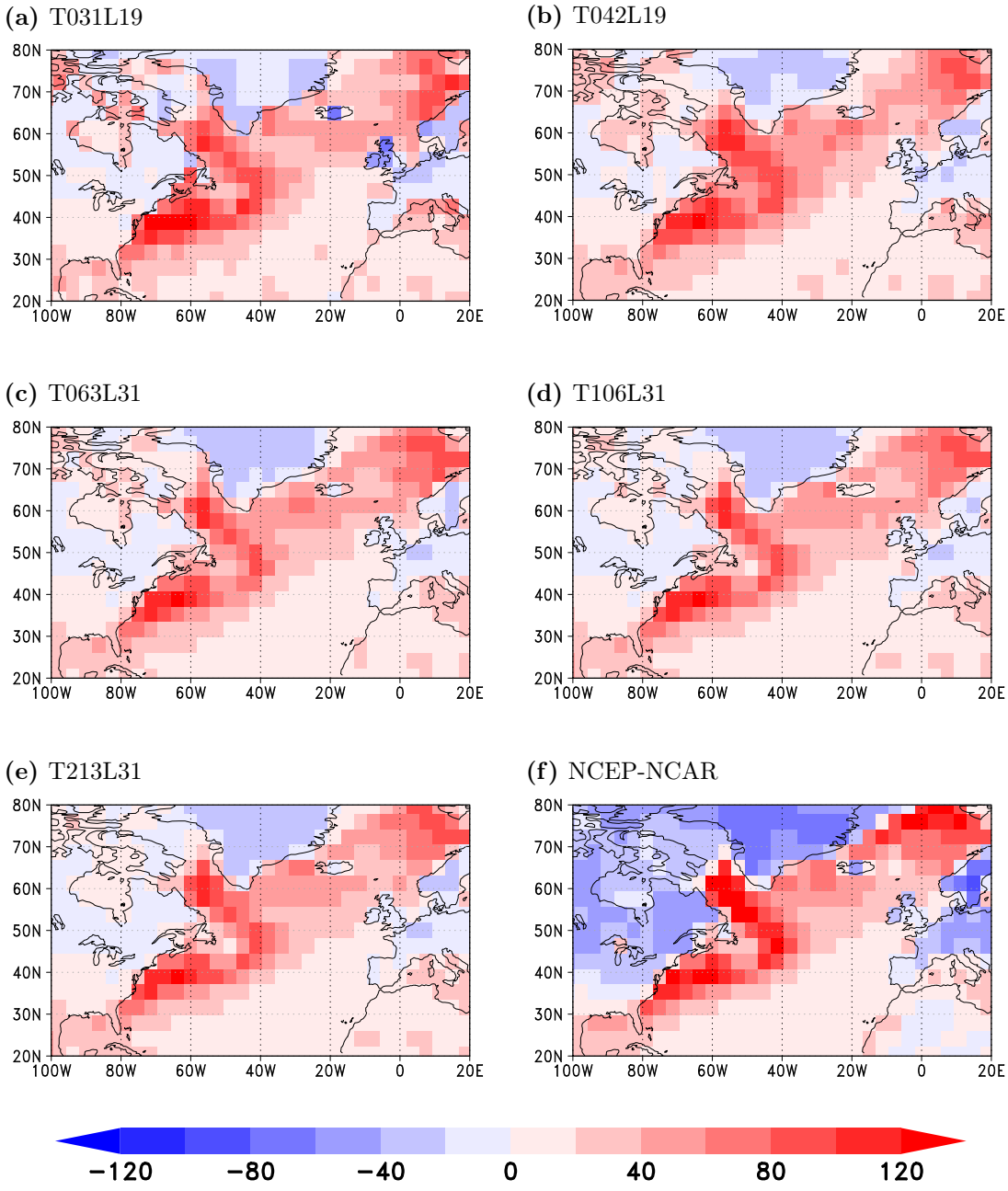

Figure 2.11: Winter-time means of upward sensible heat flux (in W/m^2) for ECHAM5 at different resolutions (a to e) and from NCEP-NCAR reanalysis data (f). For better comparability, all data were interpolated to the same horizontal grid, i.e. T31.

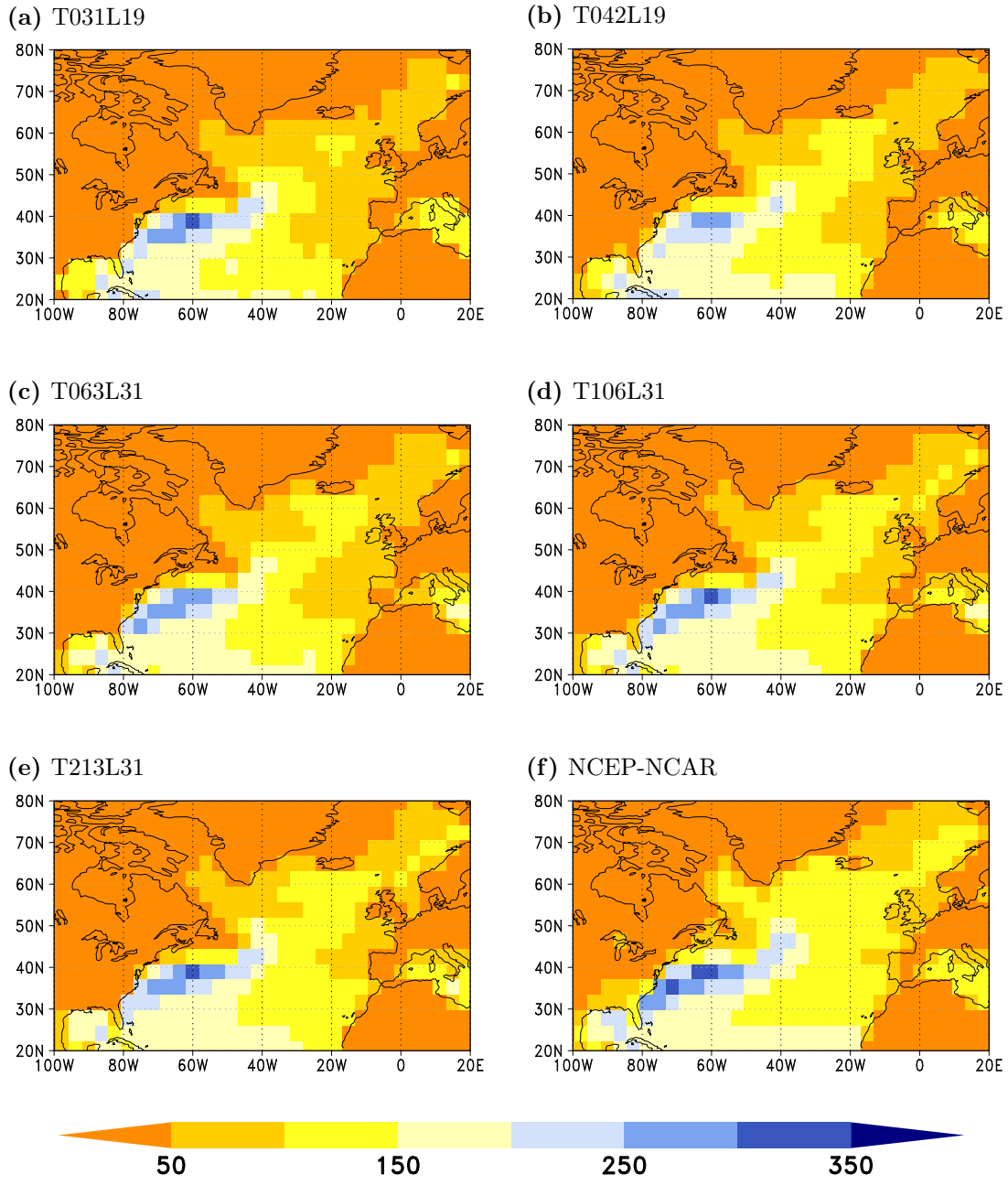

Figure 2.12: Winter-time means of upward latent heat flux (in W/m^2) for ECHAM5 at different resolutions (a to e) and from NCEP-NCAR reanalysis data (f). For better comparability, all data were interpolated to the same horizontal grid, i.e. T31.

Also the representation of the North Atlantic storm track improves in the mean with enhanced resolution. This study only focused on the resolution dependence of the mean climatological state and for the storm track analysis restricts to the bandpass-filtered 850 hPa potentiality height variability. However, this quantity only represents the integral over a variety of storms of different intensity and lifetime and therefore this kind of analysis does not provide any information about potentially useful statistics like cyclone frequency or the typical intensity. It was shown, that the resolution dependency is higher for intense and long-living systems (Jung et al., 2006). A more detailed analysis of the cyclone statistics in the model runs from this work, including application of a cyclone tracking algorithm, is provided by Kedzierski (2013).

Not only horizontal, but also vertical resolution seems to play a role for the processes analyzed. The higher vertical resolutions in our case mainly affect the model levels higher up in the atmosphere. Therefore, the changes related to enhanced vertical resolution are likely connected to a better representation of processes in the upper troposphere.

In general, the improvements in model performance are most prominent for the refinement from low to intermediate resolution. Refinement of the model grid beyond T63 only brings minor improvements in terms of the climatological mean state. However, it has to be considered that extreme events, like extreme rainfall or intense cyclones, might show a higher resolution dependency than the mean state and thus require a higher resolution (Volosciuk et al., 2015; Jung et al., 2006),.

Acknowledgements

I would like to thank Vladimir Semenov and Wan-Ling Tseng for providing the data from their NOAA-OI forced runs.

3 Simulated response to inter-annual SST variations in the Gulf Stream region

Ralf Hand[1,2], Noel Keenlyside[3], Nour-Eddine Omrani[1], and Mojib Latif[1,2]

Published in Climate Dynamics Vol. 42, 2014, Springer, Heidelberg

Abstract

Recent studies show that mid-latitude SST variations over the Kuroshio-Oyashio Extension influence the atmospheric circulation. However, the impact of variations in SST in the Gulf Stream region on the atmosphere has been less studied. Understanding the atmospheric response to such variability can improve the climate predictability in the North Atlantic Sector. Here we use a relatively high resolution (∼1 deg.) Atmospheric General Circulation Model (AGCM) to investigate the mechanisms linking observed 5-year low-pass filtered SST variability in the Gulf Stream region and atmospheric variability, with focus on precipitation. Our results indicate that up to 70% of local convective precipitation variability on these timescales can be explained by Gulf Stream SST variations. In this region, SST and convective precipitation are strongly correlated in both summer (r=0.73) and winter (r=0.55). A sensitivity experiment with a prescribed local warm SST anomaly in the Gulf Stream region confirms that local SST drives most of the precipitation variability over the Gulf Stream. Increased evaporation connected to the anomalous warm SST plays a crucial role in both seasons. In summer there is an enhanced local SLP minimum, a concentrated band of low level convergence, deep upward motion and enhanced precipitation. In winter we also get enhanced precipitation, but a direct connection to deep vertical upward motion is not found. Nearly all of the anomalous precipitation in winter is connected to passing atmospheric fronts. In summer the connection between precipitation and atmospheric fronts is weaker, but still important.

Keywords: Ocean-atmosphere interaction, Gulf Stream, SST fronts, North Atlantic

[1]GEOMAR Helmholtz Centre for Ocean Research, Kiel, Germany
[2]Christian-Albrechts-Universität, Kiel, Germany
[3]Universitet i Bergen, Bergen, Norway

3.1 Introduction

Oceanic western boundary currents (hereafter WBCs) are characterized by strong northward heat transport, resulting in strong anomalous warm SST-deviations from the zonal mean and large ocean-atmosphere fluxes of heat and moisture. The sharp SST fronts in the regions where the WBCs merge with the cold water masses of the subpolar gyre influence the climatological state of the entire troposphere (Minobe et al., 2008). Localized low sea level pressure (SLP) over the warm flank of the SST front produces low-level convergence and a tight band of precipitation. The climatological influence of the Gulf Stream SST front differs seasonally: A deep heating mode with convection mainly occurs in summer over the Florida current and the western Gulf Stream, while in winter the influence is restricted to a shallow heating mode, influencing mainly the marine boundary layer with a center of action over the eastern Gulf Stream and its extension (Minobe et al., 2010). Additionally, the maintenance of surface baroclinicity by the SST front can act as an anchoring mechanism for the Atlantic storm track (Nakamura et al., 2004). Idealized aqua planet simulations confirmed this result, showing that increased mid-latitude SST gradients lead to stronger storm tracks and the storm track response is sensitive to the position of the SST anomaly (Brayshaw et al., 2008). The dependence of the mid-latitude storm track activity on the latitude of an SST front relative to the atmospheric subpolar jet was shown by another idealized aqua planet experiment (Ogawa et al., 2012).

The distinct climatological impact of the SST front raises the question to what extent do frontal SST variations influence atmospheric variability? This question forms the main motivation of this study. The general influence of mid-latitude ocean variability on the atmosphere has been extensively investigated, but controversy still remains. AGCM forced with observed SST were used to argue that extra-tropical SST impact significantly the extra-tropical circulation (Rodwell et al., 1999). However, extra-tropical SST variability, particularly on shorter time-scales, mostly results from atmospheric variability (e.g. Cayan, 1992). Conceptional linear model studies based on this assumption show that such AGCM experiments are consistent with only a moderate influence of extra-tropical SST on the atmosphere (Barsugli and Battisti, 1998; Bretherton and Battisti, 2000). Kushnir et al. (2002) concluded in their synthesis paper that the extra-tropical ocean variability has an influence onto the atmosphere, but that this influence is only small compared to the internal atmospheric variability. Fan and Schneider (2012) showed, that the North Atlantic Tripole SST pattern is mainly controlled by weather noise, in particular to the heat flux variations related to it. However, on longer time scales ocean dynamics contribute to SST variations (e.g. Visbeck et al., 1998) and these may impact the mid-latitude atmosphere

(e.g. Bjerknes, 1964). In particular, statistical analysis using an extended reconstruction of turbulent heat-fluxes show that in the sub-polar North Atlantic on the short scales the SSTs are mainly controlled by the atmosphere, while on ten-year and longer time-scales ocean dynamics play the more important role (Gulev et al., 2013). Furthermore, recent work suggest that stratosphere-troposphere interaction, which has been poorly resolved in most models, is a key element in the atmospheric response to mid-latitude SST variability in winter (Omrani et al., 2014).

Only a limited number of studies have begun to investigate the role of mid-latitude SST fronts on the atmosphere (Xie, 2004). Recent studies of the Pacific show that the Kuroshio variability interacts with the atmospheric circulation. Positive early winter SST anomalies in the Kuroshio region cause a northward shift in the storm track and thus induce an anticyclonic circulation response in the region of the Aleutian low (Taguchi et al., 2012). For the North Atlantic the connection between extra-tropical low-frequency SST variability and the atmosphere remains a topic of current research. Since North Atlantic decadal SST variability has a predictable component (Collins et al., 2006; Griffies and Bryan, 1997; Keenlyside et al., 2008; Pohlmann et al., 2009; Robson et al., 2012; Yeager et al., 2012), improved understanding of these processes potentially will enhance climate prediction in the North Atlantic region.

Our aim here, is to better understand the mechanisms connecting low-frequency SST variations in the Gulf Stream region to the atmosphere. We focus on the locally driven precipitation changes, and as precipitation data in this region are limited we rely on AGCM experiments using a relatively high horizontal resolution that begins to resolve the Gulf Stream SST front. Additionally, we base our analysis on convective precipitation as we expect and find in our AGCM experiments that convective precipitation, by its nature, is more closely related to SST than large-scale (stratiform) precipitation. A novel aspect of our study is that we analyze the impact of the oceanic SST front on the atmosphere using an atmospherbenleric front detection method. It has be shown, that up to 90% of the precipitation in the mid-latitude storm-tracks can be connected to atmospheric fronts (Catto et al., 2012). We expect processes determining precipitation acting in winter to be more affected by the synoptic scale events compared to those acting in summer, and we would like to understand how the SST-induced synoptic scale changes affect the precipitation in the Gulf Stream region. A description of the model, experiments and the methods used in this study is given in section 2. Results are presented in section 3, followed by a summary and conclusions in section 4.

3.2 Methods

Experiments described in this study were performed using the ECHAM5 atmospheric general circulation model developed at the Max-Planck-Institute for Meteorology. ECHAM5 is a spectral model, and it was run at T106 horizontal resolution (∼100km) with 31 vertical levels and a top at 10 hPa. A comprehensive description of the model, including it's sub-grid scale physics is given by (Röckner et al., 2003). Here only details most relevant to precipitation are summarized. The convective precipitation is produced from the cumulus convection parametrization. ECHAM uses the Tiedtke (Tiedtke, 1989) mass flux scheme with modifications for penetrative convection according to Nordeng (1994). For deep convection the scheme use a closure based on convective available potential energy (CAPE), while for shallow convection the closure is based on large-scale moisture convergence. Entrainment and detrainment rates for penetrative convection are also related to CAPE. For large scale precipitation, the model uses a stratiform cloud scheme which is based on prognostic equations for the mixing ratios of the water phases, bulk cloud microphysics (Lohmann and Roeckner, 1996) and a statistical cloud cover scheme.

Hagemann et al. (2006) assess the performance of the hydrological cycle simulated by ECHAM5 in a series of SST and SIC forced experiments at different horizontal and vertical resolutions, including that used here. As most recent AGCMs, global averaged precipitation and evaporation are overestimated compared to observations, particularly over the oceans. However, observations of precipitations over oceans rely on indirect satellite measurements and have large uncertainties, since gauge data are usually not available. Nevertheless, comparison to different observational datasets shows that the biggest biases occur in the tropics, particularly in the summer season. In the midlatitudes the model performs better.

Three experiments were performed: The first is a five-member ensemble simulation driven with monthly varying observed SSTs and sea ice concentrations (SIC) from the HadISST dataset. The simulations cover the period 1870 to 2007 and ensemble members differ only in their initial conditions. The second is a 60-year long control experiment (CTL) driven with climatological SST and SIC conditions derived from the HADISST dataset for the period from 1870 to 2007. The third experiment is a sensitivity experiment (SENS), which has the same forcing as the control experiment, except in the Gulf Stream region (25°N to 55°N), where a warm SST anomaly was added. The pattern is associated with enhanced convective precipitation over the Gulf Stream region in the five-member transient simulation and was derived as follows: First, convective precipitation was averaged over

the region 65°W to 40°W and 38°N to 40°N and over the five member ensemble to form an index (Fig. 7). Second, a 5-year low-pass 10th order Butterworth filter was applied. The Butterworth filter is designed to have an abrupt decline in a small frequency range around the cutoff frequency and a flat, monotonous characteristic elsewhere. Details on how to calculate the filter coefficients can be found in Butterworth (1930). To maintain the seasonal cycle, we applied the filter to the time series of seasonal means for each season separately. The purpose of the filtering is to focus on time scales when ocean dynamics begin to control SST variations in this region (Gulev et al., 2013); however, we cannot exclude that the SST variations are also driven thermodynamically by internal atmospheric variability (Cayan, 1992; Bretherton and Battisti, 2000; Czaja and Frankignoul, 2002). Furthermore, simulated and observed precipitation have an opposite relationship to the underlying SST on inter-annual timescales (not shown), consistent with the SST variability on inter- annual timescales being mostly atmospheric forced. The forcing pattern is the composite difference between SST in years when the smoothed index exceeds plus one standard deviation and the years when it exceeds minus one standard deviation. A linear smoothing between anomaly and climatology was applied between 20-25°N and 55-60°N bands to avoid potential numerical artifacts.

Results are analyzed using linear regression and composite analysis. We perform an analysis of variance (ANOVA) of the five member ensemble simulations to detect the regions, where SST (and SIC) fluctuation have the largest influence on the atmospheric variability. We performed ANOVA as follows (see Storch (2010) for a more detailed description): First, we define the total sum of squares (TSS):

$$TSS = \sum_{i=1}^{n} \sum_{j=1}^{J} (X_{ij} - \langle \overline{X} \rangle)^2, \tag{3.1}$$

where the i denotes the ensemble member of an n-member ensemble (here n=5), and j the timestep of the total number of timesteps J (here J=138). X is an atmospheric quantity (e.g. precipitation). Angle brackets denote the ensemble mean and an overbar denotes a mean over all timesteps of an ensemble member. TSS can be decomposed into the so called "treatment sum of squares (SSA)" and the "sum of squared errors (SSE)":

$$TSS = SSA + SSE, \tag{3.2}$$

with

$$SSA = n \cdot VAR(\langle X \rangle), \tag{3.3}$$

and

$$SSE = \sum_{i=1}^{n} VAR(X_i'), \tag{3.4}$$

where $VAR(\langle X \rangle)$ denotes the time variance of the time dependent ensemble mean of X. X_i' is the time series of X in the ith ensemble member after subtracting the ensemble mean for each timestep. SSA is a measure of variability that all ensemble members have in common (i.e. as result of a common external forcing, such as sea surface temperature), and SSE of independent (internal) variability among ensemble members (i.e., not constrained by the external forcing). The ratio between SSA and TSS provides an estimate of how much of the total variance can be explained by the external forcing. However, for finite ensemble this estimate is biased, and an unbiased estimate of the "explained variance" is given by

$$R^2 = \frac{(SSA - \frac{(J-1)}{J \cdot (n-1)} SSE}{TSS}. \tag{3.5}$$

The five member ensemble is too small to make any statistically robust assumptions. ANOVA is thus used only for the detection of the region, where SST variability is potentially connected to atmospheric variability. Furthermore ANOVA can not isolate the impact of local SST variations from remote SST and SIC changes in our transient experiments. The SENS and CTL experiments address these issues.

We test the significance of our results assuming a 95% threshold. For correlation analysis we use a Student's t-test, taking into account serial-correlation. For the sensitivity experiments we considered each year as independent (i.e., providing 60 different independent realizations) and use a bootstrapping test with 1000 permutations.

Our analysis also includes the application of the atmospheric front detection algorithm described by Berry et al. (2011). The algorithm identifies maxima of the 850 hPa equivalent potential temperature gradient and joins them to fronts using a nearest neighbor method. Fronts are categorized into cold, warm, and stationary fronts, according to their speed and moving direction. Based on the results of the front detection, we created masks that extract only those grid points for each time step that fall within a 200 km radius of the detected fronts. A different, widely used way to investigate the effect of cyclones, is to identify and track local maxima in relative vorticity (e.g. Bengtsson et al., 2006). This method detects only the center of the storm system. However, precipitation in storm systems usually follows the associated fronts. The front detection method additionally

provides information about the location of these front lines. For this reason we preferred the temperature based front detection approach to vorticity tracking.

3.3 Results

3.3.1 Simulated climatology

For a rough evaluation of the simulated precipitation in ECHAM5 in the western Atlantic region we compared the seasonal climatologies of total precipitation from our transient experiment to the TRMM 3B43 satellite product for the TRMM period from 2002 to 2007 (Fig. 3.1). The model is able to reproduce the observed precipitation band along the Gulf Stream SST front in a reasonable quality, even though the observed pattern is slightly more concentrated over the front than in the model. Whereas along the SST front the modeled winter and summer precipitation is weaker than in TRMM, in the extratropical North Atlantic outside the region of the SST front the winter precipitation is stronger. In summer the overestimation of precipitation is limited to a narrow region on the southern flank of the SST front. ECHAM overestimates the precipitation over the Caribbean. The latter bias is larger in summer than in winter. For the Gulf of Mexico the simulated precipitation is stronger, particularly in winter.

Our Control Experiment shows the key features of the observed climatological atmospheric circulation associated with the Gulf Stream front that were recently described by Minobe et al. (2008, 2010): A band of precipitation located over the warm flank of the Gulf Stream that is associated with convective precipitation, convergence of low level winds, and upward motion extending over the troposphere (Fig. 3.2). In summer the center of action is closer to the coast, whereas the main features in winter are located mainly over the Gulf Stream extension. Furthermore, convective precipitation contributes to most of the precipitation in summer over this region, while in winter precipitation is mostly large scale (Fig. 3.2a-d).

As discussed in the introduction, the SST front also acts to anchor the storm track by maintaining the surface baroclinicity (Nakamura et al., 2004). This mechanisms is likely more important in winter for collocating precipitation over the front, due to enhanced baroclinicity and storm activity. The climatological distribution of atmospheric fronts (see section 2) simulated by ECHAM5 is consistent with the ERA-40 reanalysis (Berry et al., 2011). In winter, atmospheric front occurrence is greater than in summer, and it is further south and collocated with the Gulf Stream front (3.3a-b). In winter most of the convective precipitation found over the Gulf Stream is linked to atmospheric fronts (Fig. 3.3d). In the region 60°W to 30°W and 30°N to 43°N, 73% of the convective precipitation occurs within

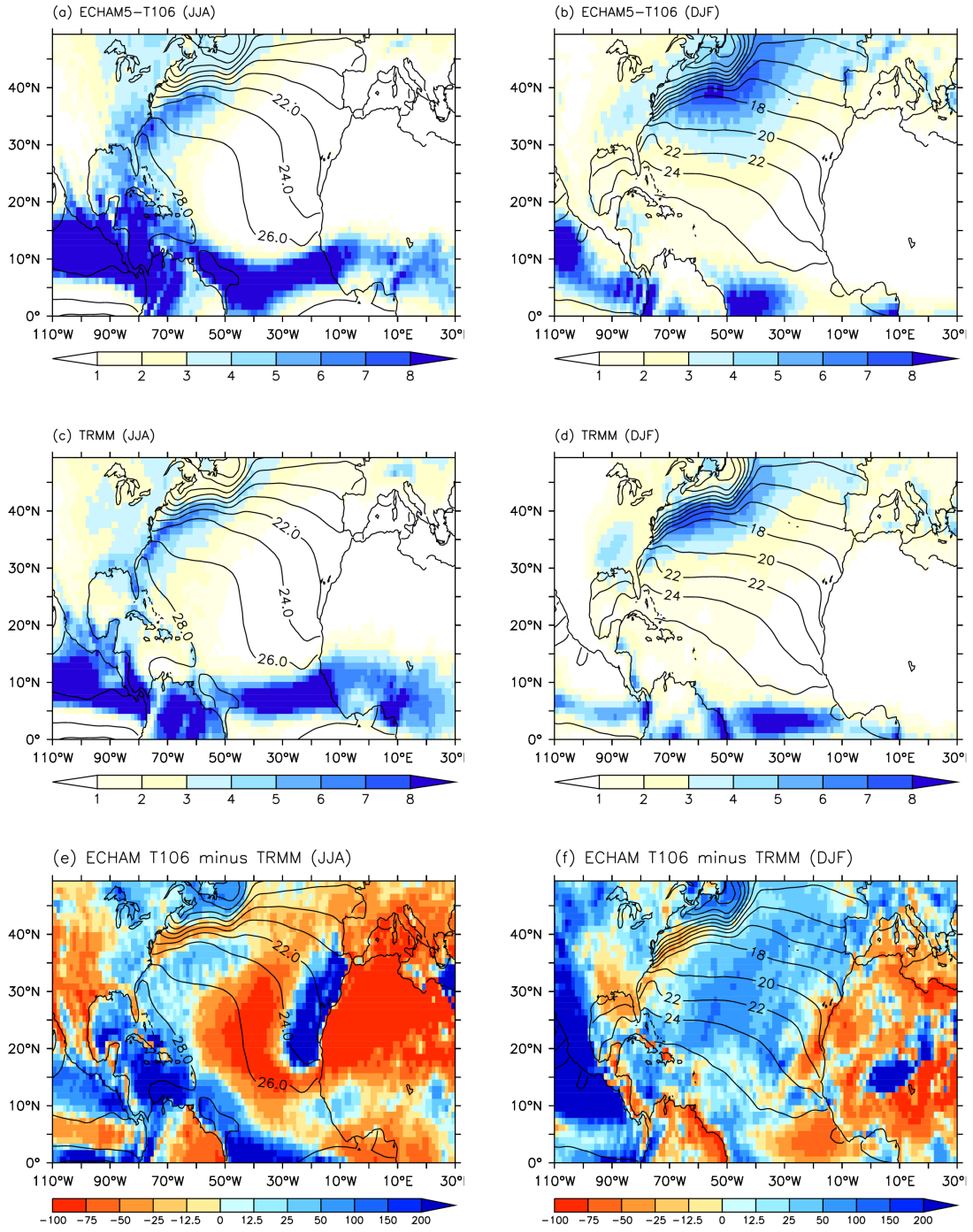

Figure 3.1: Climatological patterns of total precipitation (in mm/d) for the period 2002-2007. Left (right) column shows summer (winter) patterns from the transient ensemble simulation (a-b) and the TRMM 3B43 satellite product (c-d). (e-f) show the relative difference between ECHAM5 and TRMM (in % related to the ECHAM5 climatology). In all panels the black contours represent the climatological SST field (in °C).

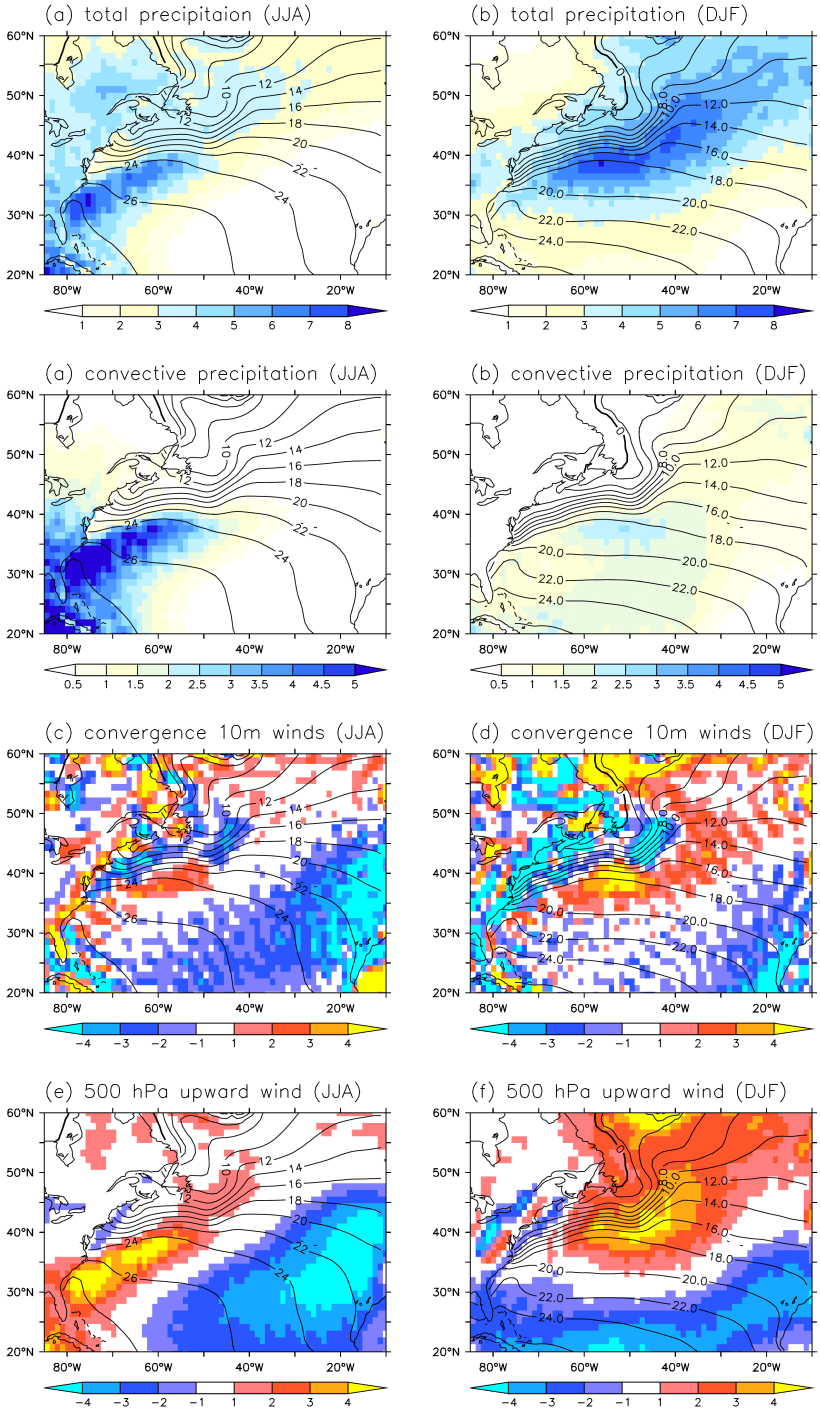

Figure 3.2: Climatological patterns of atmospheric quantities from the control simulation forced with climatological SST and SIC. Left (right) column shows summer (winter) patterns for total precipitation in mm/d (a-b), convective precipitation in mm/d (c-d), 10m wind convergence in 10^{-6}m/s^2 (e-f) and 500 hPa upward wind in hPa/s (g-h). Underlying contours are the seasonal climatological SSTs in °C.

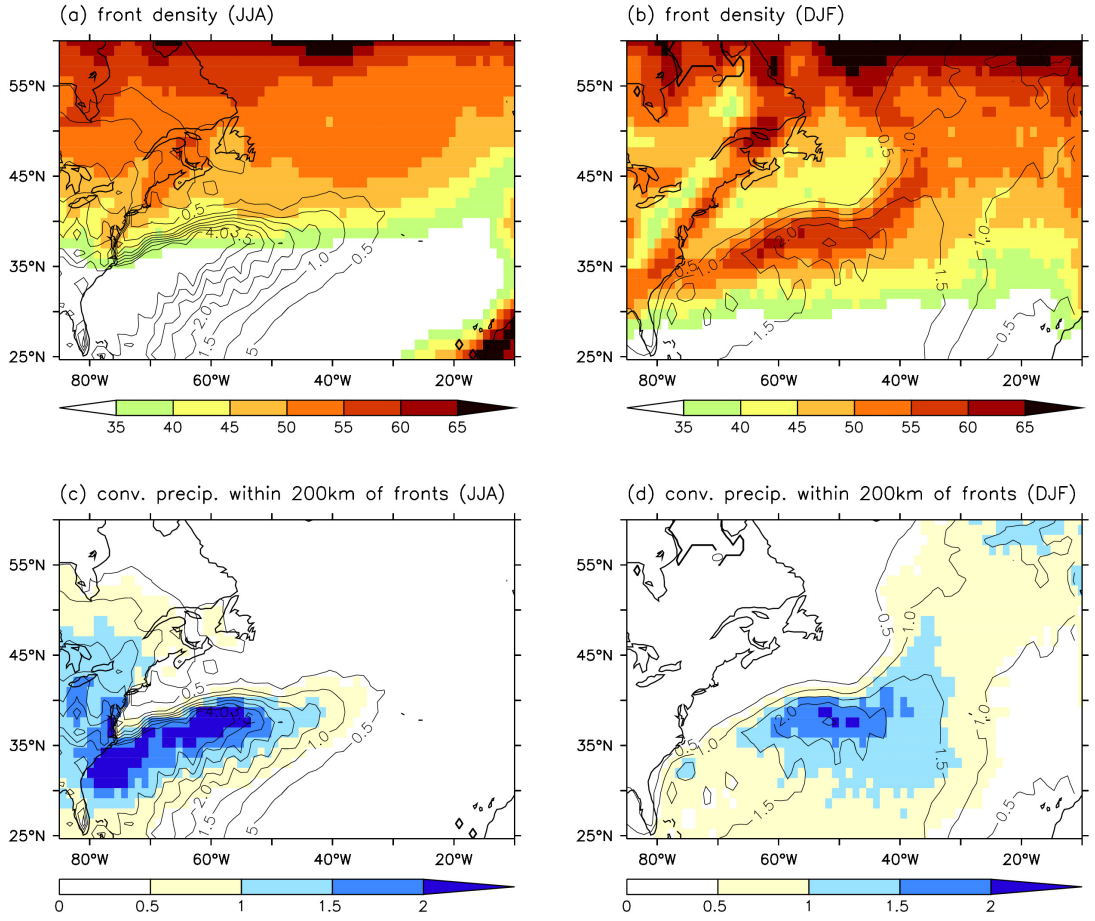

Figure 3.3: Front density and related convective precipitation (in mm/d) in the control run for summer (left column) and winter (right column). (a) and (b) Shadings show the front density plotted as relative fraction of time steps, which fall into a 200 km radius of a detected front in percent of the total number of time steps within the run. (c) and (d) Shadings show the time mean of the convective precipitation , which occurs within a 200 km radius of detected fronts. The contours represent the corresponding climatological convective precipitation.

a) Summer (JJA)

	SENS		CTL		SENS-CTL	
	mm/d	%	mm/d	%	mm/d	% of tot. resp.
total	1,675	100	1,315	100	0,36	100
all fronts	0,9583	57,19	0,7309	55,58	0,2275	63,19
cold fronts	0,5192	31	0,4079	31,02	0,1113	30,92
warm fronts	0,4073	24,32	0,2892	21,99	0,1181	32,81
stat fronts	0,3542	21,15	0,2742	20,85	0,08	22,22

b) Winter (DJF)

	SENS		CTL		SENS-CTL	
	mm/d	%	mm/d	%	mm/d	% of tot. resp.
total	2,229	100	1,682	100	0,5464	100
all fronts	1,675	75,15	1,235	73,42	0,4399	80,5
cold fronts	1,227	55,05	0,9543	56,74	0,2729	49,95
warm fronts	0,4988	22,38	0,3073	8,27	0,1915	35,05
stat fronts	0,3481	15,62	0,2547	15,14	0,0934	17,09

Table 3.1: Convective precipitation within a radius of 200km around fronts, averaged for the domain 60°W to 30°W/30 °N to 43°N for the sensitivity experiment (SENS), the control experiment (CTL) and the response (SENS-CTL) for summer (a) and winter (b). Since the same points might fall within the 200 km for more than one front type, fractions do not sum up to 100%.

the 200 km reference radius of an atmospheric front (Table 3.1a) and most (56.74%) is connected to cold fronts. Atmospheric fronts are also important in summer, as 56% of the convective precipitation occurs within the 200 km reference radius of an atmospheric front in this region, with 30% associated with cold fronts (Fig. 3.3, Table 3.1a). In both seasons, a significant fraction of convective rainfall occurs within a 200km radius of warm and stationary atmospheric fronts (Table 3.1). These results are consistent with synoptic scale observations that indicate convective rainfall is mostly associated with atmospheric cold fronts, while large-scale precipitation is mostly associated with warm and stationary fronts.

3.3.2 Ensemble AGCM simulations 1870-2007

Considering variability, the standard deviation of 5-year low-pass filtered convective and total precipitation show maxima over the warm flank of the Gulf Stream (Fig. 3.4a-d). Convective precipitation explains almost all of the precipitation variability in summer, while in winter it explains around two thirds of variability. In winter the precipitation variability is also much broader-scale. The precipitation variations in winter and summer are shifted southwards with respect to the maximum SST variability, which occurs in the region of the SST front (Fig. 3.4e-f).

ANOVA of these experimens (Fig. 3.5) provides an estimate of how much of the precipitation in the Gulf Stream region is related to the boundary forcing. ANOVA of total precipitation shows values over the Gulf Stream of around 10-30% in summer and generally less than 20% in winter (Fig. 3.5a,b). However, when concentrating on the convective part only (Fig. 3.5c,d), up to ∼70% (box mean 65°W to 40°W/38°N to 40°N: 51.6%) of the 5-year low-pass filtered variability in summer in the region of the SST front can be explained by the oceanic boundary conditions. In winter the values are slightly lower, but still reach up til about 50% (36.0% for the box mean). The difference between total and convective precipitation in terms of ANOVA indicates that large scale precipitation is dominated by internal atmospheric variability. This makes the identification of the total precipitation signal in observations and it's comparison to the model difficult, particularly in winter. We thus expect a stronger relationship between SST and convective precipitation compared to SST and large-scale or total precipitation. This stronger relationship can also be explained by the fact that convective precipitation is related to low-level moisture convergence and atmospheric stability, and that both of these are sensitive to SST. For these reasons we focus on convective precipitation (Fig 3.5c-d) only hereafter.

The time series of the box mean (65°W to 40°W and 38°N to 40°N) of low-pass filtered

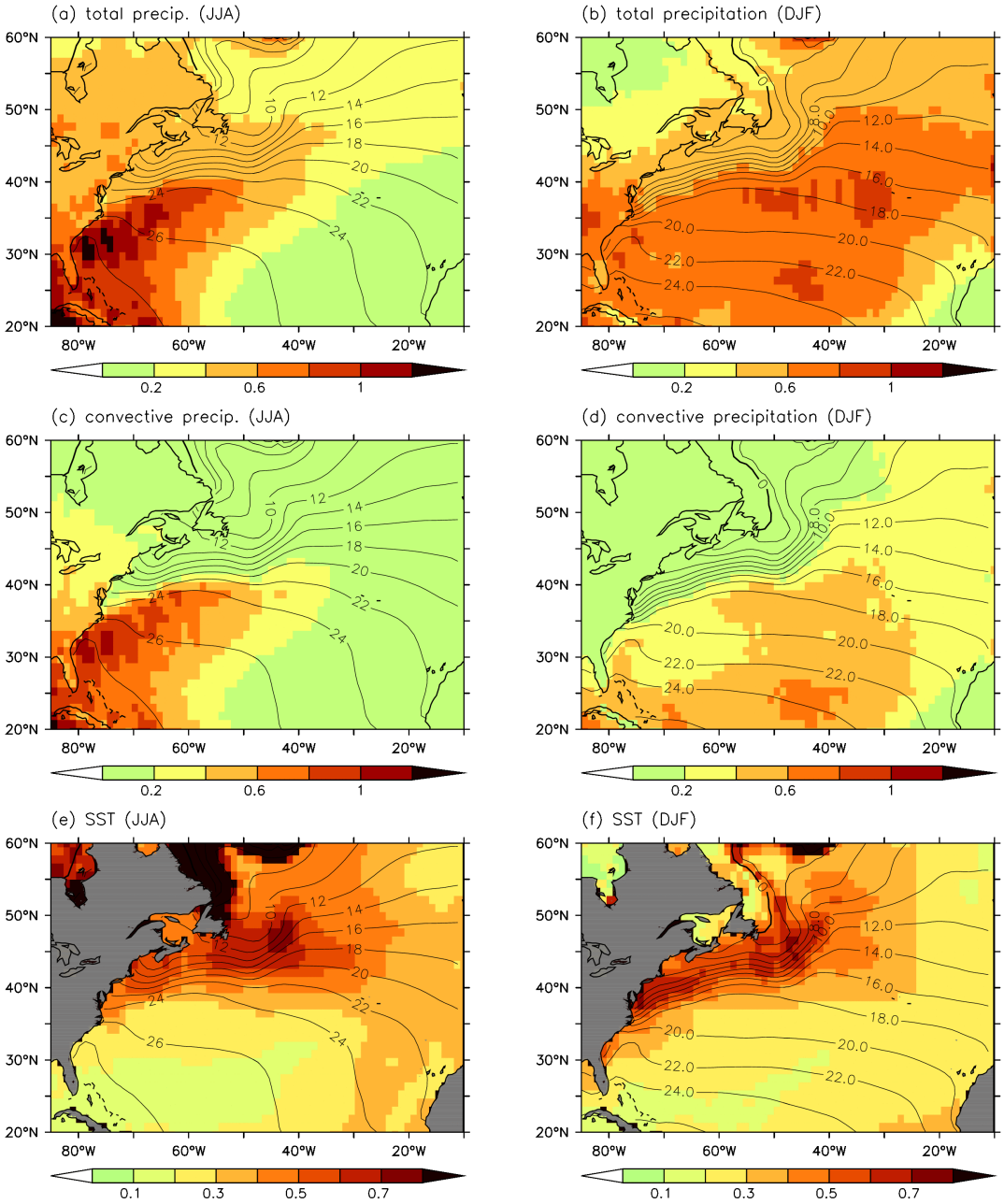

Figure 3.4: Standard deviations of 5-year low-pass filtered simulated total (a,b) and convective (c,d) precipitation (both in mm/d) over all 5 ensemble members of the transient run, and standard deviation of the observed 5-year low-pass filtered SST (e,f) for summer (left column) and winter (right column). Underlying contours is the climatological SST pattern.

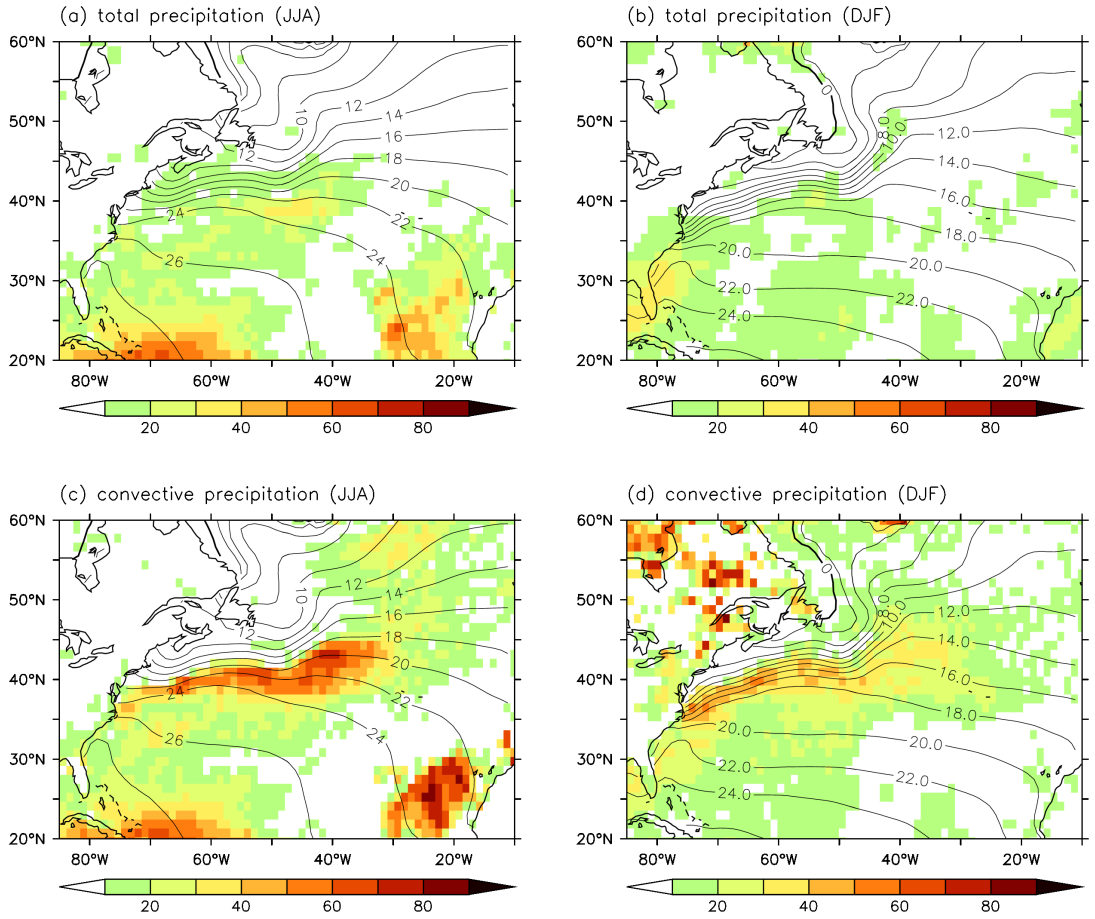

Figure 3.5: ANOVA explained variance (in %) due to the boundary forcing of total precipitation for summer (a) and winter (b) and convectice precipitation in summer (c) and winter (d). As before, climatology was removed, seasonal anomalies were calculated and afterwards a 5-year low-pass filter was applied. Contours indicate climatological seasonal SSTs in °C.

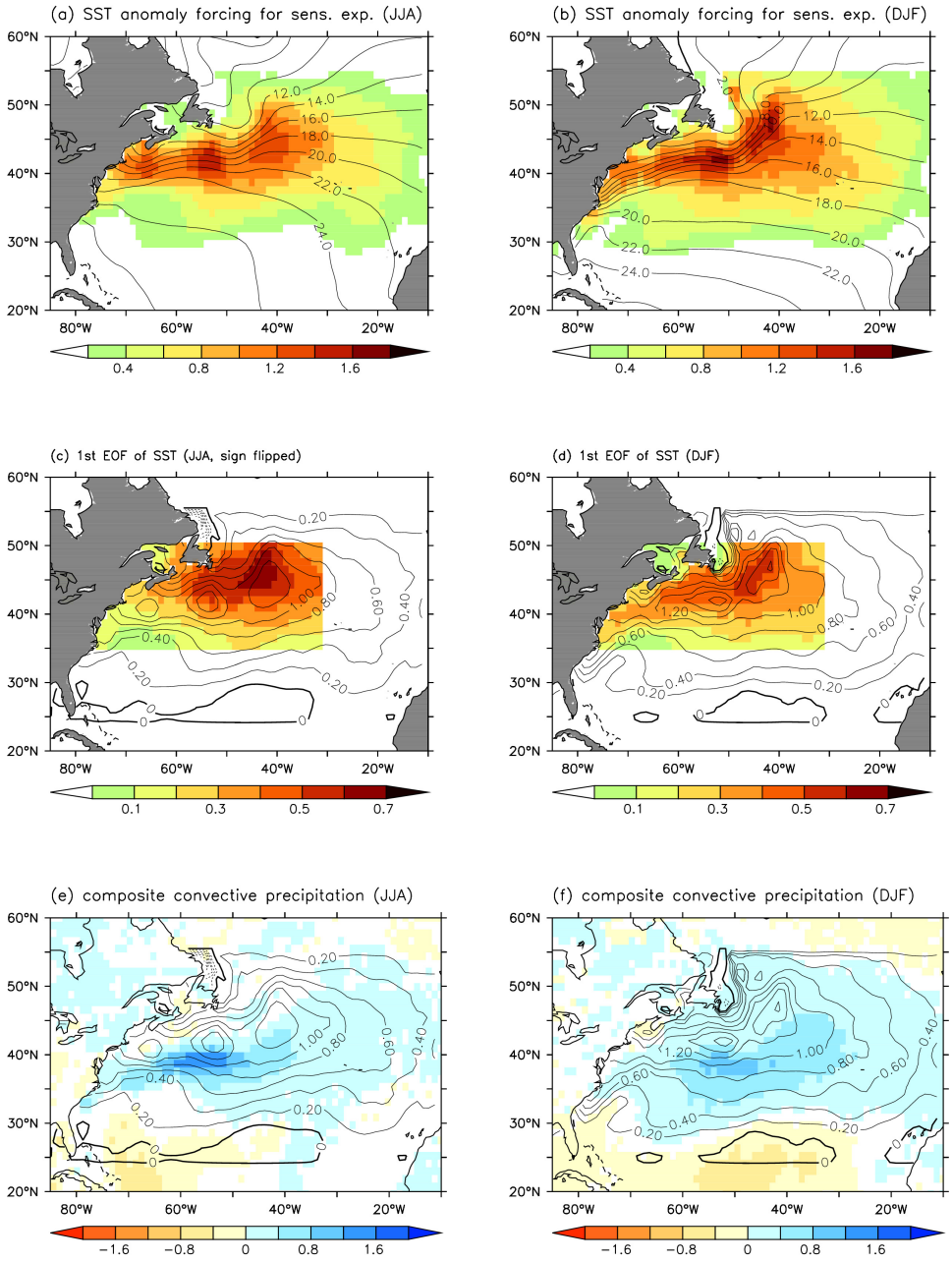

Figure 3.6: (a, b) SST anomalies (shadings, in K) for summer (a) and winter (b) used for the forcing of the sensitivity experiment. The patterns were derived from composite analysis using the convective precipitation time series box mean (65°W to 40°W, 38°N to 40°N) of 5-year low-pass filtered seasonal anomalies (Fig. 3.5) taken from the time varying run. Underlying contours are seasonal climatological SSTs in °C. (c, d) First EOF of 5-year low-pass filtered SST in the Gulf Stream Region (85°W to 30°W, 35°N to 50°N) (e, f) composite of convective precipitation from the time varying experiment. In Fig (c) to (f) the underlying contours are the SST forcing for the Sensitivity experiment.

convective precipitation and the box mean of low-frequency SST in the region with highest explained variances are highly correlated (r=0.73 for summer, r=0.55 for winter, Fig. 3.7). Composite analysis (methods) shows, that the difference between periods of high and low convective precipitation in this region is associated with a positive SST monopole over the region 25°W to 55°N, with largest anomalies in the Gulf Stream and it's extension (Fig. 3.6a-b, e-f). The SST pattern strongly resembles the first EOF mode of 5-year low-pass filtered SST (Fig. 3.6c-d). The corresponding principal components are also strongly correlated with the filtered Gulf Stream convective precipitation time series (r=0.65 for summer, r=0.7 for winter; Fig. 3.7). Thus, there are indications that the SST fluctuations in the Gulf Stream region explain a significant part of the local variability in convective precipitation.

3.3.3 Response to Gulf Stream SST anomaly

Are the simulated precipitation changes locally or remotely driven and what are the mechanisms responsible for the changes? To address these questions we perform a sensitivity experiment forced by the warm extra-tropical SST anomalies that are associated with the enhanced convective precipitation in the region of the highest explained variance (Fig. 3.5a-b, see section 3.2).

First, we consider the zonally averaged (65°W to 50°W in summer, 55°W to 35°W for winter) response over the regions where we added the SST anomaly (Fig. 3.8). In both, summer and winter, the warm SST anomaly drives increased precipitation directly to the south of the SST maximum, and a weak decrease to the north (Fig. 3.8). In summer the increased precipitation is larger and more meridionally confined than in winter. The increase is driven by enhanced convective precipitation in both seasons, while the large scale precipitation is negative and thus reduces the impact on total precipitation. Possible reasons for the latter could be that part of the available moisture for large scale precipitation is rained out by convective events (i.e., less moisture is detrained from deep convective plumes, a source term in the stratiform cloud scheme) or changes related to the large scale atmospheric circulation. The warm SST drives increased evaporation that exceeds the simulated precipitation increase (i.e., it is thus able to supply sufficient moisture for the local precipitation increase).

In summer the simulated convective precipitation pattern (Fig. 3.8a) matches that from the composite analysis, but is around 25% less (Fig. 3.6e); the latter is consistent with the ANOVA of convective precipitation (Fig. 3.5a). The associated circulation patterns (Fig. 3.9b-e) closely resemble those of the climatological annual mean (Fig. 3.2e-g; Minobe

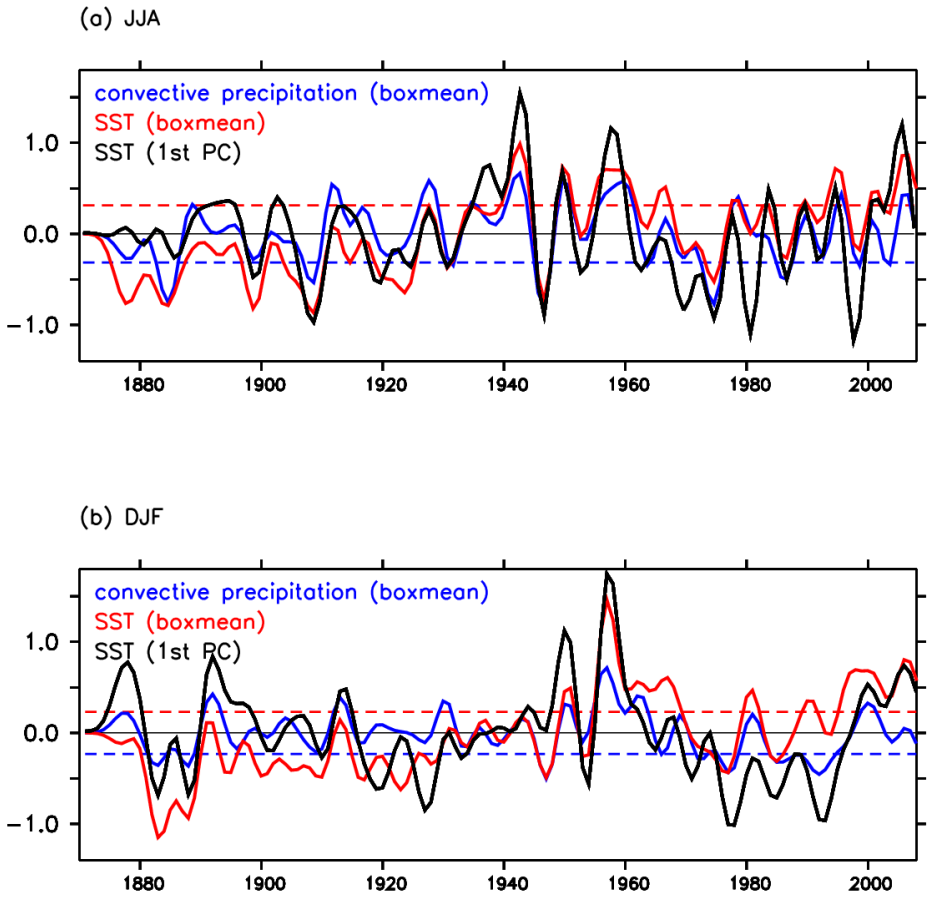

Figure 3.7: Time series of box means (65°W:40°W, 38°N:40°N) of 5 year low pass filtered seasonally averaged anomalies of ECHAM5 convective precipitation (in mm/day, blue), HadISST (in K, red) and first PC of the 5-year low-pass filtered Gulf Stream region SST (black, see figure 6 c/d for the associated EOF pattern) for summer (a) and winter (b). Dashed lines mark +/- 1 standard deviation of the convective precipitation time series, which was used as threshold to create the forcing pattern for the sensitivity experiment.

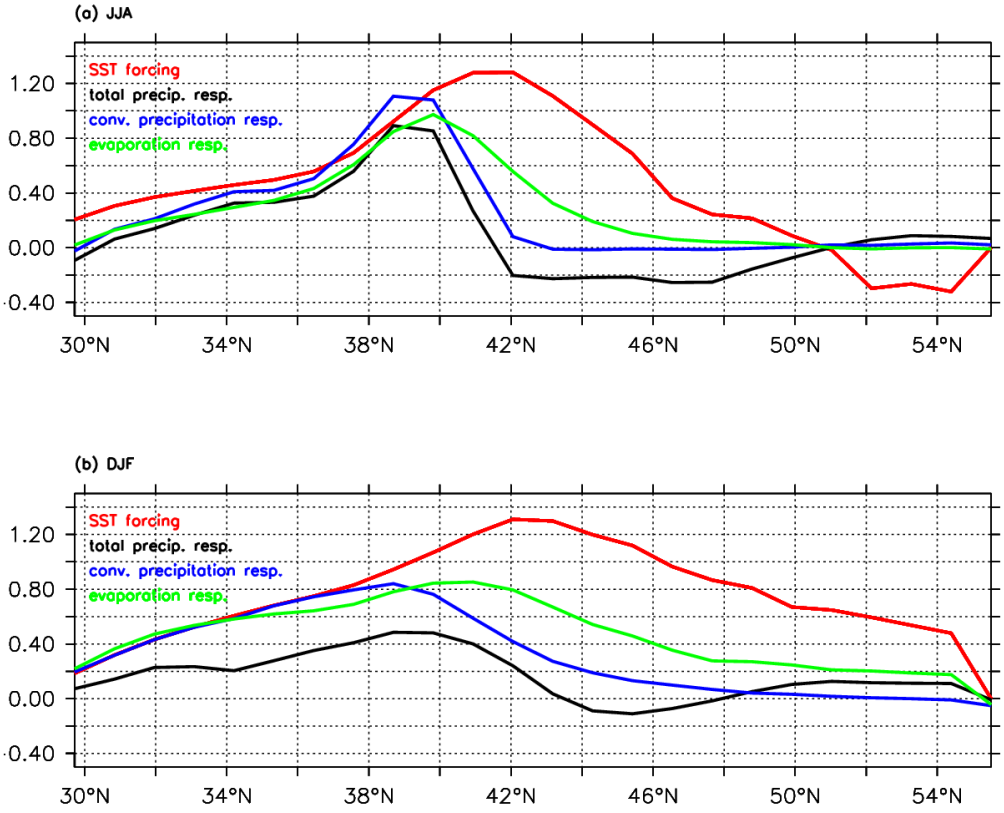

Figure 3.8: Sections of anomalous SST forcing (in K, red), total precipitation (in mm/d, black)and convective precipitation response (in mm/d, blue) and evaporation response (in mm/d, green) (a) for summer averaged for the region from 65°W to 50°W, and (b) for winter averaged for the region from 55°W to 35°W.

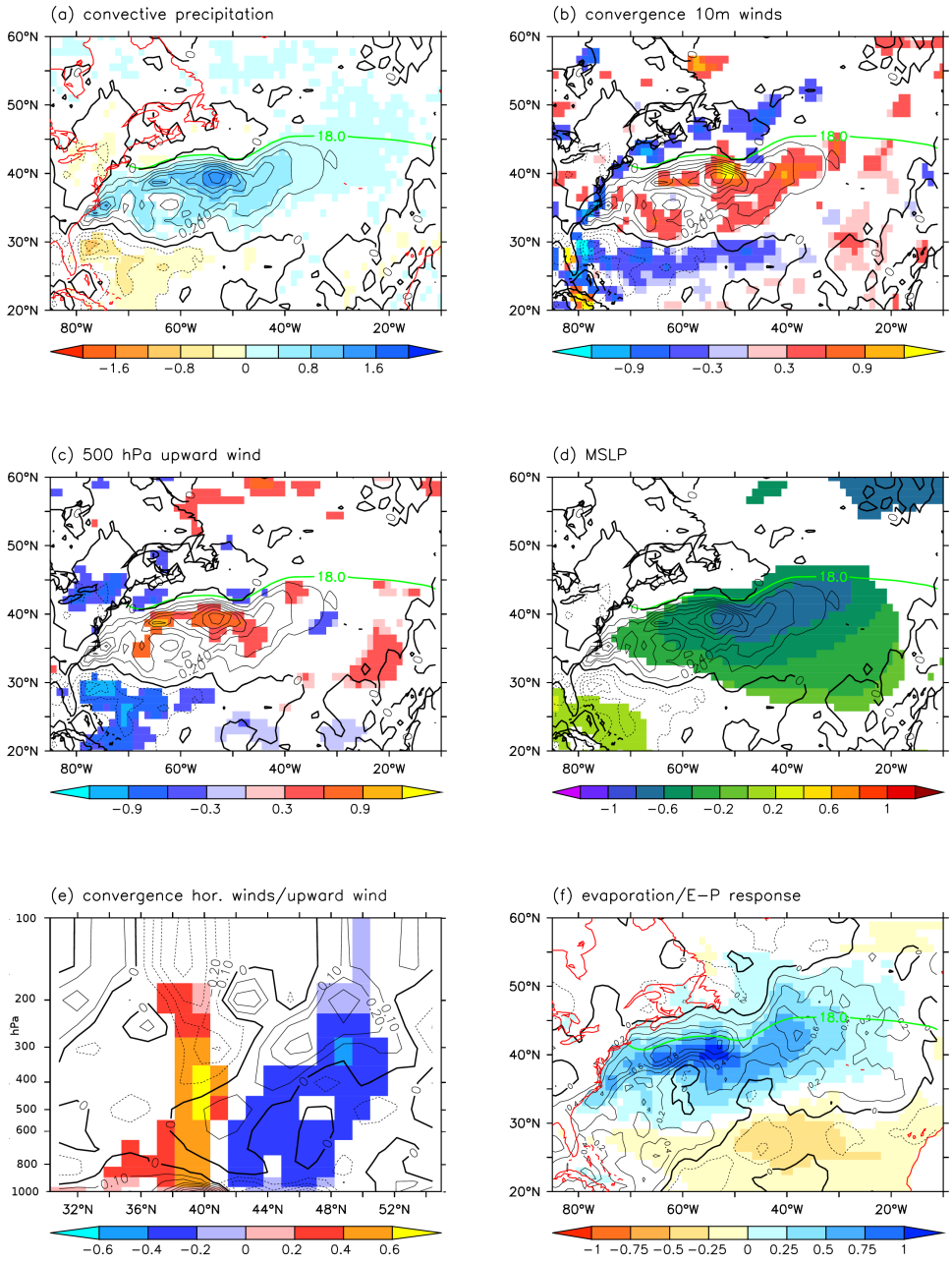

Figure 3.9: Summer response (SENS-CTL) to positive SST anomaly in the Gulf Stream region: (a) convective precipitation (in mm/d), (b) 10-m wind divergence (in 10^{-6}m/s^2) (c) upward wind (in 10^{-2} Pa/s) and (d) sea level pressure (in hPa). (e) Cross section (zonal average between 60°W and 50°W) of horizontal wind divergence (in 10^{-6}m/s^2, contours) and upward wind (in 10^{-2} Pa/s, shadings) (f) Evaporation (in mm/d, shadings) and evaporation minus precipitation (in mm/d, contours). Only values significant at the 95% level are shaded. In figure (a-d) the black contour line is the convective precipitation response. The green contour line in Fig. (a-d) and (f) marks the position of the 18°C SST isotherm in summer as an indicator for the position of the SST front.

et al. (2008)): low SLP, low level convergence and upward motion penetrating up to the mid troposphere over the anomalous SST region, but slightly shifted with respect to the maximum SST anomaly (Fig. 3.6a). The pattern of increased evaporation corresponds closely to the warm SST anomaly, as expected. Over the entire Gulf Stream and Extension region, evaporation exceeds the enhanced local precipitation.

In winter the convective precipitation pattern (Fig. 3.10a) also matches the composite analysis (Fig. 3.6f), but the response is around 40% weaker; this is also consistent with the ANOVA (Fig. 3.5b). While convective precipitation increases by up to ∼1.2 mm/day, there is a small decrease in large scale precipitation (not shown). As in summer, enhanced evaporation exceeds local precipitation over the entire Gulf Stream and extension (Fig. 3.10b). In contrast to the summer, the coherent response among SLP, low level convergence, and mid-troposphere upward motion is missing in winter (not shown).

Our SST forcing causes a northward shift in the SST gradient, and tends to strengthen the gradient to the north, while weaken it to the south. This will impact low-level baroclinicity and would tend to force a northward shift in the storm track and weakening to the south. Consistently we found indications for a slight northward shift of the atmospheric frontal activity in winter (not shown). However, the SST anomaly we add is small compared to the climatological gradient and SST variations are only one of the several factors controlling the variability in the position and the strength of the storm track. The biggest enhancements in front density are not collocated with the maximum of enhanced rainfall and the shift in atmospheric front density is too small to explain the precipitation signal.

The atmospheric front tracking analysis, however, shows that around 60% of the summertime convective precipitation simulated in response to the warm SST anomalies is associated with atmospheric fronts (Fig. 3.11a, Table 3.1a). Thus, the enhanced convective precipitation is due to more rainfall per front, rather than to an enhancement in frequency of atmospheric fronts. The increase is found for all atmospheric front categories, and can be explained by an almost equal increase in cold and warm front precipitation (Fig. 3.11b, Table 3.1a). Compared to the summer climatology this represents a proportionally stronger increase for warm fronts (Table 3.1a).

As expected, for boreal winter much more of the precipitation response is associated with atmospheric fronts. Around 80% of the increased convective precipitation is associated with atmospheric fronts (Fig. 3.10c, Table 3.1b). The largest part of the response is connected to cold fronts, which produce about half of the additional winter precipitation in

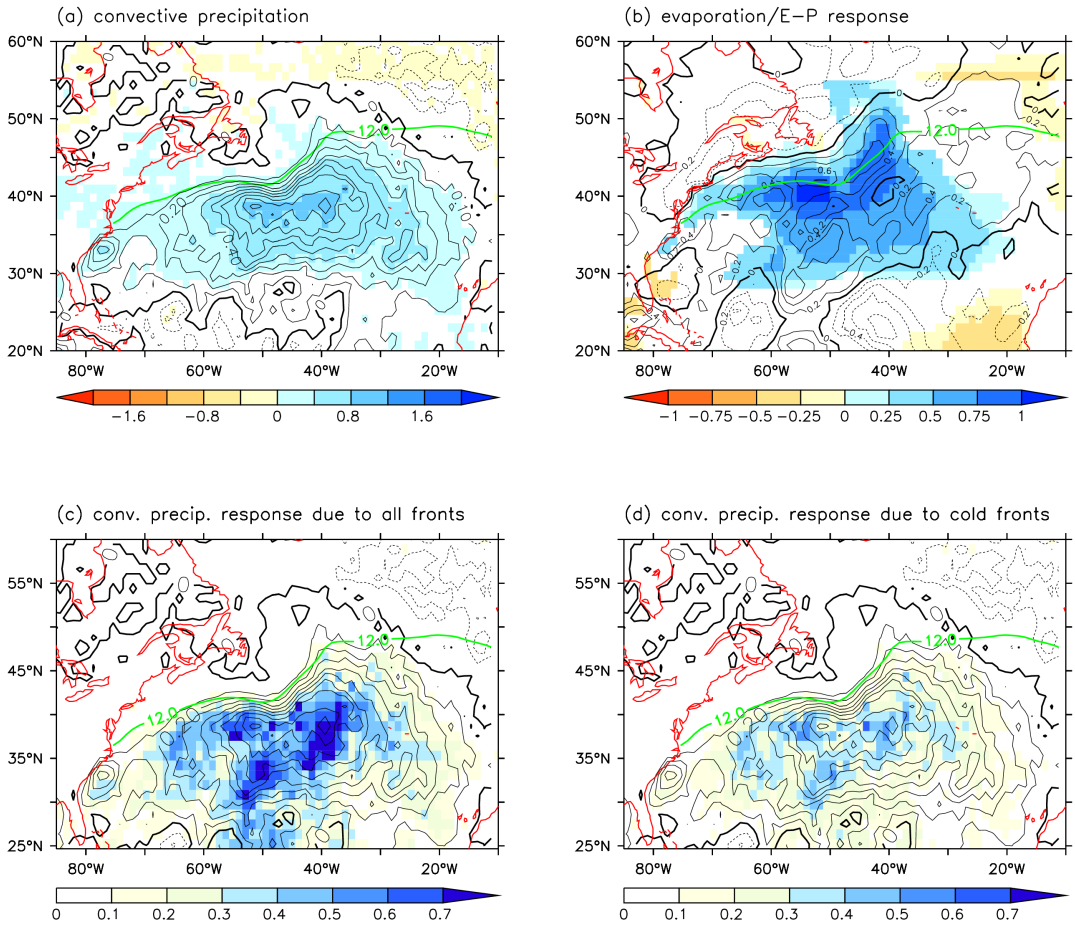

Figure 3.10: Winter response (SENS-CTL) to the positive SST anomaly in the Gulf Stream region: (a) convective precipitation (in mm/d), (b) Evaporation (in mm/d, shadings) and evaporation minus precipitation (in mm/d, contours). Only values significant at the 95% level are shaded. (c) and (d): Convective precipitation response (in mm/d, shadings), considering only that part, which is produced within a radius of 200 km around points which were detected as a front, (c) considers all fronts, and (d) cold fronts only. In Fig. (a), (c) and (d) the black contour lines are the convective precipitation response. The green contour line marks the position of the 12°C SST isotherm in winter as an indicator for the position of the SST front.

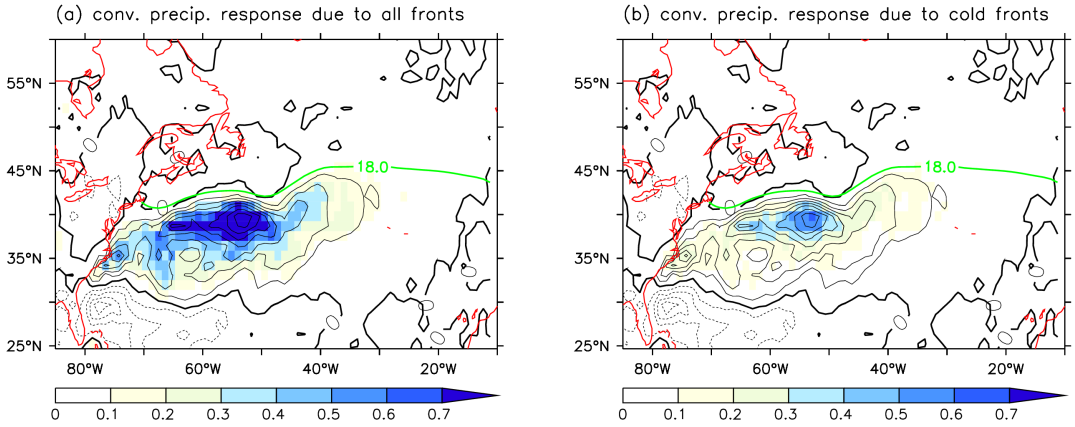

Figure 3.11: Summer response (SENS-CTL) to the SST anomaly in the sensitivity experiment: Convective precipitation response (in mm/d, shadings), considering only that part, which is produced within a radius of 200 km around points which were detected as a front. (a) considers all fronts, and (b) cold fronts only. The black contours show the total convective precipitation (in mm/d) in the sensitivity experiment, the green contour line indicates the position of the SST front.

the warm simulation (Fig. 3.10d, Table 3.1b). Thus, as in summer, the simulated increase results from increased precipitation per front rather than a change in front frequency. As in summer there is a proportionally larger increase for warm fronts. Together these results imply that the increased precipitation in winter (and to certain extent in summer) occurs through higher moisture loading of the passing atmospheric fronts that is fed by locally increased evaporation. The proportionally stronger impact on warm front precipitation is not clear, but may be due to the slower propagation speed of warm fronts.

3.4 Summary & Discussion

The aim of this work was to understand the atmospheric impact of SST variations over the Gulf Stream and its extension using an AGCM, focusing on the local precipitation changes. The ANOVA applied to a 5-member transient run forced by historical ocean conditions shows that a large part of the 5-year low-pass filtered convective precipitation variability in the Gulf Stream region (up to ∼70 % in summer, ∼50% in winter) is related to the surface boundary conditions. The precipitation changes seen in the transient run are a direct response to local SST changes as shown by an additional sensitivity experiment.

In summer the precipitation response to local SST changes over the Gulf Stream region is constricted to a tight band in the region of the climatological SST front. The response is associated with low level convergence in combination with mid-troposphere upward motion. To first order this describes a strengthening of the climatological state (Minobe et al., 2008, 2010). In contrast to the climatological state, where the highest precipitation is localized over the region with the strongest climatological SST-gradient, the highest precipitation response in our experiment is localized over the region with a weakened SST-gradient. This means, that the summer response in our model is not a response to an increased SST gradient, but to the stronger evaporation due to the anomalous warm water. However, it is the SST-front that localizes the precipitation response, causing the high SST variability in this region.

The mechanism seen in the climatological pattern (Minobe et al., 2008) could not be identified in the winter response. Instead the winter response is dominated by stronger convective events in connection with passing atmospheric fronts, especially cold fronts. Atmospheric fronts also play a role in summer, but are less important than in winter. In both seasons we found little indications of changes in front density in the region of the precipitation changes. Thus in winter, and to a certain extent in summer, the increased precipitation associated with a warming of the Gulf Stream and its extension reflects an increased water loading of passing atmospheric fronts due to locally enhanced evaporation. Our results also indicate a slightly greater increase in precipitation associated with warm fronts in both seasons.

The model resolution used in this study (T106) can not resolve properly the sharpness of the SST front. Minobe et al. (2008) showed that smoothing of the SST front leads to a significant loss in the ability to simulate the climatological precipitation band over the Gulf Stream front. On the other hand, various idealized studies indicate that the atmospheric response to the SST front may be captured with atmospheric resolution similar or low than T106 (e.g. Brayshaw et al., 2008; Ogawa et al., 2012). Whether higher resolution would lead to significant differences in the response deserves further investigations.

This study has focused largely on precipitation, which is extremely difficult to simulate as it depends on sub-grid scale processes and thus needs to be parametrized in AGCMs. A variety of different parametrizations have been developed for atmospheric convection, and the implementation of different schemes leads to big differences among in simulated precipitation (e.g. Hourdin et al., 2006)). In common with other models, ECHAM5 simulates to much precipitation over the oceans (Hagemann et al., 2006). The largest biases

are in the tropics, which may be an indication that the convective parameterisation is very sensitive to SST, as for example found in coupled model studies (Dai, 2006). The impact of convection parametrization on our results needs further investigation.

Our results should be clearly seen as a model study, and whether the link between SST and precipitation is realistic is still outstanding and cannot be easily addressed due to the lack of available long term observations of marine precipitation. Furthermore, ANOVA analysis indicates that there is only a weak link between SST and total precipitation over the Gulf Stream. Thus, even with reliable long-term observations of total precipitation it will be hard to confirm our results. Nevertheless, we compared simulated precipitation with data from the NCEP reanalysis. The low frequency part of precipitation variability shows some correlation to NCEP reanalysis in summer, where the simulated convective precipitation dominates the total precipitation in ECHAM: the low pass filtered time series of ECHAM5 convective precipitation is correlated to NCEP total precipitation by r=0.68, but in winter the correlation is low (r=0.15). However, NCEP precipitation should be considered also as a model product. We also compared shorter satellite derived precipitation (CMAP, 1979-2007) with ECHAM5 and the NCEP/NCAR reanalysis and found little agreement in any season for Gulf Stream precipitation (not shown).

Our study does not address how much of the SST variability in the Gulf Stream region on five year and longer timescales results from ocean dynamics as opposed to thermodynamic forcing of the atmosphere. Furthermore, previous studies have largely suggested that the large-scale atmospheric response to mid-latitude SST variations represents a weak feedback (Bretherton and Battisti, 2000; Czaja and Frankignoul, 2002). Nevertheless, our results indicate that at a local level there is quite a strong response in convective precipitation. Is there also a large scale response that could lead to useful climate predictability? In summer, the large scale response in our experiment is weak and consists mainly of a geopotential height maximum over Siberia. In winter the SST anomaly causes a wave train in 500 hPa geopotential height, which expands over the entire northern hemisphere (Fig. 3.12). The pattern shows some similarities to previous studies (Palmer and Zhaobo, 1985), although it's centers are shifted a little. We see this as a hint of possible interaction with large scale circulation in the Gulf Stream region.

Concerning the large scale response, observational studies found that warm SST anomalies in the Gulf Stream region were followed by a positive NAO response with a lag of about two weeks (Ciasto and Thompson, 2004). Models show a very heterogeneous response to mid-latitude SST anomalies. Deser et al. (2007) found a zonal, NAO/NAM-like response

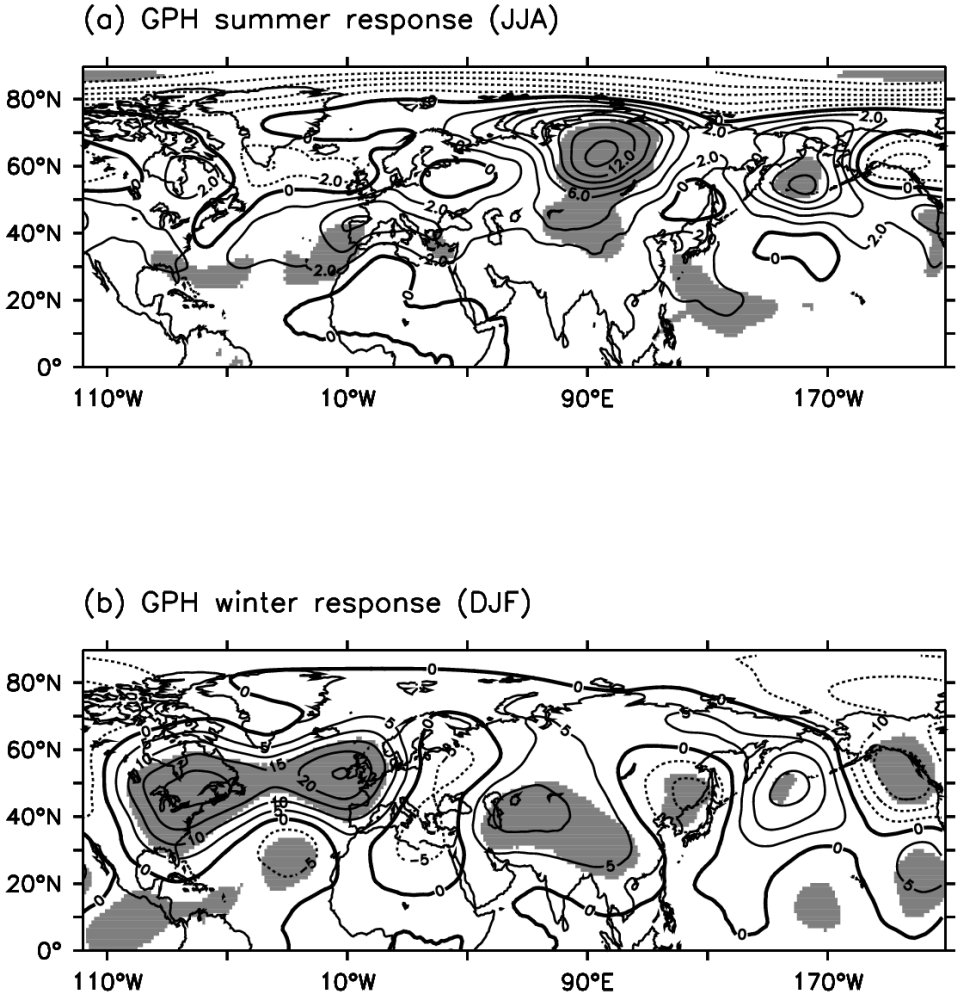

Figure 3.12: 500hPa GPH response response (in m) in the sensitivity run for summer (a) and winter (b). Values 95% significance level are indicated by grey shadings.

in winter. In contrast to our experiment, the SST anomaly they used was slightly shifted to the north, was more extended and had a much higher amplitude than our forcing pattern. Earlier studies showed, that the atmospheric response to wintertime midlatitude SST anomalies furthermore strongly depends on the background state of the atmosphere (Peng et al., 1995). It also differs among models (Hodson et al., 2010) and is very sensitive to the structure and location of the forcing pattern. Furthermore, accurate representation of stratosphere-troposphere interaction could be important to capturing the observed large-scale winter response (Omrani et al., 2014). Thus, the realism of the large scale features simulated by ECHAM5 is uncertain. Nevertheless, the significant response found to SST variations in the Gulf Stream region is potentially important and deserves further attention, particular as ocean dynamics is known to be important in driving SST in this region and on low-frequency timescale (Bjerknes, 1964; Yeager et al., 2012; Gulev et al., 2013).

Acknowledgements

We thank Richard Greatbatch, Shoshiro Minobe, Bunmei Taguchi, and Akira Kuwano-Yoshida for fruitful discussions and Michael Reader and Gareth Berry for providing code and support for the frontal tracking analysis. Further, we thank the two anonymous reviewers for their constructive comments. Ralf Hand was supported by the German Federal Ministry of Education and Research (BMBF) through the MiKliP program, Noel Keenlyside and Nour-Eddine Omrani were funded by the German Research Foundation (DFG) through the Emmy Noether program. Ralf Hand, Noel Keenlyside and Nour-Eddine Omrani benefited from travel grants through the DFG-JSPS cooperation program, which stimulated the collaboration with the groups from Hokkaido University and JAMSTEC on this topic. We thank the MPI for providing the ECHAM5 model and support, and we acknowledge computing resources and technical support from the North-German Supercomputing Alliance (HLRN) and the German Climate Computing Center (DKRZ).

4 The role of ocean-atmosphere interaction in shaping climate change in the North Atlantic sector

4.1 Abstract

Here, we present an analysis of North Atlantic ocean-atmosphere interaction in a warming climate, based on a long-term coupled general circulation model experiment forced by the RCP 8.5 (Representative Concentration Pathways 8.5) scenario. In addition to the direct radiatively forced increase in sea surface temperature (SST), the model run shows a distinct change of the local SST pattern in the Gulf Stream region. This includes changes of the SST gradients in the region of the Gulf Stream SST front, likely as a response of the wind-driven part of the oceanic surface circulation. Furthermore the northern North Atlantic shows a much weaker warming than the other ocean basins that is likely caused a massive slow-down of the Atlantic Meridional Overturning Circulation.

The feedback of these changes on the atmosphere was studied in a set of sensitivity experiments based on the SST climatology of the coupled runs. The set consists of four runs: a control experiment based on the historical run, a run using the full SST from coupled RCP 8.5 run and two runs, where where we deconstructed the SST signal into a homogenous mean warming part and a local SST pattern change. In the region of the precipitation maximum in the historical run, the future simulation shows a significant decrease in precipitation, despite a strong increase in the underlying SST. Instead, this local change in precipitation is caused by a weakening of the SST gradients. Consistently, the model shows enhanced precipitation north of this region, where the SST gradients are enhanced. The warming causes a decreased low-level convergence and upward motion in the region with reduced SST gradient. However, the response is restricted to the low and mid-troposphere and there is little evidence for a large-scale atmospheric response to the SST pattern changes in the Gulf Stream region. Instead, the large-scale response is mainly controlled by either warming remote to the Atlantic or the large-scale warming pattern in the Atlantic. In a warmer climate the same change in the SST gradient has a stronger

effect on precipitation and an enhanced North Atlantic storm track is found in the model.

4.2 Introduction

Anthropogenic greenhouse gas emissions are expected to have a major impact on the Earth's atmosphere. Beyond a strong increase in the global mean temperature, recent climate projections show changes in the large scale atmospheric and oceanic circulation (IPCC, 2013) which can give rise to pronounced regional effects (Xie et al., 2010). Understanding the processes linking atmospheric and oceanic changes therefore is of great importance for a comprehensive understanding of climate change. Our work is based on a long-term climate projection forced by the RCP 8.5 scenario, a climate scenario used by many modeling groups to estimate the climate feedbacks to the injection of large amounts of greenhouse gases (GHG) into the atmosphere. Here, we focus on understanding the atmospheric response to future North Atlantic SST changes. We focus on precipitation, a quantity that has been shown to be highly sensitive to the position of the SST front (Ogawa et al., 2012) and the absolute value of SST (Hand et al., 2014). The change in SST simulated by the CMIP5 projections exhibits a distinct and rather robust pattern that consists of minimum warming in the subpolar gyre region and more pronounced warming in the vicinity of Gulf Stream and its extension (fig. 4.1). These features have been linked to oceanic processes (Drijfhout et al., 2012).

Recent studies have shown that mid-latitude regions with strong SST gradients, as found in the Gulf Stream and its extension, are a key-region for mid-latitude ocean-atmosphere interactions. The CMIP5 climate projections exhibit distinctive precipitation changes in winter that appear related to the underlying SST changes in winter, while in summer there is less correspondence (fig. 4.1). One focus of this paper is on understanding the processes connected to changed mid-latitude SST fronts in the context of climate change. Previous studies have shown that the SST front causes a narrow band with strong precipitation on its equator-ward side (Minobe et al., 2008) and a model study has shown that SST variability on inter-annual to decadal timescales in this region has a distinct impact on the overlying atmosphere (Hand et al., 2014). Furthermore the SST front is thought to anchor the North Atlantic storm track by maintaining low-level baroclinicity in the atmosphere (Nakamura et al., 2004). Conceptional model studies have shown that the position of the SST front has an impact on the strength of the atmospheric subpolar jet (Ogawa et al., 2012). It was found that both, the absolute SST in the North Atlantic as well as the SST gradient along the US east coast are controlling factors for the strength of the storm track (Keeley et al., 2012). Climate scenarios show a strengthening of the

storm track over western Europe in a warming climate and a high level of agreement in terms of the storm track response (Woollings et al., 2012; Harvey et al., 2012). Woollings et al. (2012) showed, by comparison of a set of CMIP5 scenario runs, that the intensity of the storm track response can be related to the strength of the response of the Atlantic Meridional Overturning Circulation (AMOC). In future climate projections, most models show a northward shift of the baroclinic regions and the northern hemisphere storm track (Bader et al., 2011). However, ECHAM5/MPIOM (i.e. the previous version of MPI-ESM, the model used in this study) forms an exception in this point (Yin, 2005).

In this study, we use MPI-ESM, the Earth System Model of the Max-Planck-Institute for Meteorology to investigate the role of ocean-atmosphere interaction in the North Atlantic in shaping the global warming response. The model shows good agreement with the CMIP5 ensemble mean in terms of the simulated surface temperature and precipitation response (fig. 4.1 and supplementary fig. A.14; pattern correlation for the region shown: 0.95 for surface temperature, 0.83 for precipitation). Using a single model offers the advantage that the SST gradients are enhanced compared to the multi-model ensemble mean. We focus on the far future to enhance the signal to noise ratio. In the context of mid-latitude ocean-atmosphere interactions, this CGCM experiment forms an interesting extreme case, combining two features of interest: On the one hand, the surface temperatures are globally strongly increased as a direct response to the high GHG concentrations. On the other hand, the coupled model setup allows feedbacks from the atmosphere onto the ocean circulation. The thermohaline circulation in the ocean to large extent is driven by water masses cooling down to very low temperature in the high latitudes in boreal winter, leading to deep ocean convection and the formation of North Atlantic Deep Water. In MPI-ESM the AMOC response to the RCP 8.5 scenario is a significant slowdown in the future (Fischer, M., pers. communication). This feature is likely related to two factors: Firstly, there is a strong warming of these parts of the North Atlantic where we find the main regions of deep convection in the present-day climate; secondly fresh water input from enhanced precipitation and from the continental ice sheet melting due to higher air temperatures. Additionally, the experiment shows a northward shift of the boundary between the subtropical and the subpolar gyre in the North Atlantic, likely as a response of the wind-driven part of the ocean surface circulation. As a result, the SST gradients in the Gulf Stream region change with respect to that simulated with the historical conditions.

In summer the most prominent feature in terms of precipitation is a decrease in the region off the US east coast, where the historical control experiment had the strongest SST gradients, but shows weaker gradients in the future. In winter the coupled models show a large

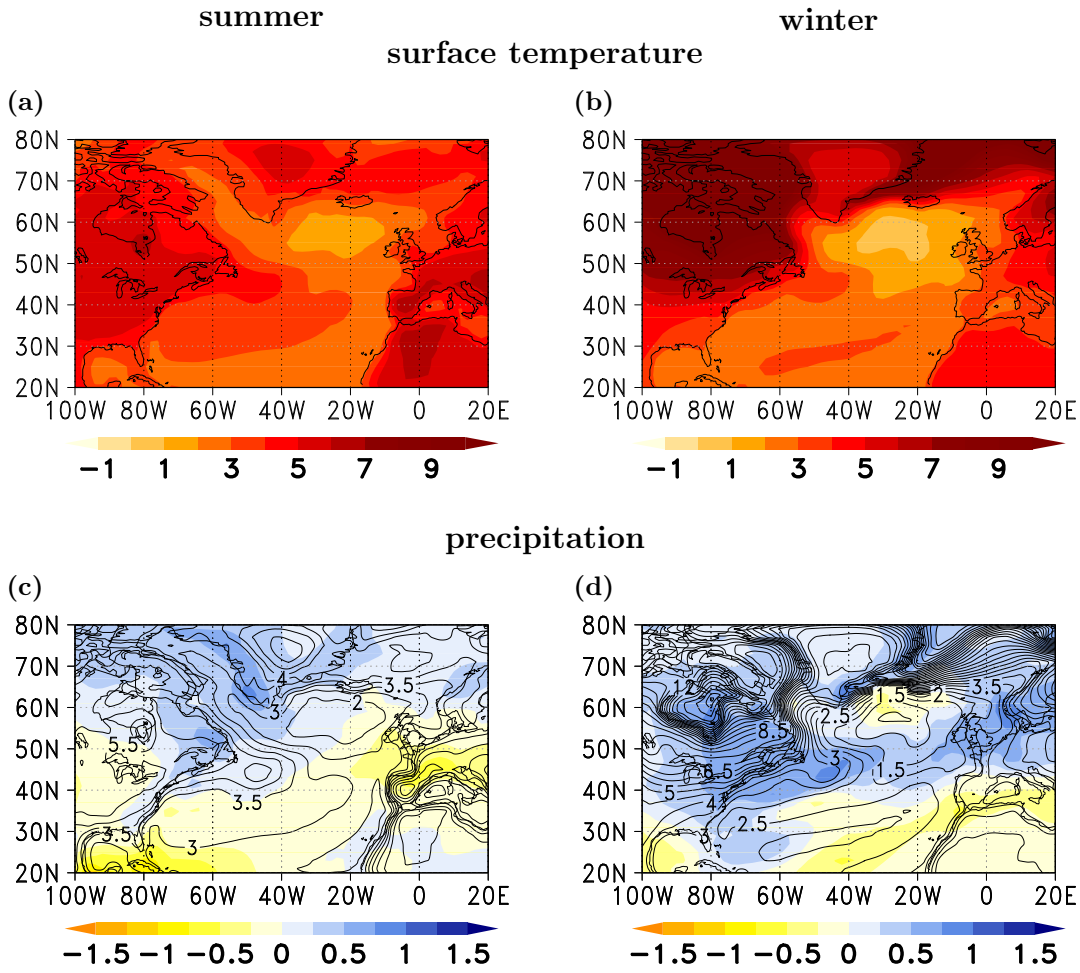

Figure 4.1: Surface temperature response (top, in K) and precipitation response (bottom, in mm/day) to the RCP 8.5 scenario for summer (left column) and winter (right column) for the CMIP5 multi-model ensemble mean. Climatological differences between the periods from 2050 to 2100 and 1900 to 1999. In panels c & d contours repeat the surface temperature change.

region with strongly enhanced precipitation southeast of Newfoundland. The precipitation changes in winter seem to be closely linked to the SST changes in the North Atlantic sector (fig. 4.1d). This is not the case for summer; therefore we investigate only winter in this study. A preliminary analysis of the hydrological cycle gives indications that the precipitation changes are induced by a combination of (globally) warmer air temperatures, enhancing the hydrological cycle, and an effect due to shifted SST patterns and related changes in the atmospheric circulation (fig 4.6).

For a better understanding of the processes controlling the atmospheric response in this scenario we performed sensitivity experiments with the atmospheric component of the model. The aim of these experiments is to partition the atmospheric response to global warming into a part that arise from local SST changes in the North Atlantic, including, in particular, SST gradient changes in the Gulf Stream region from those caused by large-scale atmospheric changes, changed radiative forcings and (potentially) remote SST changes.

The rest of this chapter is structured as follows: In section 4.3 we describe the experiments used in this study, complemented by a short assesment of the model performance of MPI-ESM. Section 4.4 presents the results, separated into the atmospheric features in the coupled experiment and the response to the SST anomalies taken as forcing for the sensitivity runs with the AGCM. In section 4.5 we provide a summary and discussion of the results.

4.3 Models and methods

4.3.1 Coupled model experiments

First, we analyse a set of transient simulations with the Earth System Model of the Max-Planck-Institute for Meteorology, Hamburg (MPI-ESM) that were performed for CMIP5. The MPI-ESM consists of the ECHAM6 atmospheric model coupled to the MPIOM ocean model. The model horizontal spectral resolution is T63 (approx. 1.8° x 1.8°) with 47 vertical levels and a top at 0.01 hPa. ECHAM6 includes the land-surface model JSBACH to provide the lower-atmospheric boundary conditions over land. For the coupled runs ECHAM is combined with the MPI Ocean Model (MPIOM) with a resolution of GR15L40 (approx. 1.5° horizontal resolution, 40 vertical levels), using the OASIS 3 coupler. Giorgetta et al. (2013) give a detailed model description. The coupled runs consist of a historical run, covering the period from 1850 to 2005 and a subsequent projection extending up to 2300. The projection follows the IPCC RCP 8.5 scenario for atmospheric forcings (IPCC, 2013).

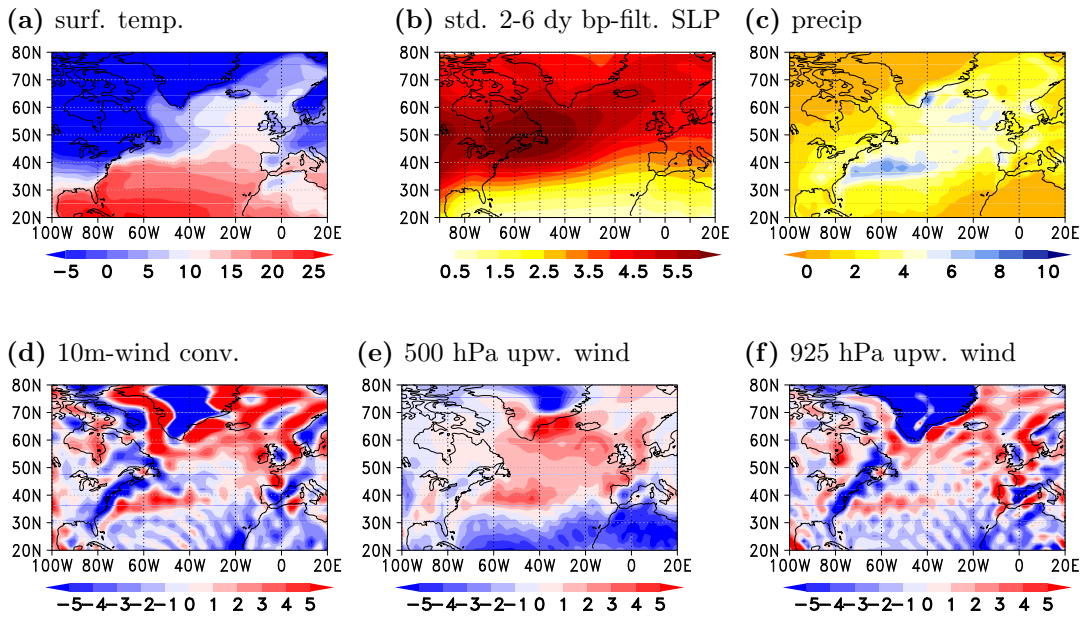

Figure 4.2: Winter-time (DJF) climatologies of different atmosperic quantities in the historical run. Surface temperature (a, i.e. SST over the oceans, in °C), standard deviation of 2-6 day bandpass-filtered SLP anomalies (b, in hPa), total precipitation (c, in mm/day), 10m-wind convergence (d, in 10^{-6} s^{-1}), and upward wind (in Pa/s) for 500 hPa (e) and 925 hPa (f).

Precipitation is parametrized in the model. For convective precipitation, ECHAM uses the Tiedtke (1989) mass flux scheme with modifications for penetrative convection according Nordeng (1994). The deep convection scheme uses a closure based on convective available potential energy (CAPE), while for shallow convection the closure is based on large-scale moisture convergence. Entrainment and detrainment rates for penetrative convection are also related to CAPE. For large scale precipitation, the model uses a stratiform cloud scheme, which is based on prognostic equations for the mixing ratios of the water phases, bulk cloud microphysics (Lohmann and Roeckner, 1996) and a statistical cloud cover scheme.

4.3.2 Coupled model performance in the North Atlantic region

The performance of MPI-ESM to reproduce ocean-atmosphere interaction in the NA sector is assessed by plotting climatolgies of key quantities from the historical run (fig. 4.2, averaged for DJF in the historical run from 1850 to 2005). As most recent coupled ocean-

atmosphere models, MPI-ESM has problems to reproduce a realistic Gulf Stream path (Jungclaus et al., 2013), which are reflected by the SST pattern (fig. 4.2a). Compared to observations, the separation of the Gulf Stream from the coast is dislocated slightly northward of the observed position. The northward turn at the Grand Banks is not simulated by the model and the path of the North Atlantic current is too zonal.

For the previous version of the model, a detailed analysis of the hydrological cycle has been performed (Hagemann et al., 2006). The relevant parametrizations are unchanged, and therefore these results are to large extend transferable to ECHAM6; the precipitation bias patterns are widely conserved in the newer model, but slight improvement has been made concerning the amplitude of the precipitation biases (Stevens et al., 2013). ECHAM overestimates global averaged precipitation compared to observations, particularly over the oceans. The strongest biases occur in the the tropics, while the model has a much better performance in the mid-latitudes. Particularly, the model reproduces the Gulf Stream precipitation band considerably well (fig. 4.2c). The precipitation band can be associated to low-level convergence (even though week, fig. 4.2d) and upward motion, penetrating deep into the atmosphere (figs. 4.2f & 4.2e), supporting the pressure adjustment mechanism (Minobe et al., 2008). The climatological storm track (fig. 4.2b) shows good agreement with the NCEP-NCAR reanalysis.

4.3.3 Sensitivity experiments

For the sensitivity experiment we use ECHAM6, the atmospheric component of MPI-ESM. The experiments are designed to decompose the atmospheric response into the component driven by local SST pattern changes in the North Atlantic (including the location and strength of the Gulf Stream SST front) and a part that covers all other relevant processes. The latter includes the direct response to changed radiative forcings as well as the response to remote SST changes outside the North Atlantic and the warmer North Atlantic SSTs, neglecting changes in the structure of the SST pattern (i.e. equivalent to a homogenous warming of the North Atlantic). The experiment consists of four runs. The winter-time patterns of absolute SSTs taken as forcing for these runs and the SST anomalies (with respect to the control run) are shown in fig. 4.3. For the complete global forcing fields see supplementary fig. A.15.)

The setup of the four individual runs is as follows: The 60-year control run (CTL) uses averaged radiative forcings and monthly climatologies of the SST from the period 1850 to 2005 in the historical coupled run (fig. 4.3a). The second run (FULL) is also 60 years long, but uses atmospheric forcings and SST boundary conditions from the coupled RCP

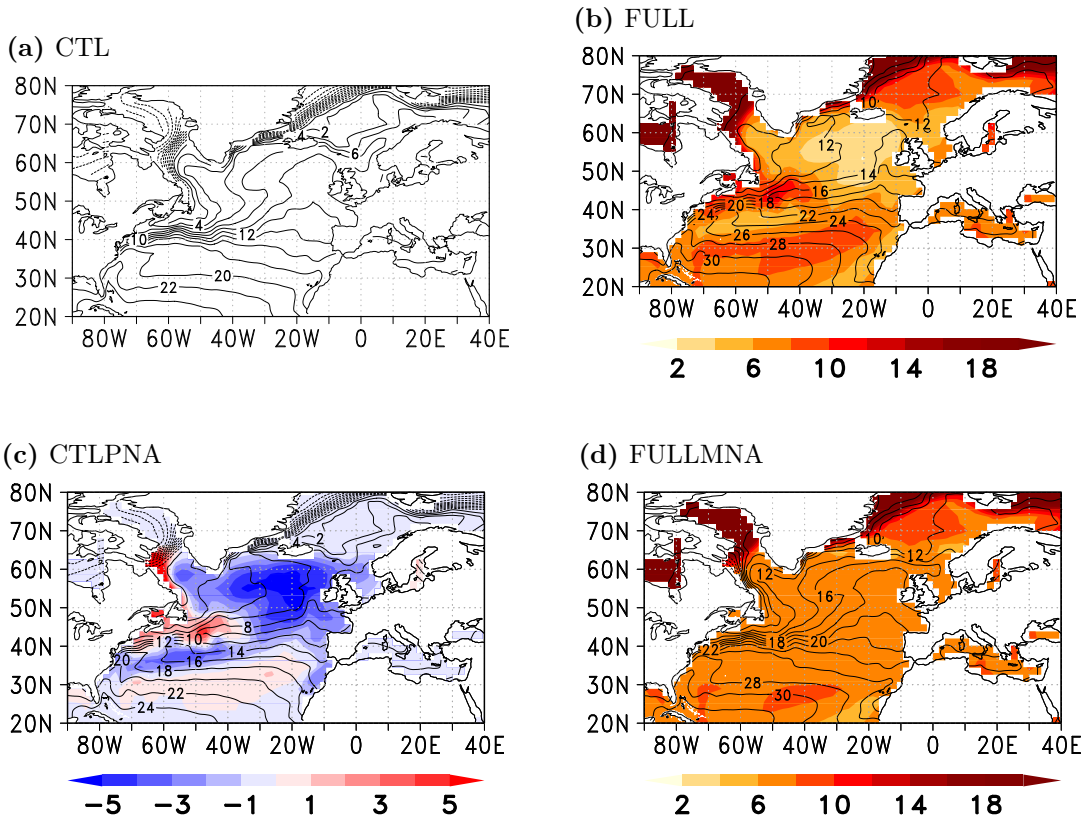

Figure 4.3: Winter-time SST forcing for the sensitivity experiment. The contours show absolute SSTs (in °C) for each run, averaged for the winter months (DJF). In panels (b) to (d) he shadings are the SST anomaly (in K) with respect to CTL.

8.5 scenario projection, averaged for the period from 2200 to 2300 (fig. 4.3b).

The third and fourth run are each 30 years long and except in the North Atlantic region (25°N to 31°N and 60°N to 66°N) they are identical in all other aspects to CTL and FULL, respectively. The third run (CTLPNA) assess the impact of only the changes in the SST pattern in FULL excluding homogenous global warming: The North Atlantic SST is identical to FULL minut the global mean change between 2200-2300 and 1850-2005, elsewhere the SST is from CTL (fig. 4.3c). These SST changes likely represent the first order the effect of ocean circulation changes in the North Atlantic on SST. The pattern shows a relative cooling of the North Atlantic, likely as a result of a AMOC slowdown by approximately 50% in the coupled experiment (Fischer, M., pers. communication). Furthermore it includes a relative cooling of the southern side of the historical Gulf Stream region and a relative warming north of it, likely as a result of a northward shift of the Gulf Stream axis in the coupled experiment. However, it should be considered that other processes, such as surface heat fluxes, may contribute to the SST pattern.
The fourth run (FULLMNA) assess the impact of global warming minus the changes in SST patterns in the North Atlantic. The SST anomaly in the North Atlantic equals the global mean change between 1850-2005 and 2200-2300. Outside the North Atlantic the SST is identical to FULL (fig. 4.3d).

The anomalous SST pattern added in CTLPNA (subtracted in FULLMNA) was modified to avoid artificial gradients at the northern and southern boundary. Therefore, the anomaly was multiplied by a weighting factor, increasing linearly from 0 to 1 in 6°-wide latitude bands at the northern and southern edge of the SST anomaly regions (i.e. 25°N to 31°N and 60°N to 66°N) before adding (subtracting) it. For all sensitivity runs, we assumed a spin-up time for the atmospheric model of 5 years, and thus limited our analysis to the last 55/25 years of the runs, as appropriate. For all runs, the sea ice forcing was generated, by assuming all regions to be ice-covered (ice-free) where the SST is colder (warmer) than -1.8°C.

4.4 Results

4.4.1 Local simulated response in the coupled model

For the period from 2050 to 2100 the temperature and precipitation responses to the RCP 8.5 scenario simulated by MPI-ESM are in good agreement with the CMIP5 multi-model ensemble mean. For the far future (2200 to 2300, fig. 4.4) the shape of the patterns remain the same, but the amplitude of the signal is strongly enhanced. The pattern correlation

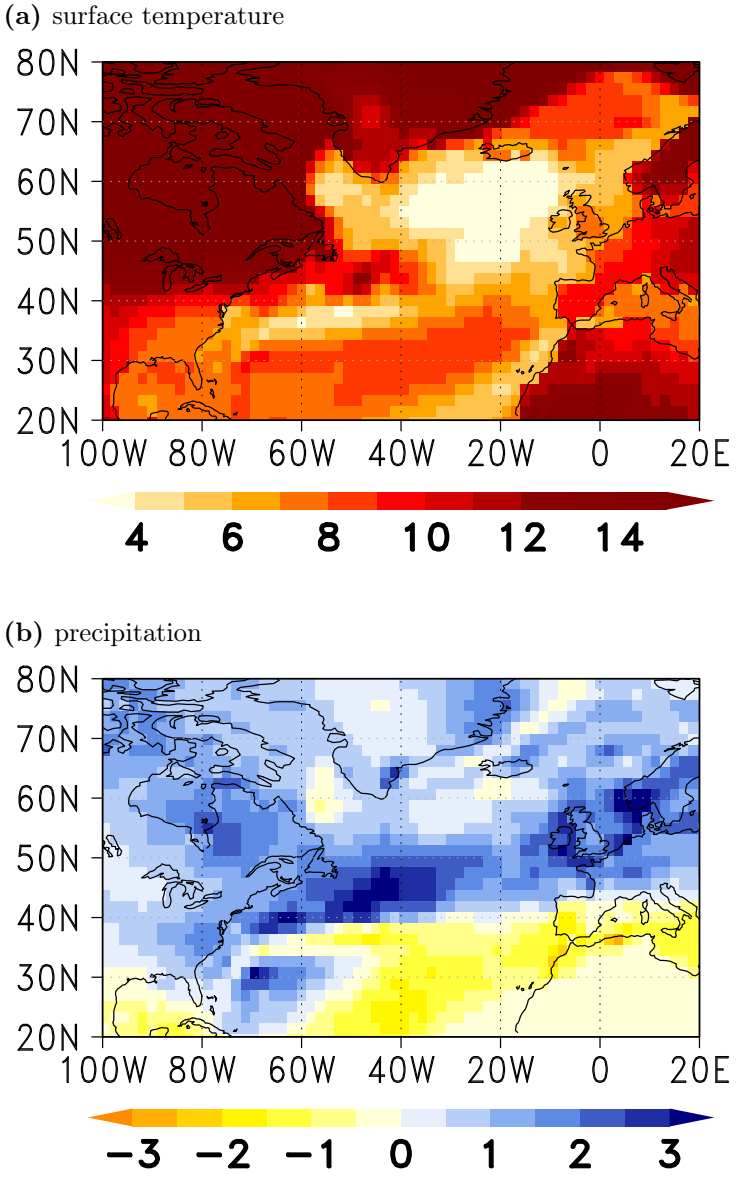

Figure 4.4: Winter-time surface temperature response (a, in K) and precipitation response (b, in mm/day) to the RCP 8.5 scenario in MPI-ESM. Climatological differences between the periods from 2200 to 2300 and 1850 to 2005.

between the two periods is 0.96 for surface temperature and 0.88 for precipitation. The signal is dominated by a strong warming over the entire North Atlantic, but the pattern shows distinct regional differences. In agreement with the CMIP5 ensemble mean, MPI-ESM shows a local minimum of the warming in the north east North Atlantic and a local maximum in the region of the Grand Banks. In MPI-ESM the latter maximum is flanked to the south by a zonally oriented band of only moderate warming.

In the historical simulation the strongest meridional gradients in surface temperature are located at the Gulf Stream front (fig. 4.5a). The most prominent feature of the projected future changes of the SST gradient, is a weakening of the SST gradient in the region of the historical Gulf Stream front (figs. 4.5b & 4.5c). However, this region remains the region with the strongest meridional SST gradients in the future projection, albeit values are reduced by up to 50% with respect to the historical run (fig. 4.5c). North of the area with reduced gradients we find a region with enhanced gradients east of Newfoundland. Both, surface temperature changes and gradient changes are much more pronounced in winter, than in summer (not shown). It is likely that large-scale changes in the ocean circulation drive the SST changes (Drijfhout et al., 2012). The wind-driven part of the ocean circulation underlies key changes in the coupled run and the boundary between the subtropical and subpolar gyre is shifted northward, while the strength of the AMOC is decreased by approximately 50% (Fischer, M., pers. communication). These changes are consistent with the modeled banded structure in the temperature pattern in the Gulf Stream region and the weaker warming of the North East Atlantic. However, part of the pattern may be driven by changed heat fluxes from the atmosphere into the ocean.

The precipitation response (fig. 4.4b) consists of a zonally banded dipole structure with heavily enhanced precipitation south and south-east of Newfoundland, flanked by a region on the southern side of the historical Gulf Stream SST front, that becomes dryer. The drying is contrary to the usual expectation that wet regions are will become wetter and dry regions drier in a warmer climate (IPCC, 2013; Held and Soden, 2006). This indicates that the precipitation changes are not exclusively related to a higher moisture content of the atmosphere due to the warming, but there must also be changes in the atmospheric circulation. The north east of the North Atlantic shows a slight drying, while Europe becomes wetter.

A relatively simple relation for the response of the hydrological cycle to global warming can be obtained if the circulation is assumed not to change, then the response of the water vapour transport may scale with the lower tropospheric water vapour mixing ratio. As

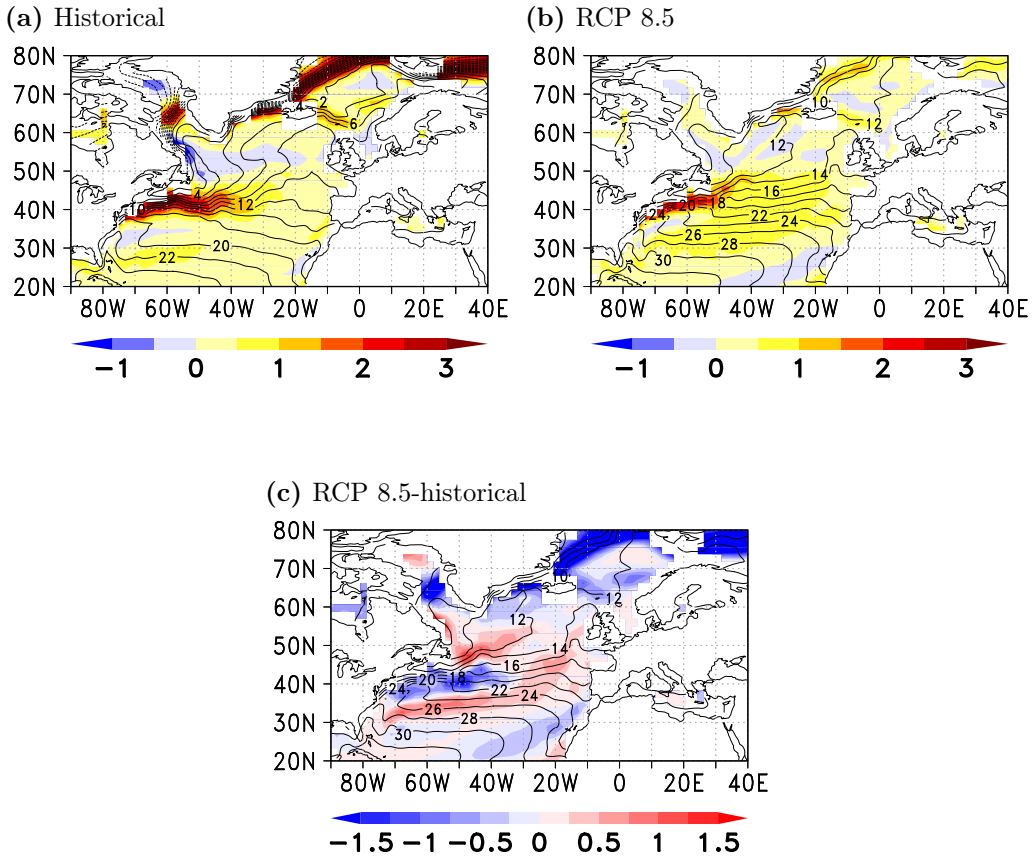

Figure 4.5: Winter-time (DJF) response of the meridional SST gradient (in K/100km, positive values indicate a southward increase of SST) to the RCP 8.5 scenario in the transient runs, averaged for the periods from 1850 to 2005 in the historical run (a) and from 2200 to 2300 in the RCP 8.5 scenario run (b) and difference between the two periods (c). Underlying contours show the climatological seasonal mean SSTs for the according period from the historical run (a) and for the period from 2200 to 2300 in the RCP 8.5 scenario run (b & c).

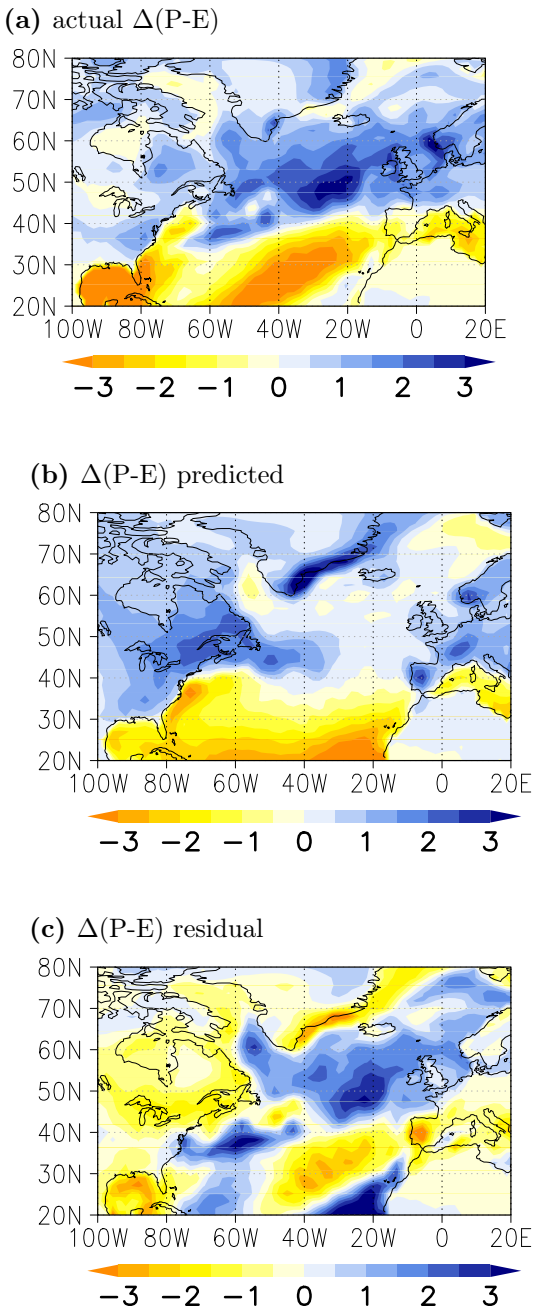

Figure 4.6: Precipitation minus evaporation change (in mm/d) in the RCP 8.5 scenario run (2200 to 2300) with respect to the historical run (1850 to 2005): Actual P-E change in the model (a), P-E change as predicted after Held and Soden (2006) (b) and the difference between these two (c).

the P-E equals the divergence of water vapour transport, we may expect it to also scale following the Clausius-Clapeyron scaling (Held and Soden, 2006). The model simulates an increase in P-E over the extra-tropical NA and reduction over the subtropics 4.6a. The P-E predicted assuming a fixed circulation and CC scaling only partly reproduces the pattern 4.6b. In particular, the model shows far greater P-E changes over over extra-tropical NA and dipole like changes over the GS region. These differences provide further indications that the precipitation changes also result from atmospheric circulation does changes that may partly relate to the underlying SST pattern.

4.4.2 Sensitivity experiments to assess the impact of local SST changes in the North Atlantic sector

Our hypothesis is, that the dynamical changes, suggested by the analysis in the previous section, can be linked to local SST pattern changes in the North Atlantic. We perform experiments with the atmospheric model component to isolate the impact of the SST changes; a detailed description of the experimental setup is given in section 4.3. We start with a description of the precipitation response in the individual runs, and additionally provide some figures investigating the atmospheric circulation related to it.

Figs. 4.7a to 4.7b show the winter-time seasonal mean precipitation response in the sensitivity experiments with respect to the control experiment (CTL). First, we started to compare FULL, a run performed with climatological forcings from the future scenario coupled run, to CTL, forced with the climatological conditions from the historical run. The idea of this experiment is, to verify that it is possible to reproduce the main features of the precipitation response in the coupled run with climatological forcings and an atmosphere-only setup. Indeed, in terms of total precipitation, FULL reproduces the winter-time precipitation changes from the coupled transient experiment well (Figs. 4.4b and 4.7a). The strongest precipitation increase in the experiment with the full future conditions (FULL) occurs southeast of Newfoundland, where the northward shifted Gulf Stream causes a strong SST warming (fig. 4.3b) and strongly enhanced meridional SST gradients. In the region of the southern flank of the historical Gulf Stream front (approx. 33°N to 39°N and 70°W to 40°W) precipitation decreases, even though SSTs are slightly increased. Also, as described in the previous section, this is a region where we find wet conditions in present-day climate. Therefore these precipitation changes are likely due to the changes in the SST gradient.

Now, we separate the SST forcing into a mean warming and local pattern changes in the

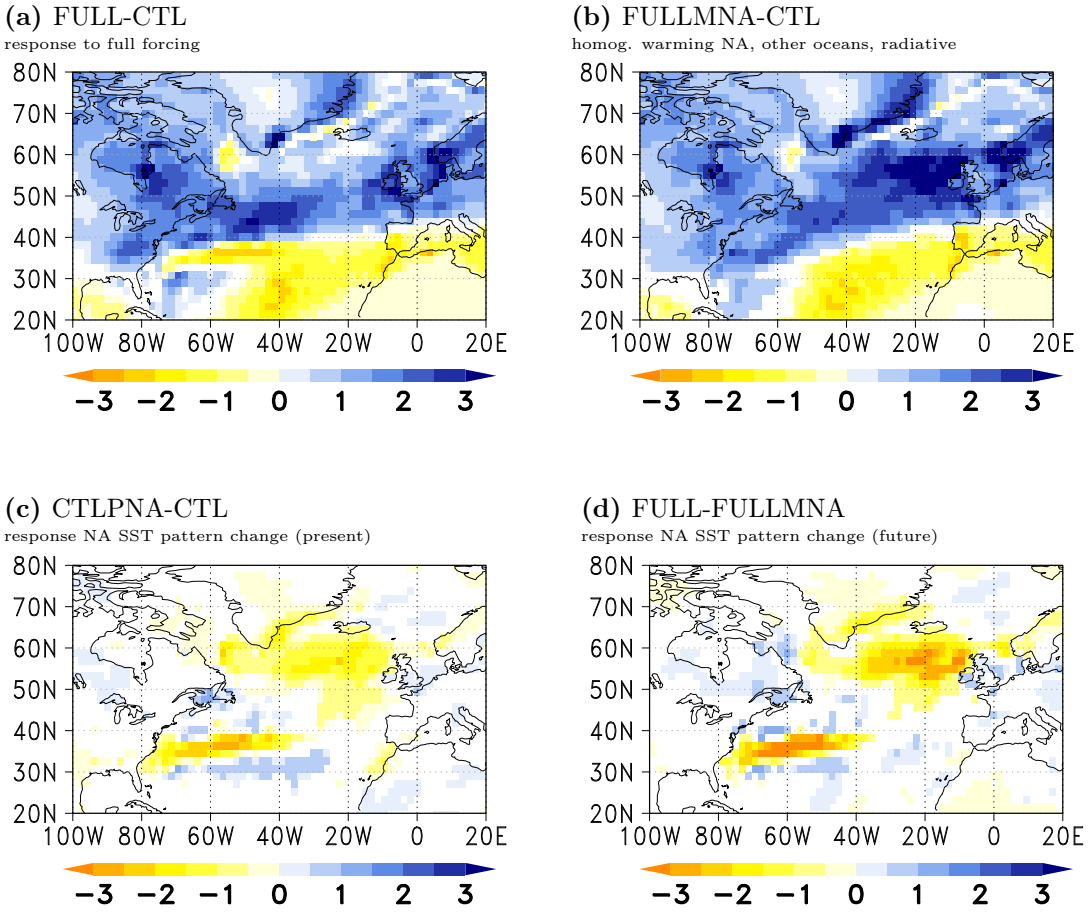

Figure 4.7: Winter-time total precipitation response (in mm/day) in the sensitivity experiment. Plottd are climatological differences in FULL (a), CTLPNA (b) and FULLMNA (c) with respect to CTL and climatological difference of FULL with respect to FULLMNA (d). Non-significant values (based on a bootstrapping test at a confidence level of 95%) are masked.

North Atlantic: In the FULLMNA experiment we consider the effects resulting from a homogenous warming of the North Atlantic (conserving the shape SST of the local SST pattern, but adding a constant temperature offset), changed radiative forcings and remote SST changes outside the North Atlantic (fig. 4.3d). FULLMNA reproduces the gross changes in precipitation across the North Atlantic, with a wetter extra-tropics and drier subtropics (fig. 4.7b). However, there are key differences to the FULL response. These include stronger precipitation changes west of the British Isles (fig. 4.7b). Furthermore, the structure of the local response pattern in the Gulf Stream region, particularly the drying found in the coupled experiment and in FULL, is not reproduced in this experiment.

In contrast, the experiment with local pattern changes (CTLPNA, fig. 4.7c) reproduces this drying. This supports our hypothesis that this feature is primarly driven by local SST gradient changes. Furthermore, we find an extended drying of the north eastern Atlantic basin (fig. 4.7c), where the absolute SST shows a distinct cooling that is likely a result of the MOC slowdown. In this case, we assume the absolute SST to be the driving factor for the precipitation change.

For analysis of the linearity of the response and to investigate the effects from a changed atmospheric background state due to changed radiative forcings, we also included a comparison between FULL and FULLMNA (fig. 4.7d). The patterns shows high similarity to that from CTLPNA minus CTL (fig. 4.7c), except that the same SST gradient change causes an enhanced amplitude of the pattern in a warmer background state.

To better understand the processes causing the precipitation response, we split the response into convective (fig. 4.8a & 4.8b) and large scale (fig. 4.8c & 4.8d) components, as distinguished by the model. For the response to the homogenous warming both components contribute almost equally to the total precipitation response (figs. 4.8a & 4.8c). In contrast, the precipitation response to the local SST pattern changes mainly result from the large-scale component (figs. 4.8b & 4.8d). This is contrary to Hand et al. (2014), where evidence was found that convective precipitation is much more sensitive to extra-tropical SSTs, particularly in the Gulf Stream region. However, when concerning the basin-wide precipitation response to the ocean warming, the convective precipitation also contributes. (fig. 4.8a).

The local response to the SST pattern change in the Gulf Stream region is associated with a zonally orientated dipole structure in the the low-level wind convergence (fig. 4.9b) and the vertical wind field (figs. 4.9d & 4.9f). The low-level convergence and the vertical motion

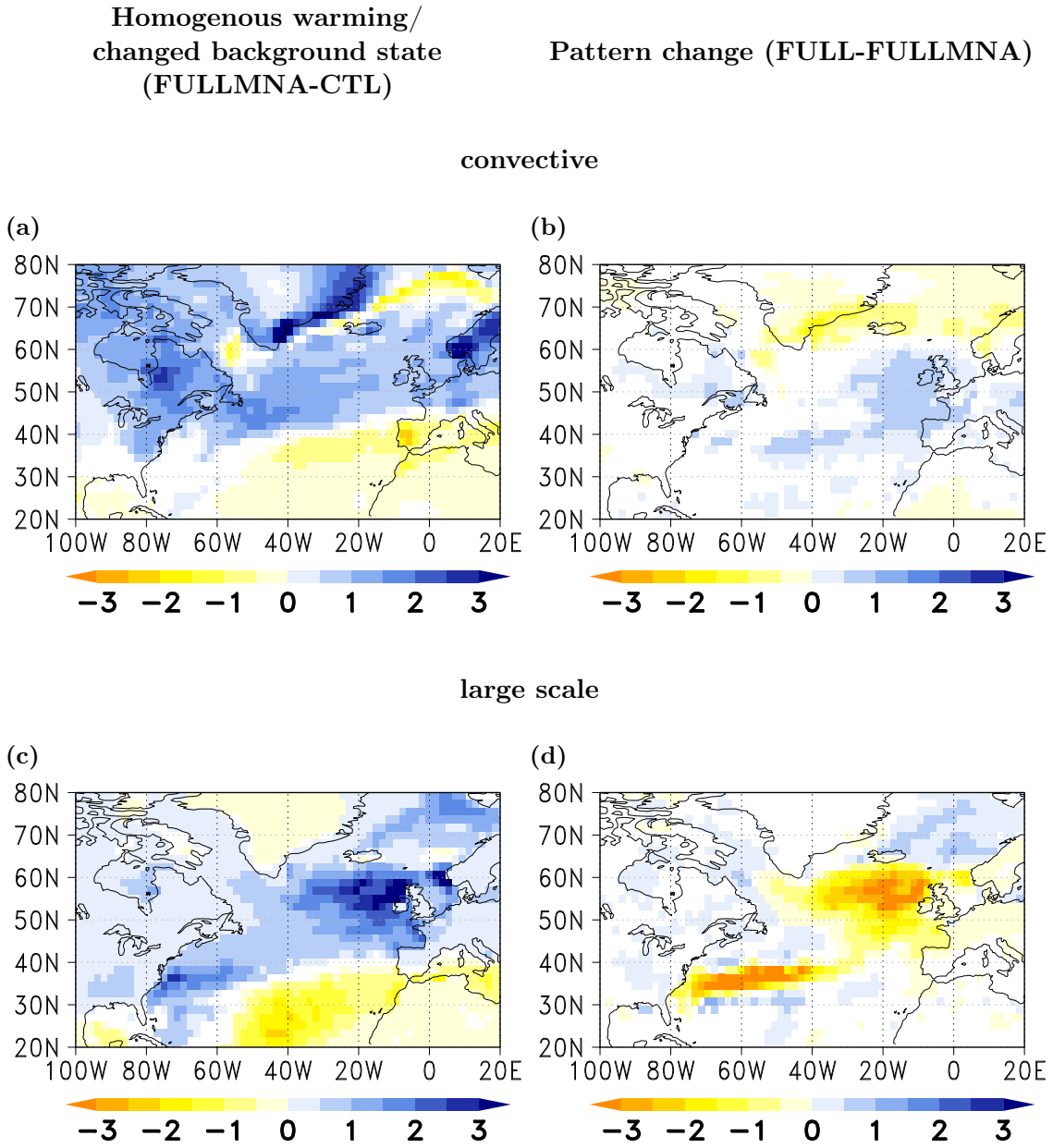

Figure 4.8: Convective and large scale precipitation response (in mm/day) in the sensitivity experiment. Climatological differences between FULLMNA and CTL (left, i.e the impact of homogenous warming and the changed background state) and between FULL and FULLMNA (right, i.e. the effect of local SST pattern changes) for convective (top) and large-scale precipitation (bottom). Non-significant values (based on a bootstrapping test at the 95% confidence level) are masked.

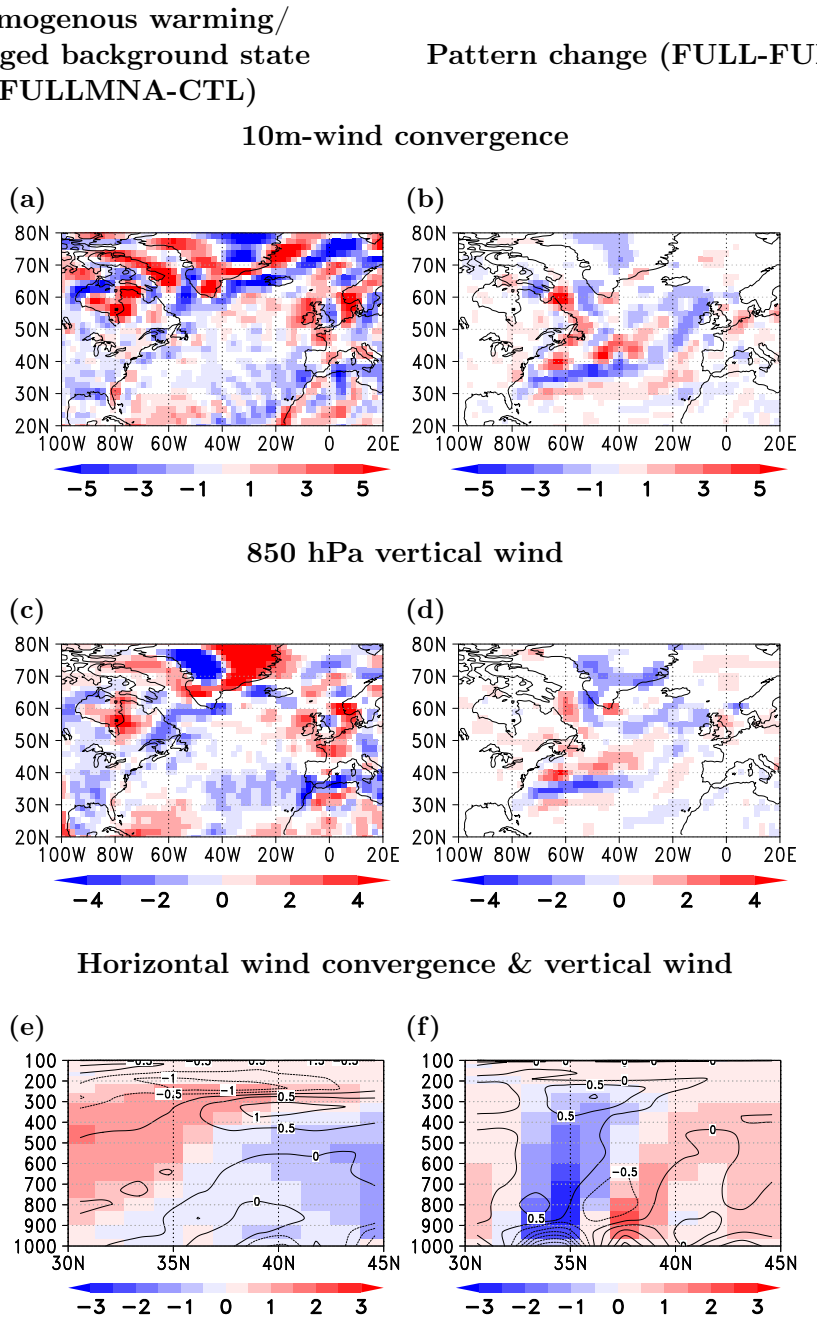

Figure 4.9: Winter-time response of the 10m-wind convergence (top, in 10^{-6} s^{-1}), the vertical wind at 850hPa (middle, in Pa/s, red denotes a strengthening of the upward direction) and vertical cross sections (bottom) of the vertical wind response (in Pa/s, red denotes a strengthening of the upward direction) and the horizontal wind convergence (contours, in 10^{-6} s^{-1}) zonally averaged between 65°W and 50°W. As before, the left column shows the response to homogenous warming and the changed background state and the right column the response to local SST pattern changes. In subfigures a to d non-significant values (based on a bootstrapping test at the 95% confidence level) are masked.

is intensified in the north, and weakened south of the position of the historical SST front. This pattern is consistent to the structure of the SST gradient changes in this region, as well as with the precipitation changes. For the case with the homogenous warming (figs. 4.9a, 4.9c & 4.9e) these changes are absent.

4.4.3 Response of the North Atlantic storm track and large-scale response

The large-scale response in the coupled model shows a wave number two response in the high latitudes while a wave number one pattern dominates in the mid-latitudes (fig. 4.10a). These changes are mainly caused by remote SST changes and uniform warming (fig. 4.10b).

The region with the strongest storm track change is located on the south eastern flank of the storm track's climatological position (fig. 4.11a), consistent with the findings from Woollings et al. (2012). The cyclones are usually associated with atmospheric cold and warm fronts on their southern side, that cause the major part of precipitation in this region (Catto et al., 2012). The precipitation changes west of the British Isles therefore are likely linked to the enhanced storm track slightly north this region. The sensitivity experiments indicate that these changes are mainly associated with uniform warming and the direct atmospheric response to the changed radiative forcings (figs. 4.10b, 4.11b, 4.12a & 4.12c). In contrary, the storm track changes east of Newfoundland are consistent with being driven by changes of the local SST gradients, by changes in the stability of the low-level atmosphere (fig. 4.12b) and low-level baroclinicity (fig. 4.12d). However, these changes are weak compared to the climatological values and the changes in the eastern part of the North Atlantic.

4.5 Summary and Discussion

Analysis of the coupled MPI-ESM experiment forced with the RCP 8.5 scenario shows a band of intensified winter-time precipitation crossing the North Atlantic from the region south of Newfoundland towards the British Isles. This band is flanked to the south by a region becoming drier. This region corresponds to the southern flank of the historical Gulf Stream extension SST front. This pattern is a robust feature of the CMIP5 multi-model ensemble mean (IPCC, 2013, ch.12). The sensitivity experiments driven by climatological boundary conditions from the coupled experiments can reproduce the precipitation climatology from the coupled experiment quite well. This demonstrates the importance of the boundary conditions in driving the precipitation changes.

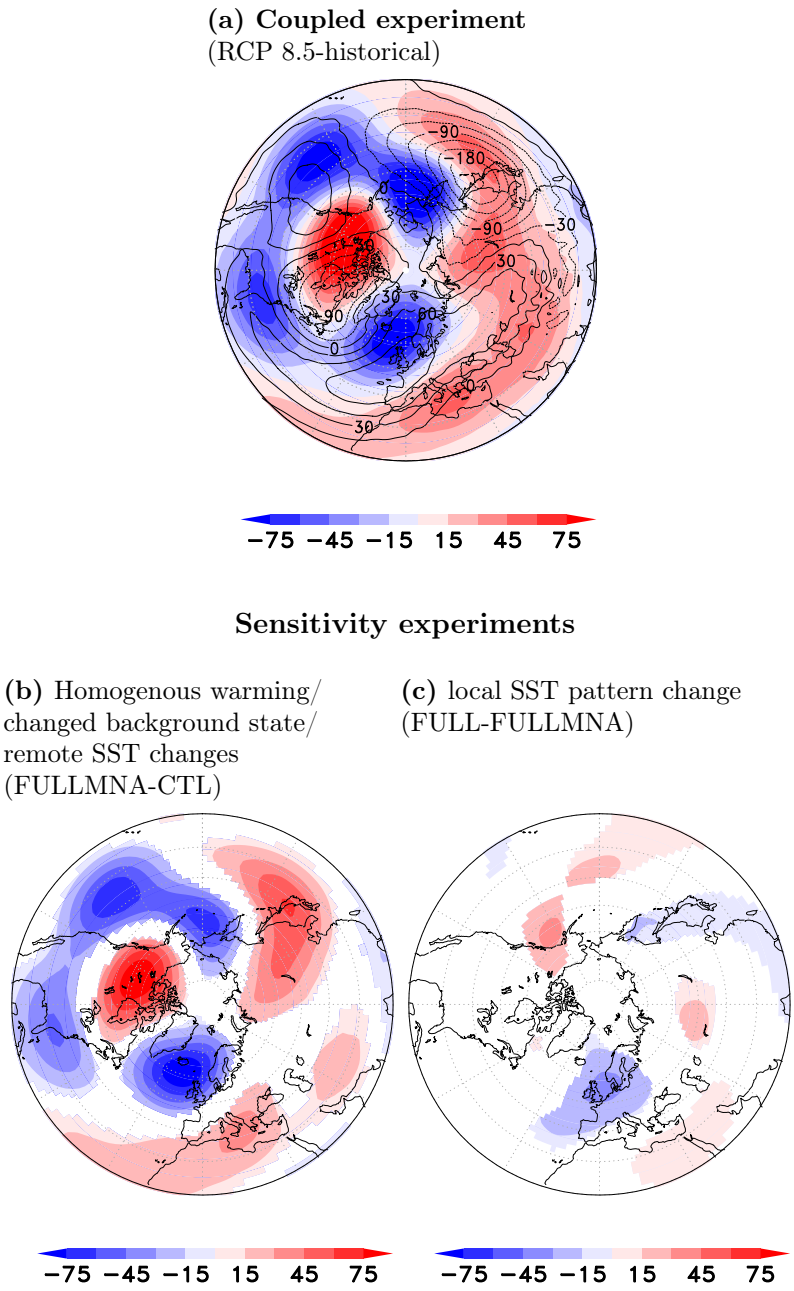

Figure 4.10: Stationary wave response, as indicated by the climatological winter-time 500 hPa geopotential height anomalies (in m) with the zonal mean response removed. Differences between (a) the RCP 8.5 coupled run (averaged for the period 2200 to 2300) and the historical run (averaged for the period 1850 to 2005), (b) between FULLMNA and CTL (i.e the impact of homogenous warming, changed radiative forcings and remote SST changes) and (c) between FULL and FULLMNA (i.e. the effect of local SST pattern changes). In (a) the contours show the climatological values from the historical run, in (b) and (c) non-significant values (based on a bootstrapping test at the 95% confidence level) are masked out.

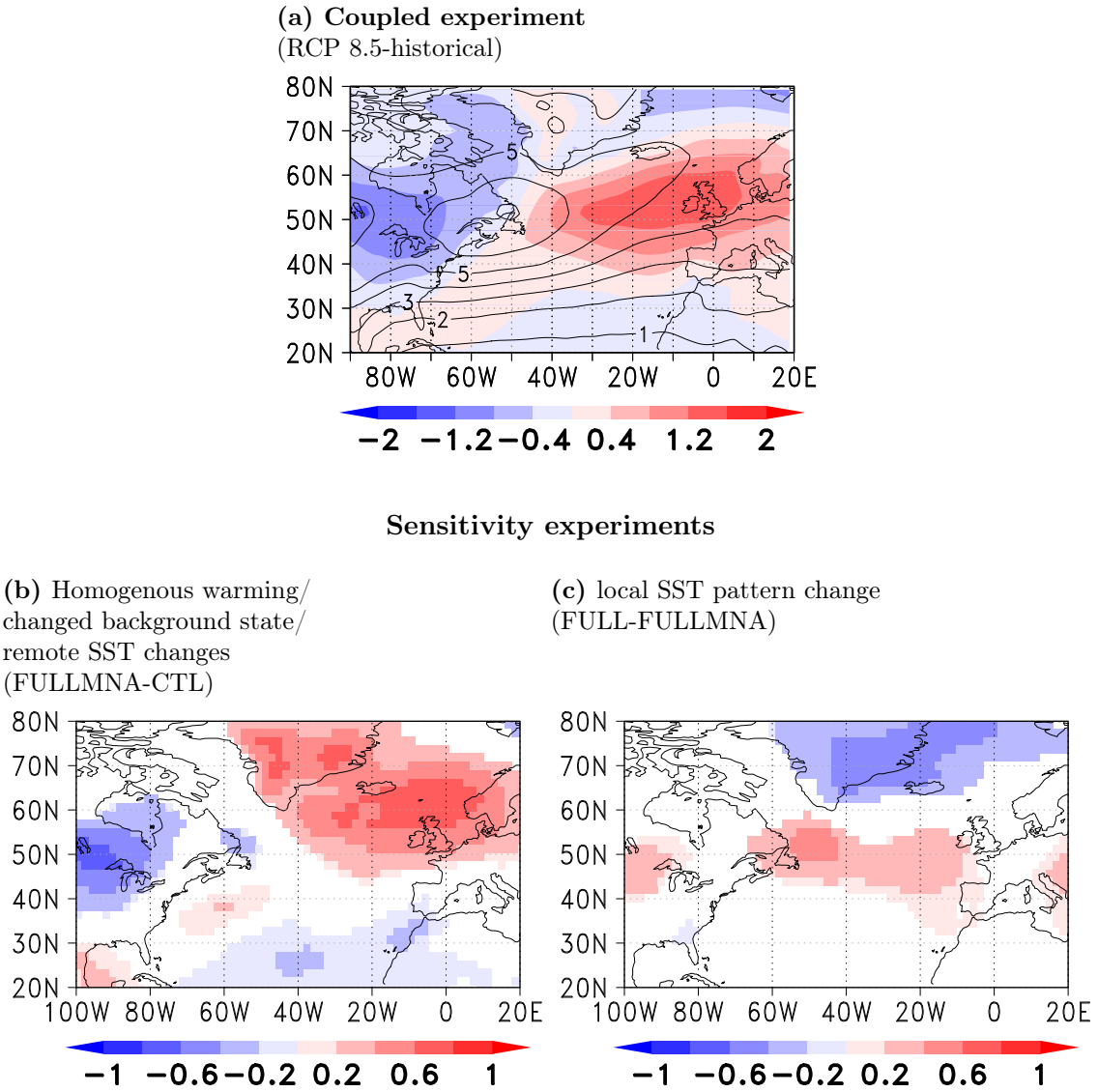

Figure 4.11: Climatological winter-time storm track response as indicated by the 2-6 day bandpass-filtered anomalies of sea level pressure (in hPa). Differences between (a) the RCP 8.5 coupled run (averaged for the period 2200 to 2300) and the historical run (averaged and averaged for the period 1850 to 2005), (b) between FULLMNA and CTL (i.e the impact of homogenous warming, changed radiative forcings and remote SST changes) and (c) between FULL and FULLMNA (i.e. the effect of local SST pattern changes). In (a) the contours show the climatological values from the historical run, in (b) and (c) non-significant values (based on a bootstrapping test at the 95% confidence level) are masked out.

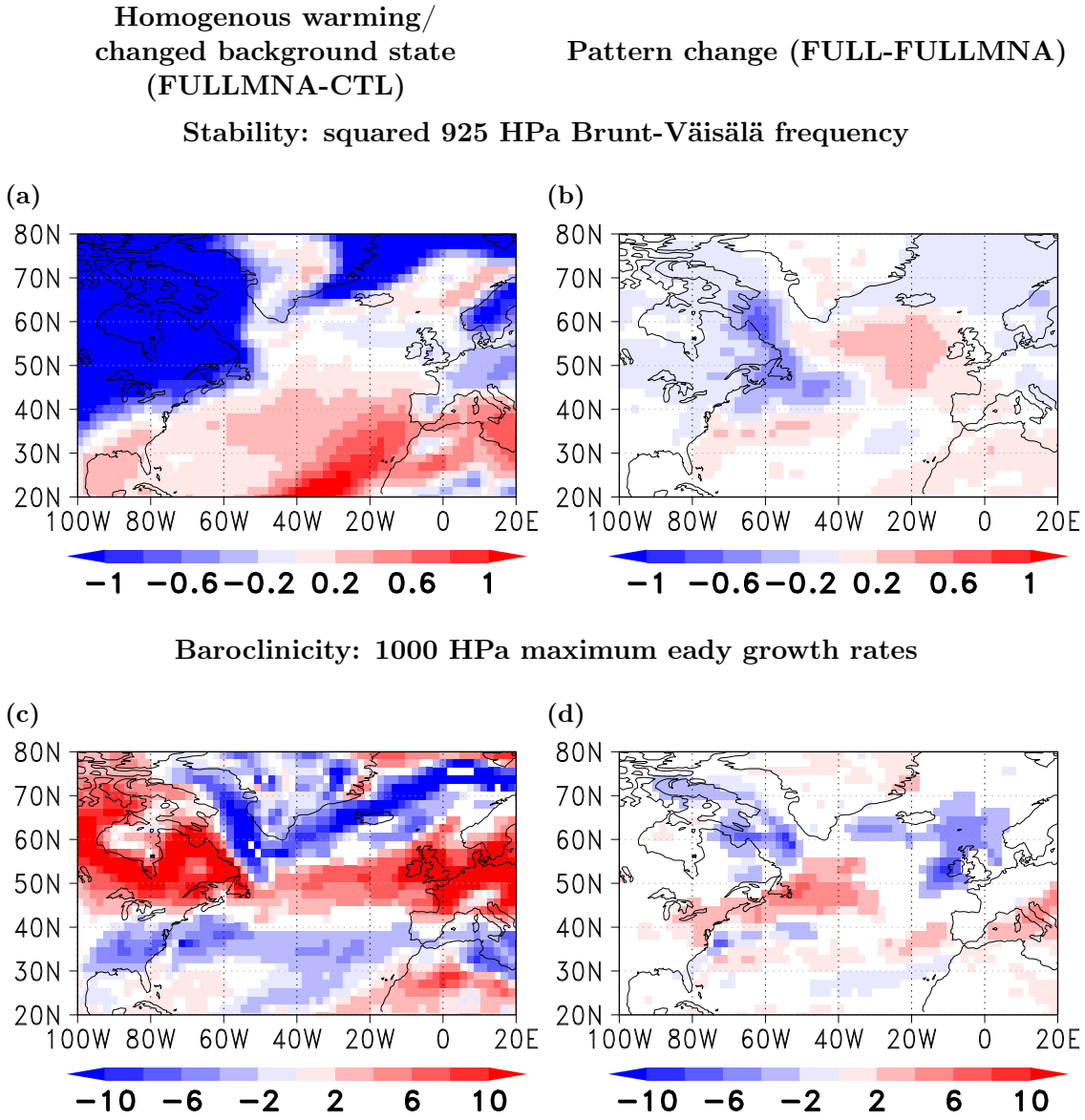

Figure 4.12: Large-scale response in the sensitivity experiment. Climatological differences between FULLMNA and CTL (left, i.e the impact of homogenous warming and the changed background state) and between FULL and FULLMNA (right, i.e. the effect of local SST pattern changes) for the vertical stability of the atmospere indicated by the squared Brunt-Väisälä frequency (top, in 10^{-2} s^{-1}) and the low-level baroclinicity, indicated by the maximum eady growth rates (in 10^{6} s^{-1}, bottom). Non-significant values (based on a bootstrapping test at the 95% confidence level) are masked.

Our sensitivity experiments show that local SST pattern changes in the North Atlantic shape the winter-time precipitation changes locally. In agreement with observations, the Gulf Stream region shows strong precipitation when forcing the model with historical conditions. A warming of the region therefore in principle would lead to enhanced rainfall. In contrast forcing the model with future SSTs locally causes a decrease in precipitation, even though the absolute value of SST is enhanced. This indicates that in ECHAM6 the local precipitation changes in the Gulf Stream region are mainly controlled by weakened local SST gradients rather than by absolute SST.

When only adding local SST pattern changes to the historical climate background state we indeed get a pronounced local response pattern that is capable to explain this initially unexpected local drying over warmer SSTs. The amplitude of this pattern is enhanced when prescribing the same local SST anomalies in a warmer background climate, while the shape of the pattern is highly robust. The local precipitation changes in the Gulf Stream region are mainly driven by changes in large-scale precipitation. In contrast, the precipitation response outside the Gulf Stream region has contribtions from both precipitation types, that are related to the large-scale SST warming of the North Atlantic, remote SST changes and the changes in the radiative forcings.

The mechanism behind the local precipitation changes is consistent with previous experiments (Minobe et al., 2008; Hand et al., 2014). The enhanced precipitation goes along with enhanced low-level convergence and upward motion. However, our sensitivity experiment indicates that the response to local SST gradient changes only has a very localized impact on the atmosphere. Even though we found a significant impact on local baroclinicity and the static stability of the atmosphere, the changes in storm track activity and the large-scale atmospheric circulation found in the coupled experiment are dominated by the response to changes in the atmospheric background state and large-scale SST warming. These also explain the precipitation changes in the eastern North Atlantic. In this context, it might be a limitation that our experiments were performed at relatively coarse resolution. Particulary the reproduction of a realistic storm track is expected to benefit from higher horizontal resolution and therefore the response may change when moving to a finer grid.

Finally, it has to be considered that as most recent ocean models, MPI-ESM is not able to reproduce a fully realistic Gulf Stream path in present-day climate. An extended cold SST bias in the North Atlantic is the consequence of a too zonal North Atlantic current. This problem occurs across most of the IPPC models and affects the exact localization of

the related atmospheric patterns. Even though MPI-ESM reproduces the main features of the North Atlantic sector climate quite well, our study therefore should be seen more as an evaluation of the sensitivity of the atmosphere to changes in certain regions, rather than as a completely realistic simulation of present-day and future states of the coupled ocean-atmosphere system.

Acknowledgements

I would like to thank Jürgen Bader and Felix Bunzel for help with setting up the model runs and Matthias Fischer for inspiring discussion.

5 Summary & Conclusion

We have shown that current climate models are able to reproduce the observed climatological response to mid-latitude SST fronts quite well. The first issue analysed in this thesis is the sensitivity of the climatological atmospheric mean state in the North Atlantic sector to model resolution. Therefore, three-member ensemble simulations with ECHAM5 were analysed. The model runs cover a range of different horizontal and vertical resolutions (i.e. T31L19, T42L19, T63L31, T106L31 and T213L31) and were all forced by NOAA-OI SSTs for a period of 28 years. Precipitation showed a relative high sensitivity to model resolution. The convective part of the precipitation in general shows a tendency to decrease with enhanced resolution. This effect is partly compensated by an increase in large-scale precipitation, especially in winter. The other quantities which were analysed during this work show clearly less sensitivity to resolution than precipitation does. This indicates, that the resolution dependency found for precipitation is a matter of how precipitation is parametrised in the model. In general, our analysis suggests that in terms of climatological patterns, enhancement of resolution beyond intermediate resolution (T63L31) brings less benefit, than enhancement from low to intermediate resolution (i.e. enhancement from T31L19 to T63L31). However, for a representation of localized structures and for a highly realistic representation of the North Atlantic storm track, high resolution is favorable.

Analysis of a transient ensemble run with ECHAM5 at intermediate resolution (i.e. T106) showed that local SSTs and local convective precipitation show a high correlation on multi-annual time scales in the Gulf Stream area. An analysis of variance indicates that this correlation is caused by the boundary conditions. These results motivated a sensitivity study with a local warm SST anomaly to prove that it is local SST that drives precipitation variability in this region. Concerning the response to this SST anomaly, our experiments show a consistent behaviour. For both, winter and summer season, local warm SST anomalies cause a plausible enhancement of local precipitation. In summer the atmosphere responds to SST anomalies consistent to the mechanism described in Minobe et al. (2008). In our sensitivity experiment this precipitation signal is confined to the region of the SST anomaly and mainly increases convective precipitation, which appears much more sensitive to local SST variation than large scale precipitation. The signal goes along with a

convective-like signal with low-level wind convergence and upward winds penetrating into higher tropospheric levels and a local minimum in SLP. In winter, the mechanism is not as clear as in summer, but our analysis gives an indication that the winter signal is connected to a higher moisture loading of atmospheric fronts. Especially cold fronts seem to play an important role. Even though we did not find evidence that the frequency of atmospheric front activity changes over a warmer Gulf Stream area, enhanced evaporation seems to be an important factor controlling the precipitation signal. In contrast to summer, we found indications for a large scale impact of Gulf Stream SST anomalies in winter: The 500 hPa geopotential height anomalies show indication for a significant circumpolar wave pattern in the northern hemisphere.

The last part of the work investigates the atmospheric response to shifts in the SST pattern in a RCP 8.5 scenario run. This includes a set of sensitivity experiments using the SST patterns from the coupled MPI-ESM run, to assess the impact of local ocean-atmosphere interaction in shaping the response to global warming. These runs were performed with the atmospheric component of MPI-ESM at T63L47 resolution, which is a common set up for contemporary Earth System Models when performing multi-decadal to centennial climate projections. The main question to be addressed in this context, was how far it is possible to separate the effects of SST front shifts found in the ESM run from the effect of a generally warmer ocean-atmosphere system due to the direct radiative effect of the greenhouse gas forcing. Therefore we deconstructed the SST signal from the coupled run into a mean warming part and a local pattern change. The atmospheric component of the model was forced with these separated SST anomalies as well as with the full (combined) signal. The run with the full forcing reproduced the precipitation pattern of the coupled run sufficiently. The run considering changes of the SST gradient only, shows a precipitation response that includes a decrease in precipitation in regions where the SST gradient is weakened and vice versa. Even though looking at winter season here, the mechanism seems to be consistent to Minobe's pressure adjustment mechanism with low-level convergence and upward motion over regions with strong SST gradients. Furthermore, there is a slight increase in local low-level baroclinicity. However, the atmospheric response to local SST pattern changes is week beyond the local scale. The large-scale atmospheric response in the RCP 8.4 run, in contrast, is dominated by features, that are well reproduced by the run neglecting the local SST pattern changes (FULLMNA). In particular, these run show an intensification of the North Atlantic storm track, higher evaporation connected to the increased SSTs and, as a result, heavily enhanced precipitation in the North Atlantic sector. Our experiments therefore indicate that these features are only little influenced by the local SST patterns in the Gulf Stream region, but are mainly caused by large-scales SST warming, changes

in the radiative forcing, and remote SST changes. In this context, a response of the large-scale circulation over the extra-tropical North Atlantic to tropical SST, as investigated in ongoing studies (Nour-Eddine Omrani, personal communication), potentially has an impact. As chapter 2 shows, the representation of the storm track benefits from very high model resolutions. Therefore it is possible that interactions between the SST front and the storm track at higher model resolution might get relavant for the large-scale atmospheric response.

Appendix

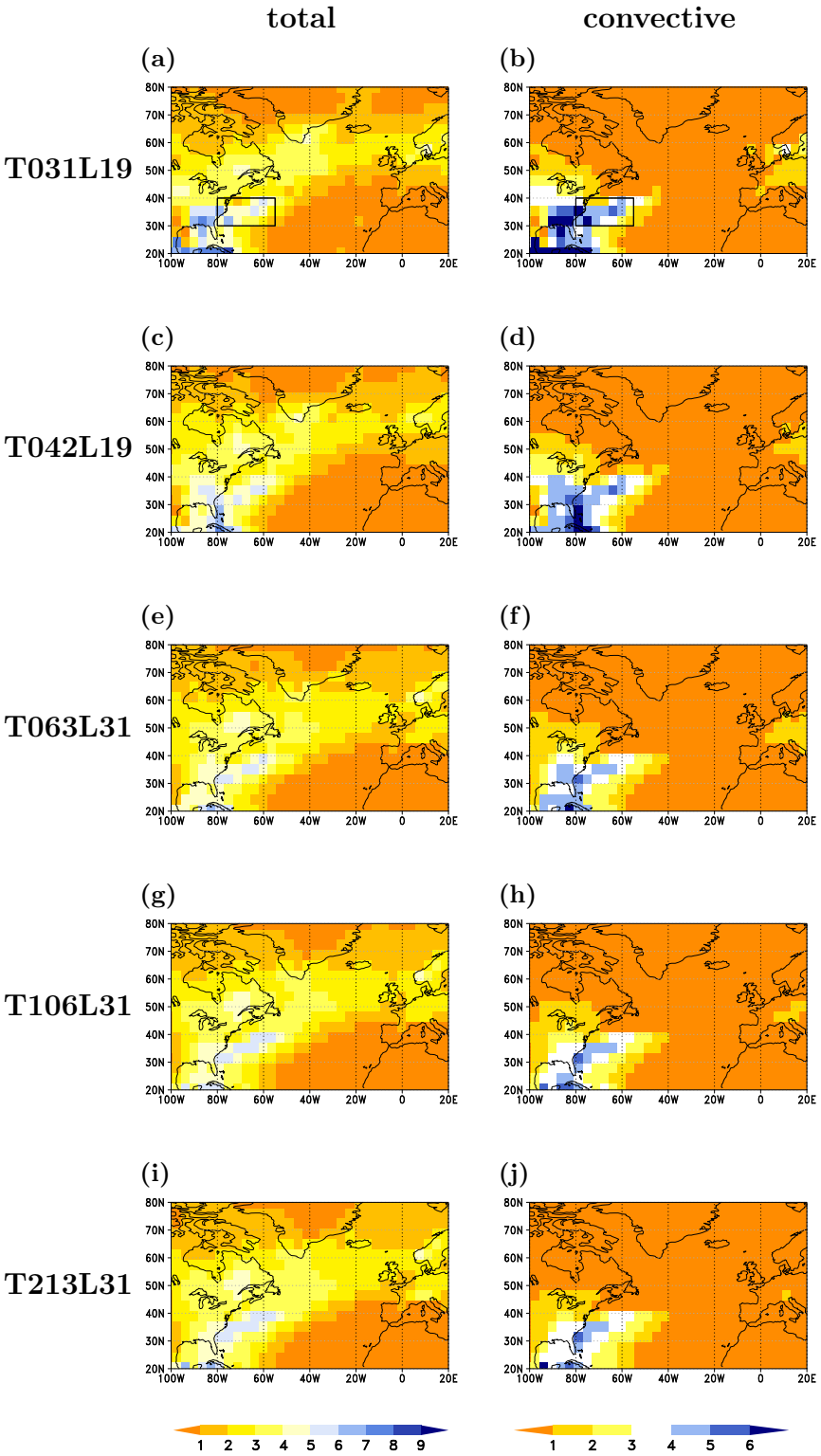

Figure A.1: Same as 2.2, but with all data interpolated to T31 for better comparability.

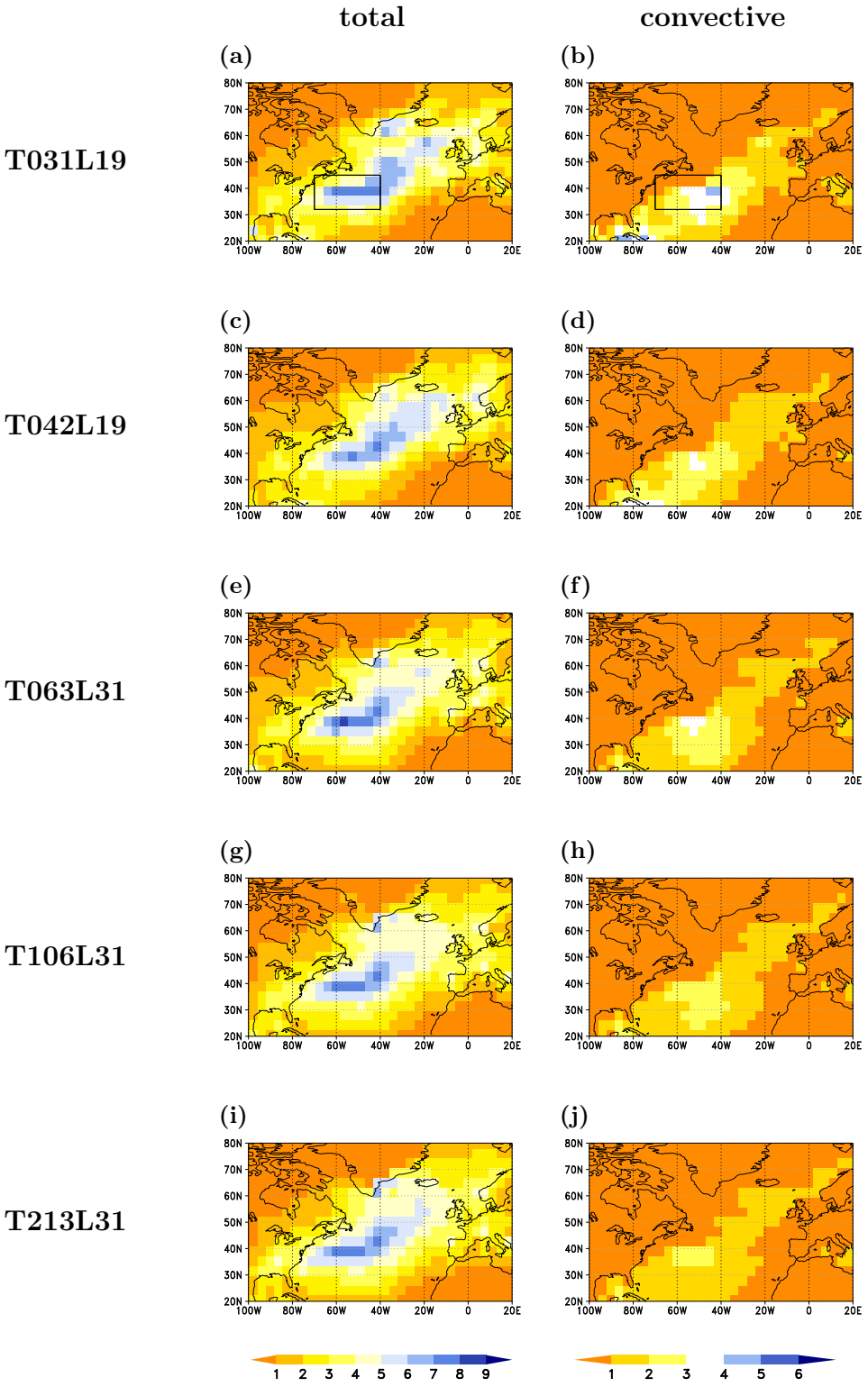

Figure A.2: Same as 2.3, but with all data interpolated to T31 for better comparibility.

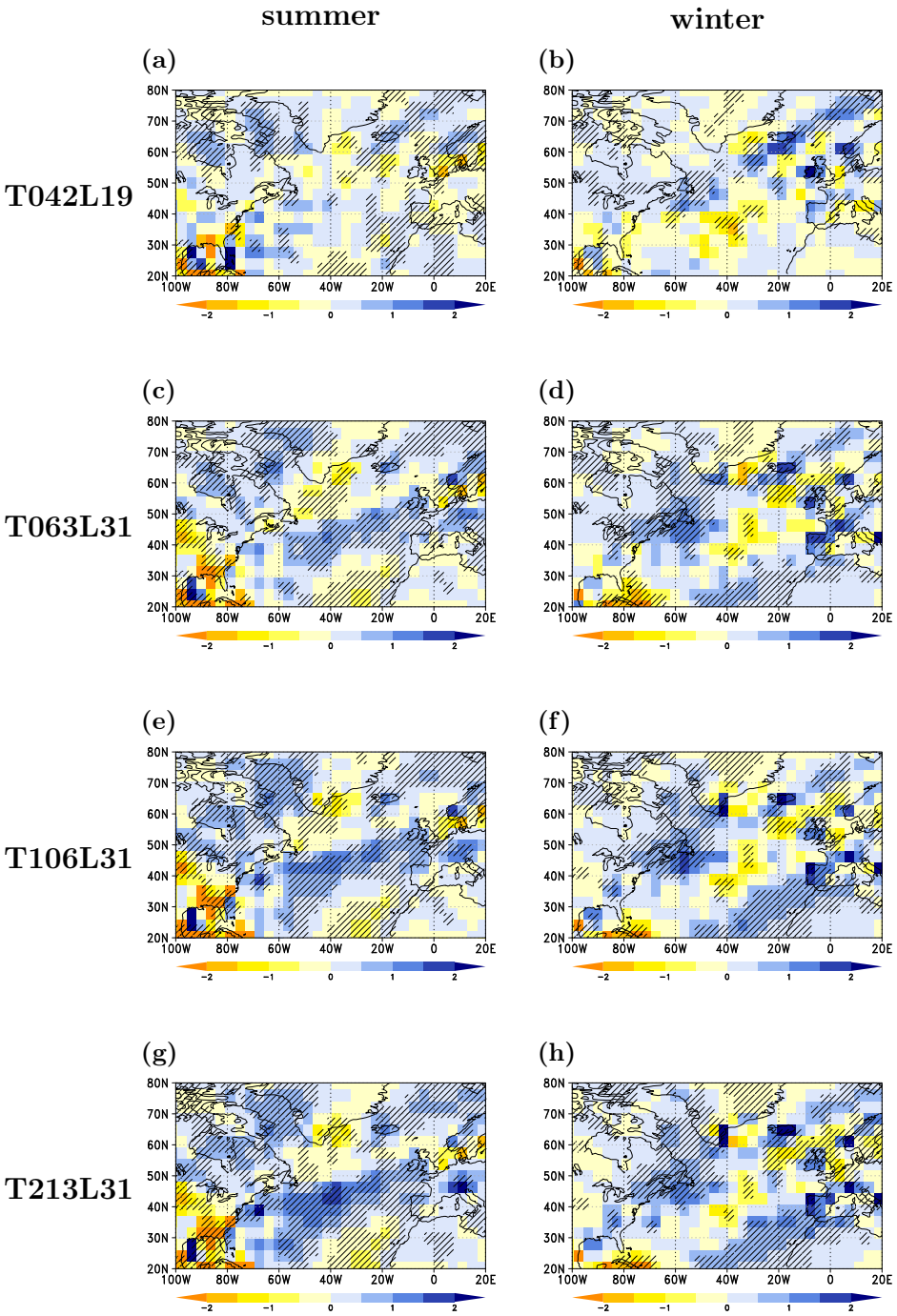

Figure A.3: The effect of model resolution on total precipitation. The figures show the difference in seasonal mean total precipitation (in mm/d) between the runs performed at different vertical and horizontal resolutions (refer to the labelling on the left side of each row) and averaged to T31 afterwards and the run originally performed in T031L19 resolution. Results are shown for summer (JJA, left column) and winter (DJF, right column). Hatching indicates regions, where the differences pass a bootstrapping test at the 95% confidence level.

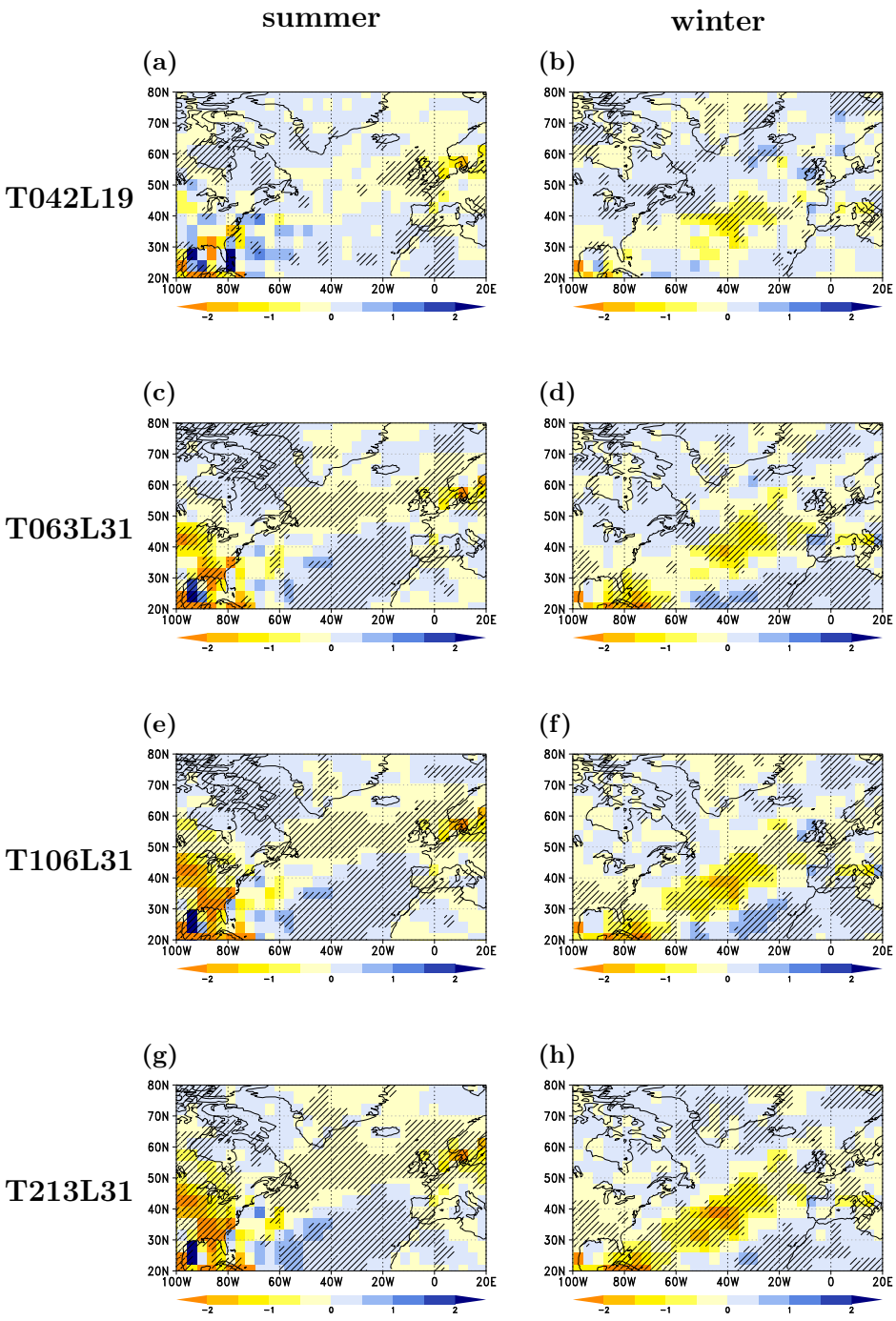

Figure A.4: same as A.3, but for convective precipitation only.

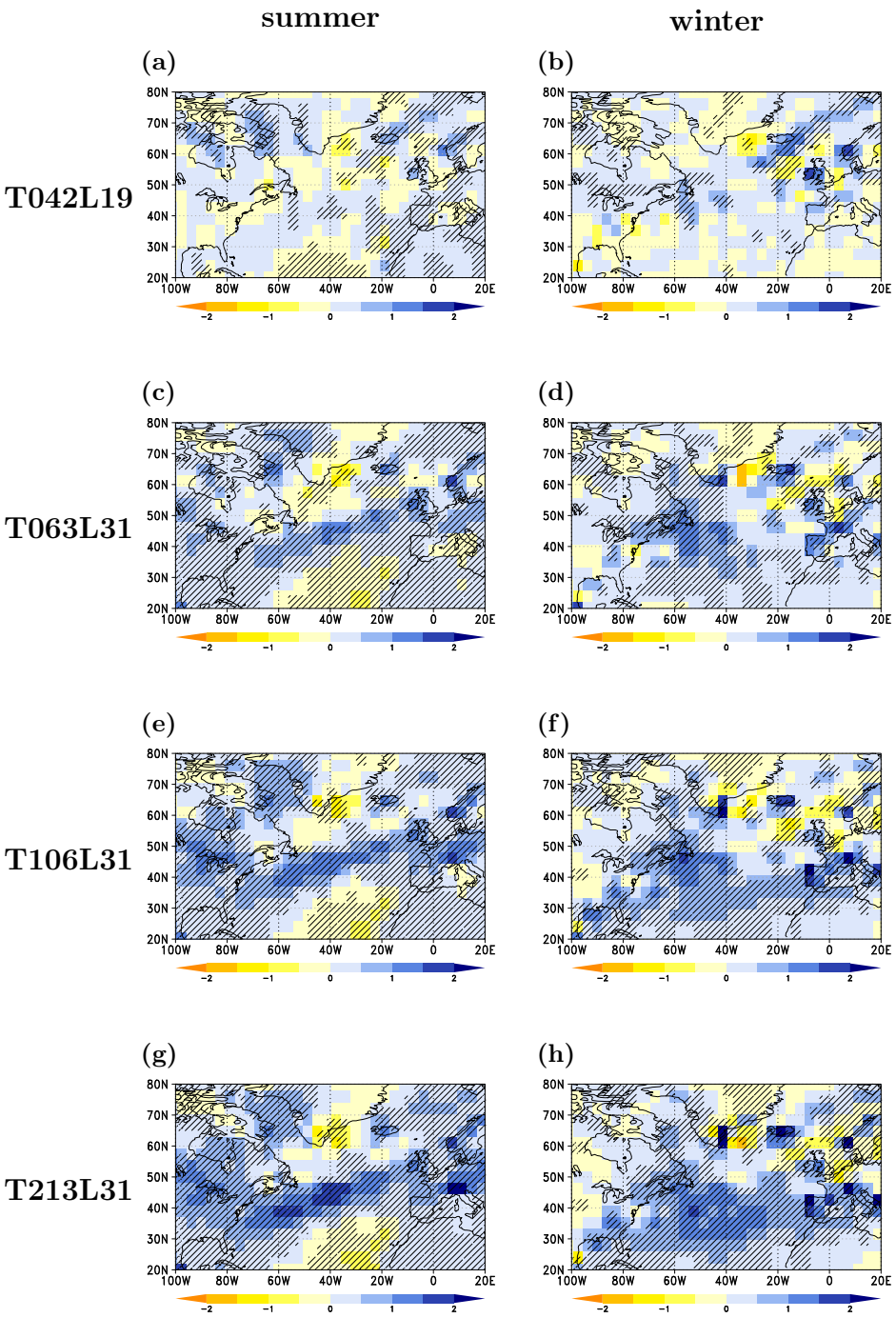

Figure A.5: same as A.3, but for large-scale precipitation only.

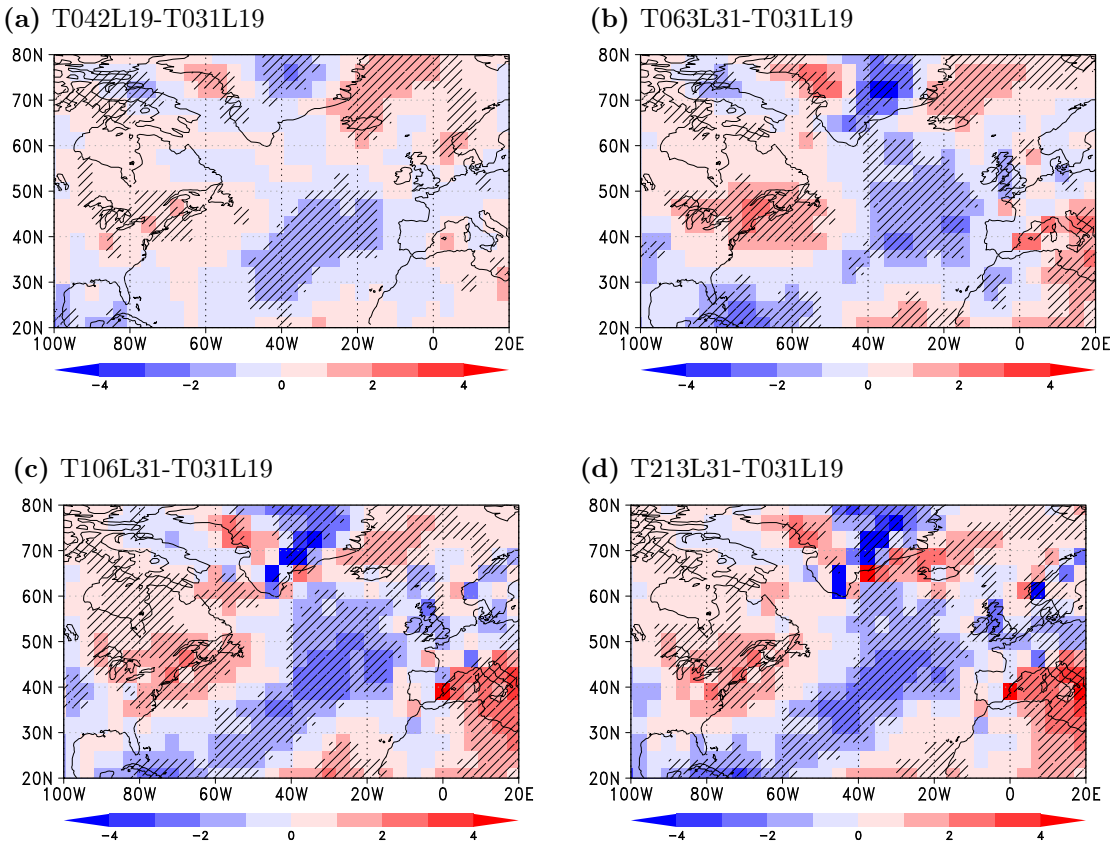

Figure A.6: Winter-time 500 hPa upward wind. Differences (in Pa/s) of the runs performed at different horizontal and vertical resolutions with respect to the run performed in T031L19. Regions where the signal is significant at the 95% confidence level using a bootstrapping test are hatched.

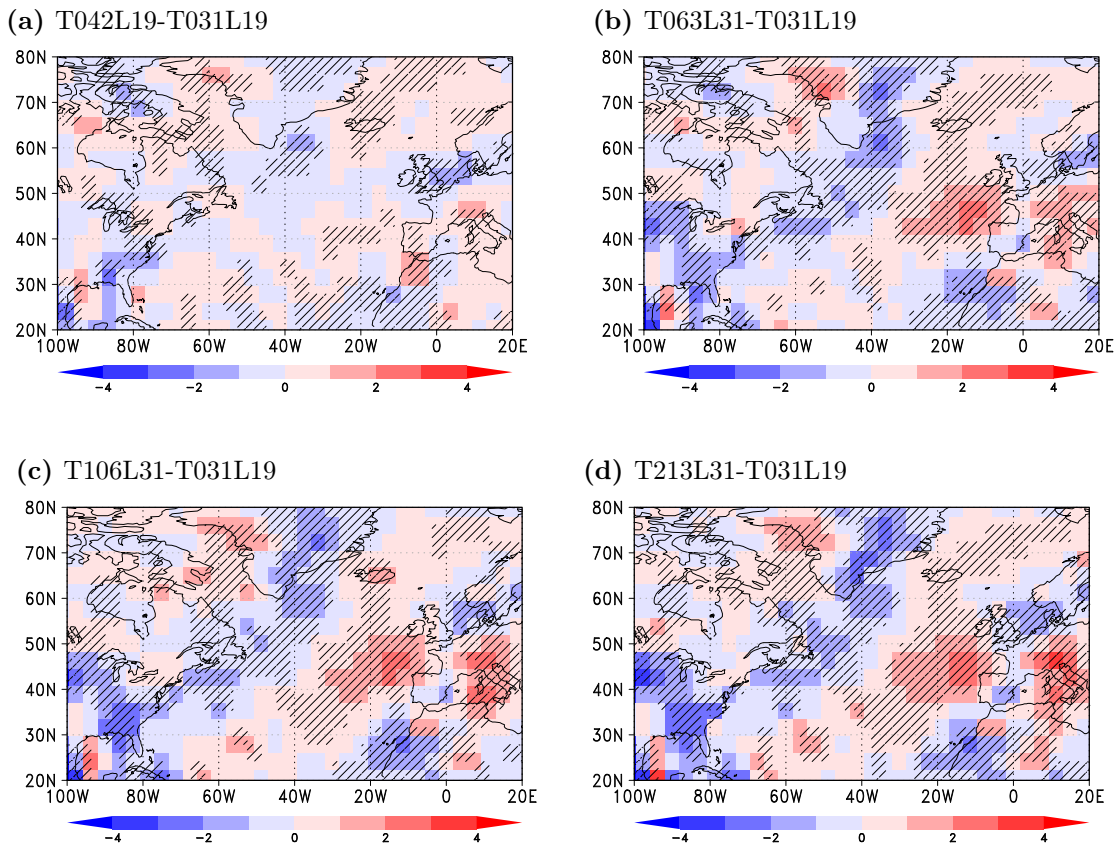

Figure A.7: Same as A.6, but for summer.

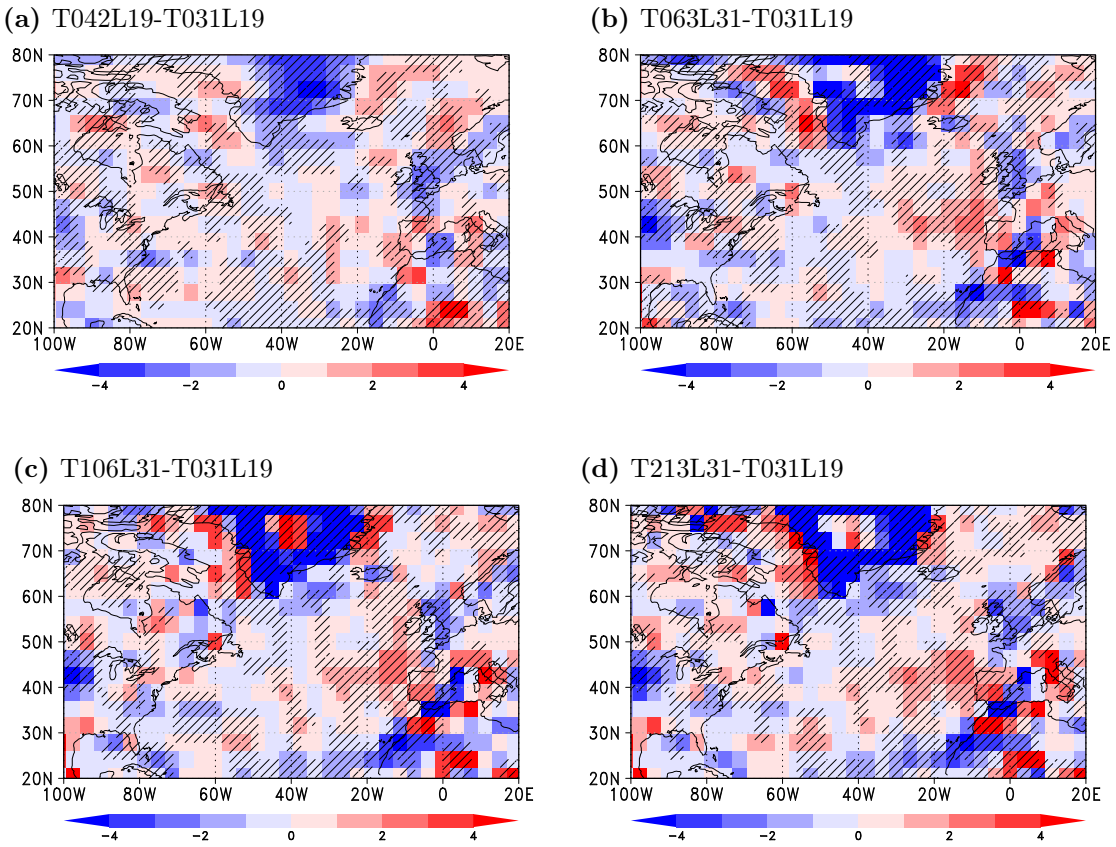

Figure A.8: Same as A.6, but for summer-time 850 hPa upwward wind (in Pa/s).

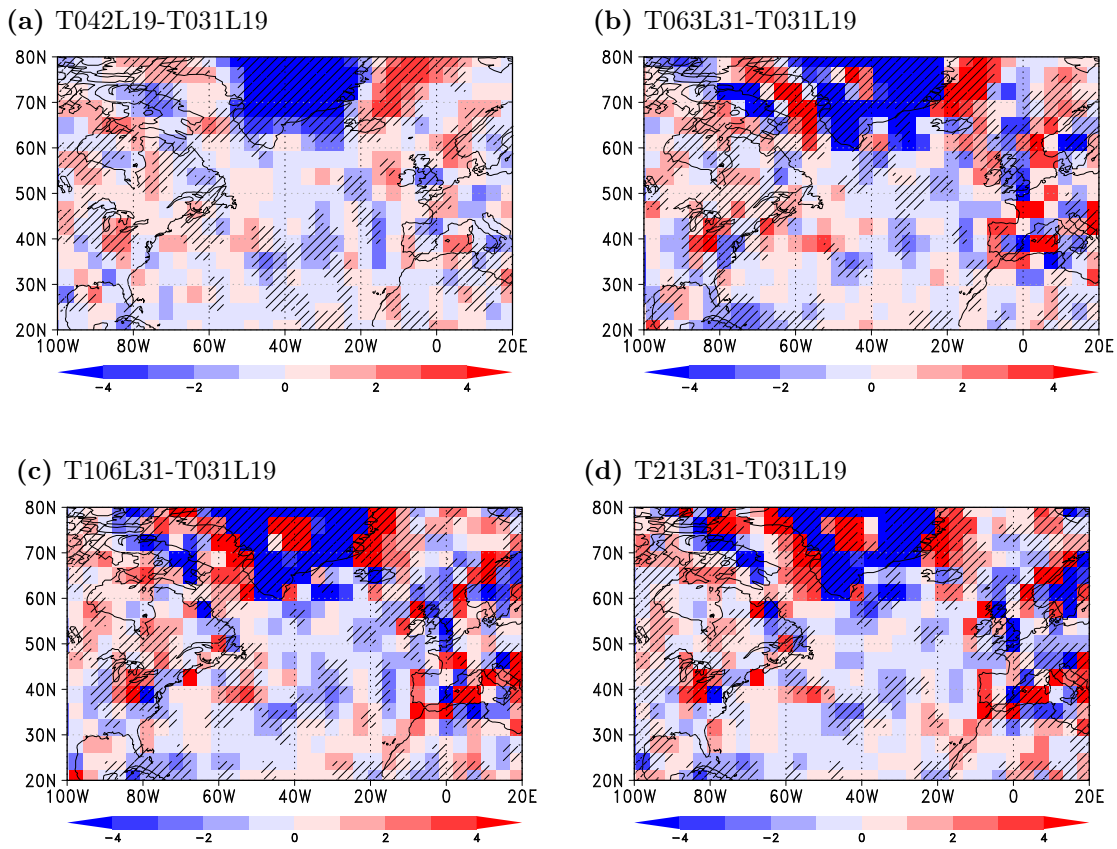

Figure A.9: Same as A.7, but for winter-time 850 hPa upwward wind (in Pa/s).

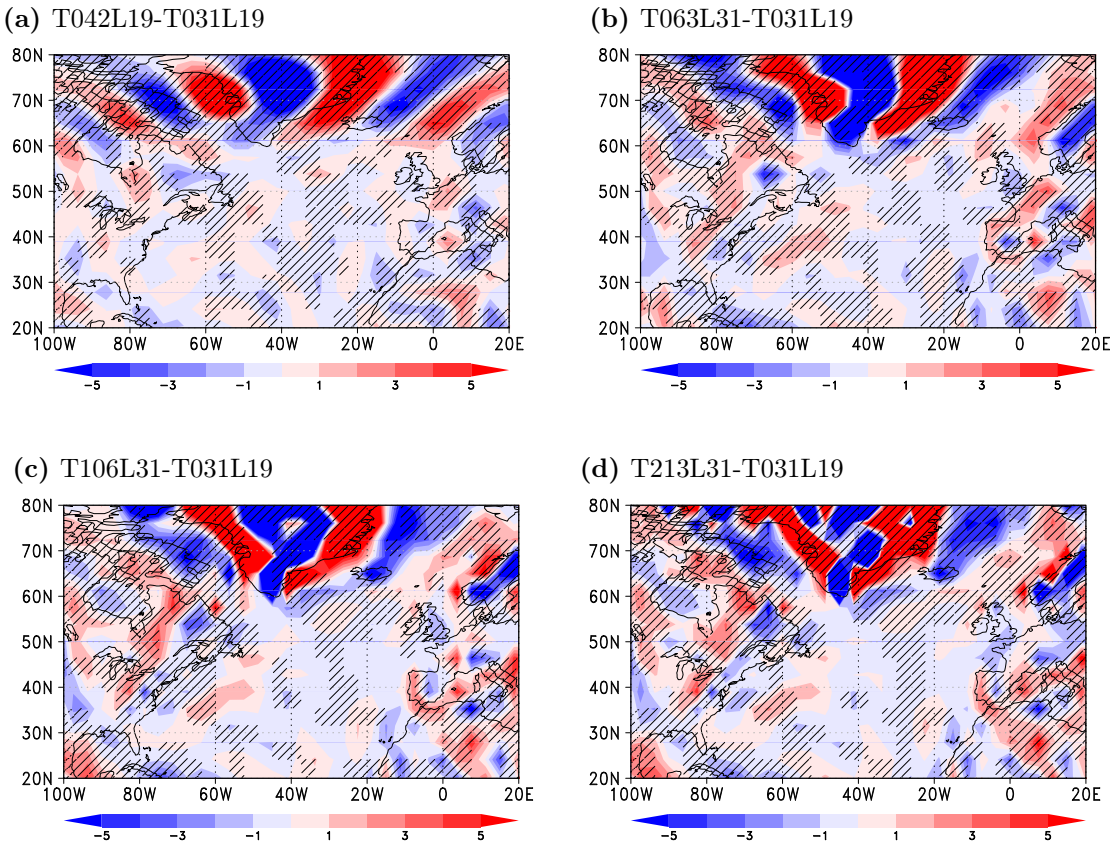

Figure A.10: same as A.7, but for winter-time 925 hPa horizontal wind convergence (in 10^{-6}/s).

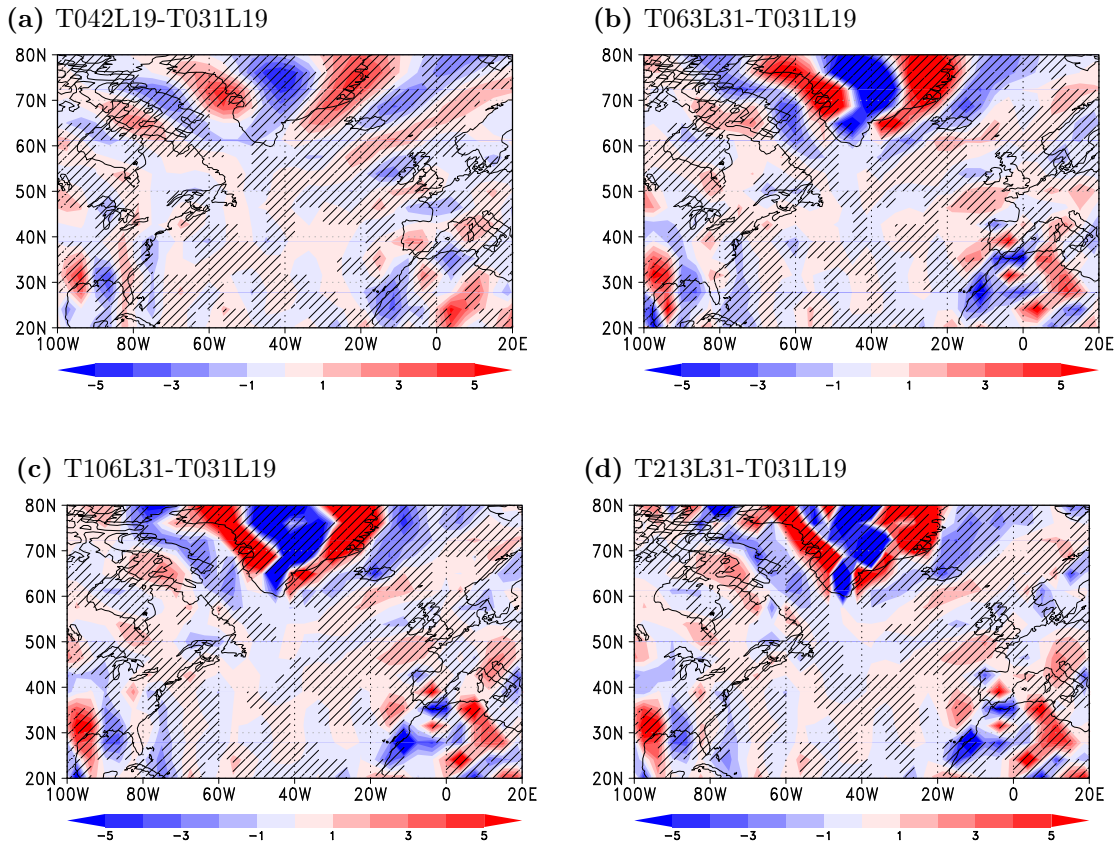

Figure A.11: Same as A.6, but for summer-time 925 hPa horizontal wind convergence (in 10^{-6}/s).

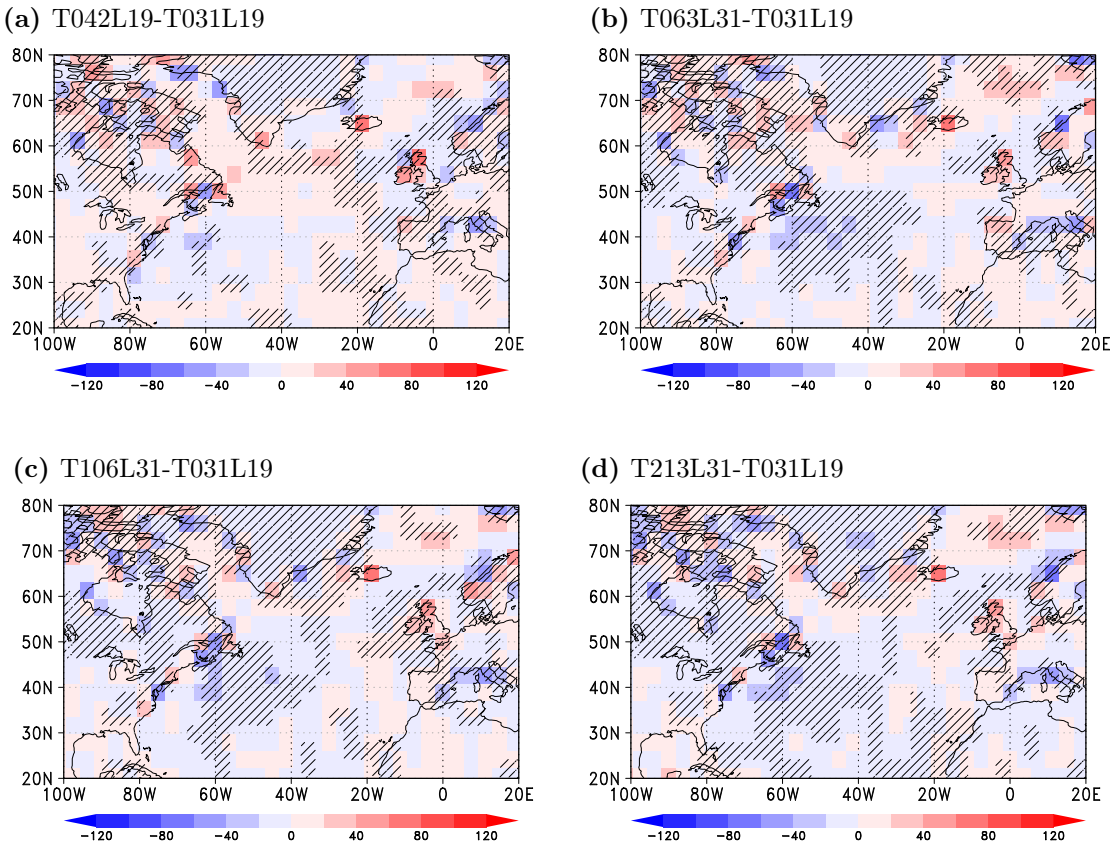

Figure A.12: Same as A.7, but for winter-time upward sensible heat flux (in W/m^2).

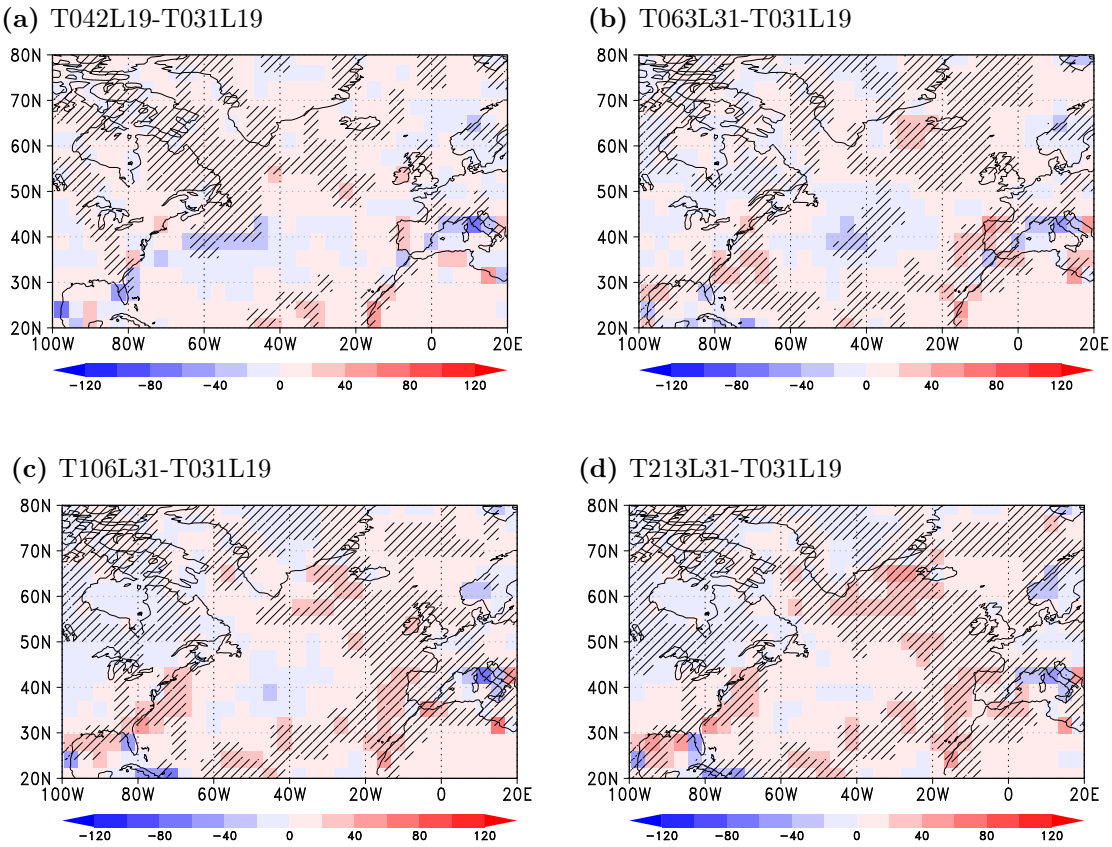

Figure A.13: Same as A.7, but for winter-time upward latent heat flux (in W/m^2).

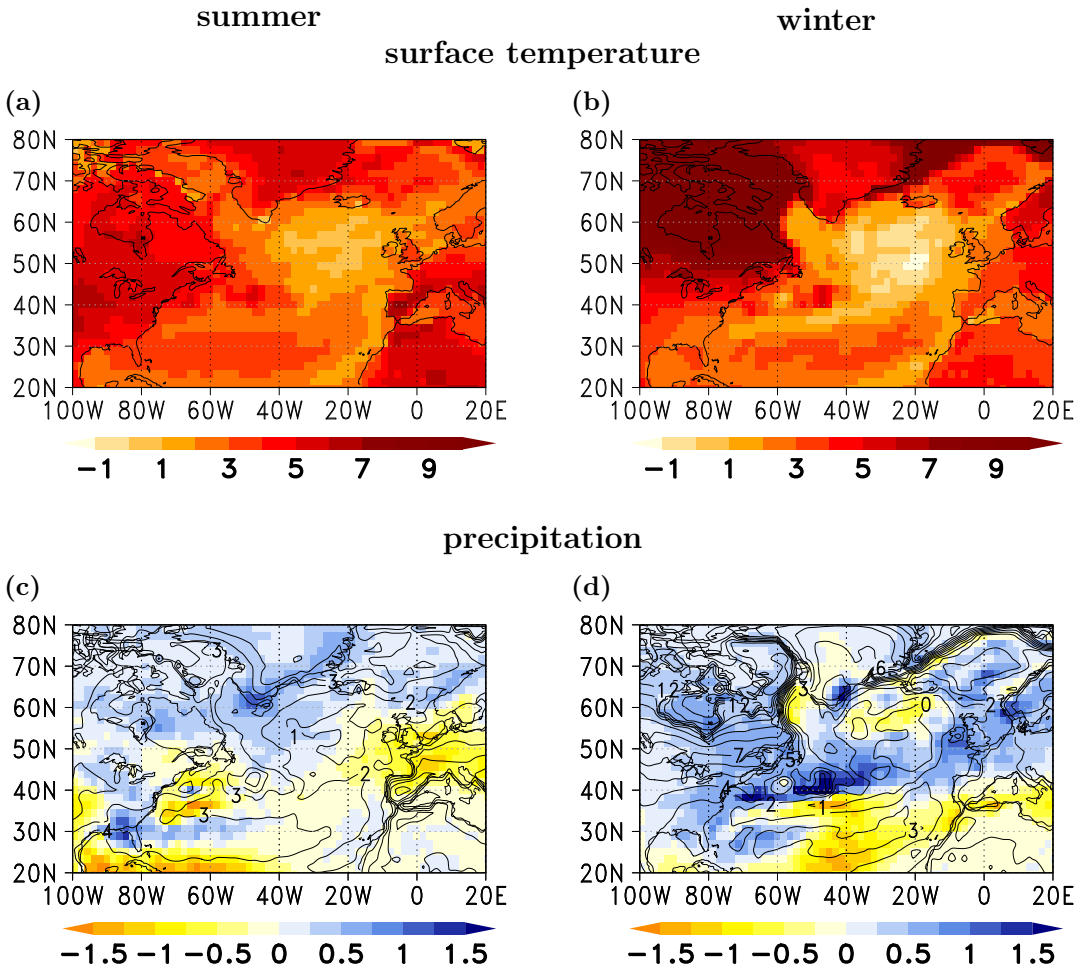

Figure A.14: Same as fig. 4.1, but for MPI-ESM as individual model: Surface temperature response (top, in K) and precipitation response (bottom, in mm/day) to the RCP 8.5 scenario for summer (left column) and winter (right column) for MPI-ESM. Climatological differences between the periods from 2050 to 2100 and 1900 to 1999. In fig. b contours repeat the surface temperature change.

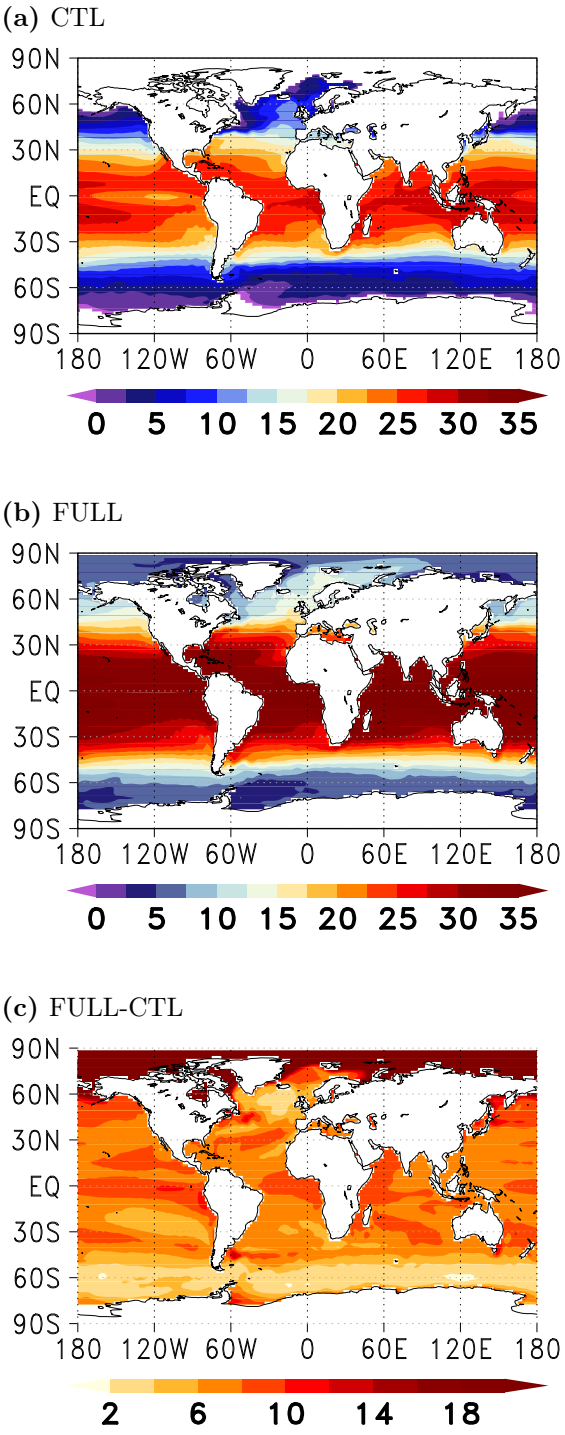

Figure A.15: Winter-time (DJF) SST forcing for the sensitivity experiment. Absolute SSTs (in °C) for CTL (a) and FULL (b) and the difference FULL-CTL (c). In a and b white areas over the ocean indicate sea ice.

Abbreviations

AGCM	atmospheric general circulation model
AMOC	Atlantic Meridional Overturning Circulation
CGCM	coupled general circulation model
CMIP5	Coupled Model Intercomparison Project (5^{th} phase)
ECHAM	atmospheric general circulation model of the Max-Plack-Institute for Meteorology, Hamburg (ECMWF Hamburg), based on the ECMWF forecast model
ECMWF	European Centre of Medium Range Weather Forecast
EOF	empirical orthogonalfunction
GHG	greenhouse gases
GS	Gulf Stream
IPCC	Intergovernmental Panel on Climate Change
NA	North Atlantic
NAO	North Atlantic Oscillation
NCEP	National Center for Environmental Prediction
NOAA	National Oceanic and Atmospheric Administration
MPI-ESM-LR	Max-Planck-Institute Earth System Model, low resolution version (i.e. T63L47)
PC	principal component
RCP8.5	Representative Concentration Pathways. Greenhouse gas concentrations used for the IPCC model experiments. The following number quantifies the equivalent radiative forcing with respect to the pre-industrial conditions, in the experiments analyzed during this work 8.5 W/m^2
SLP	sea level pressure
SST	sea surface temperature
Sv	Sverdrup, unit of ocean volume transport; 1 Sv=$10^6 m^3 s^{-1}$

List of Figures

List of Tables

Bibliography

Bader, Jürgen; Mesquita, Michel D. S.; Hodges, Kevin I.; Keenlyside, Noel; Østerhus, Svein and Miles, Martin. 2011. A review on Northern Hemisphere sea-ice, storminess and the North Atlantic Oscillation: Observations and projected changes. Atmospheric Research, **101**(4), 809–834.

Barsugli, Joseph J. and Battisti, David S. 1998. The Basic Effects of Atmosphere–Ocean Thermal Coupling on Midlatitude Variability*. Journal of the Atmospheric Sciences, **55**(4), 477–493.

Bengtsson, Lennart; Hodges, Kevin I. and Roeckner, Erich. 2006. Storm Tracks and Climate Change. Journal of Climate, **19**(15), 3518–3543.

Berry, Gareth; Reeder, Michael J. and Jakob, Christian. 2011. A global climatology of atmospheric fronts. Geophysical Research Letters, **38**(Feb.). WOS:000287808400006.

Bjerknes, J. 1964. Atlantic Air-Sea Interaction. Advances in Geophysics, **10**, 1.

Boville, Byron A. 1991. Sensitivity of Simulated Climate to Model Resolution. Journal of Climate, **4**(5), 469–485.

Brayshaw, David James; Hoskins, Brian and Blackburn, Michael. 2008. The Storm-Track Response to Idealized SST Perturbations in an Aquaplanet GCM. Journal of the Atmospheric Sciences, **65**(9), 2842–2860.

Bretherton, C. S. and Battisti, D. S. 2000. An interpretation of the results from atmospheric general circulation models forced by the time history of the observed sea surface temperature distribution. Geophysical Research Letters, **27**(6), 767–770. WOS:000085868600008.

Butterworth, Stephen. 1930. On the Theory of Filter Amplifiers. Wireless Engineer, 536–541.

Catto, J. L.; Jakob, C.; Berry, G. and Nicholls, N. 2012. Relating global precipitation to atmospheric fronts. Geophysical Research Letters, **39**(10), n/a–n/a.

Cayan, Dr. 1992. Latent and Sensible Heat-Flux Anomalies Over the Northern Oceans - Driving the Sea-Surface Temperature. Journal of Physical Oceanography, **22**(8), 859–881. WOS:A1992JF12800003.

Chang, Edmund K. M. 2009. Are band-pass variance statistics useful measures of storm track activity? Re-examining storm track variability associated with the NAO using multiple storm track measures. Climate Dynamics, **33**(2-3), 277–296.

Chen, Cheng-Ta and Knutson, Thomas. 2008. On the Verification and Comparison of Extreme Rainfall Indices from Climate Models. Journal of Climate, **21**(7), 1605–1621.

Ciasto, Laura M. and Thompson, David W. J. 2004. North Atlantic Atmosphere–Ocean Interaction on Intraseasonal Time Scales. Journal of Climate, **17**(8), 1617–1621.

Collins, M.; Botzet, A.; Carril, A. F.; Drange, H.; Jouzeau, A.; Latif, M.; Masina, S.; Otteraa, O. H.; Pohlmann, H.; Sorteberg, A.; Sutton, R. and Terray, L. 2006. Interannual to decadal climate predictability in the North Atlantic: A multimodel-ensemble study. Journal of Climate, **19**(7), 1195–1203. WOS:000237226700010.

Czaja, Arnaud and Frankignoul, Claude. 2002. Observed Impact of Atlantic SST Anomalies on the North Atlantic Oscillation. Journal of Climate, **15**(6), 606–623.

Dai, Aiguo. 2006. Precipitation Characteristics in Eighteen Coupled Climate Models. Journal of Climate, **19**(18), 4605–4630.

Deser, Clara; Tomas, Robert A. and Peng, Shiling. 2007. The Transient Atmospheric Circulation Response to North Atlantic SST and Sea Ice Anomalies. Journal of Climate, **20**(18), 4751–4767.

Drijfhout, Sybren; van Oldenborgh, Geert Jan and Cimatoribus, Andrea. 2012. Is a Decline of AMOC Causing the Warming Hole above the North Atlantic in Observed and Modeled Warming Patterns? Journal of Climate, **25**(24), 8373–8379.

Fan, Meizhu and Schneider, Edwin K. 2012. Observed Decadal North Atlantic Tripole SST Variability. Part I: Weather Noise Forcing and Coupled Response. Journal of the Atmospheric Sciences, **69**(1), 35–50.

Giorgetta, M.A.; Roeckner, E.; Maurits, T.; Bader, Jürgen; Crueger, Traute; Esch, Monika; Rast, Sebastian; Kornblueh, Luis; Schmidt, Hauke; Kinne, Stefan; Hohenegger, C.; Möbis, B.; Krismer, T.; Wieners, K.-H. and Stevens, Bjorn. 2013. The atmospheric general circulation model ECHAM6 - Model description. Tech. Rept. 135. Max-Planck-Institut für Meteorologie, Hamburg.

Griffies, S. M. and Bryan, K. 1997. A predictability study of simulated North Atlantic multidecadal variability. Climate Dynamics, **13**(7-8), 459–487. WOS:A1997XX04700001.

Gulev, Sergey K.; Latif, Mojib; Keenlyside, Noel; Park, Wonsun and Koltermann, Klaus Peter. 2013. North Atlantic Ocean control on surface heat flux on multidecadal timescales. Nature, **499**(7459), 464–467.

Hagemann, Stefan; Arpe, Klaus and Roeckner, Erich. 2006. Evaluation of the Hydrological Cycle in the ECHAM5 Model. Journal of Climate, **19**, 3810.

Hand, Ralf; Keenlyside, Noel; Omrani, Nour-Eddine and Latif, Mojib. 2014. Simulated response to inter-annual SST variations in the Gulf Stream region. Climate Dynamics, **42**(3-4), 715–731.

Harvey, B. J.; Shaffrey, L. C.; Woollings, T. J.; Zappa, G. and Hodges, K. I. 2012. How large are projected 21st century storm track changes? Geophysical Research Letters, **39**(18), n/a–n/a.

Held, Isaac M. and Soden, Brian J. 2006. Robust Responses of the Hydrological Cycle to Global Warming. Journal of Climate, **19**(21), 5686–5699.

Hodson, Daniel L. R.; Sutton, Rowan T.; Cassou, Christophe; Keenlyside, Noel; Okumura, Yuko and Zhou, Tianjun. 2010. Climate impacts of recent multidecadal changes in Atlantic Ocean Sea Surface Temperature: a multimodel comparison. Climate Dynamics, **34**(7-8), 1041–1058.

Hourdin, Frédéric; Musat, Ionela; Bony, Sandrine; Braconnot, Pascale; Codron, Francis; Dufresne, Jean-Louis; Fairhead, Laurent; Filiberti, Marie-Angèle; Friedlingstein, Pierre; Grandpeix, Jean-Yves; Krinner, Gerhard; LeVan, Phu; Li, Zhao-Xin and Lott, François. 2006. The LMDZ4 general circulation model: climate performance and sensitivity to parametrized physics with emphasis on tropical convection. Climate Dynamics, **27**(7-8), 787–813.

IPCC. 2013. Climate Change 2013: The Physical Science Basis. Contribution of Working Group I to the Fifth Assessment Report of the Intergovernmental Panel on Climate Change. Tech. Rept. Cambridge, United Kingdom and New York, NY, USA.

Jung, T.; Gulev, S. K.; Rudeva, I. and Soloviov, V. 2006. Sensitivity of extratropical cyclone characteristics to horizontal resolution in the ECMWF model. Quarterly Journal of the Royal Meteorological Society, **132**(619), 1839–1857.

Jungclaus, J. H.; Fischer, N.; Haak, H.; Lohmann, K.; Marotzke, J.; Matei, D.; Mikolajewicz, U.; Notz, D. and von Storch, J. S. 2013. Characteristics of the ocean simulations in the Max Planck Institute Ocean Model (MPIOM) the ocean component of the MPI-Earth system model. Journal of Advances in Modeling Earth Systems, **5**(2), 422–446.

Kalnay, E.; Kanamitsu, M.; Kistler, R.; Collins, W.; Deaven, D.; Gandin, L.; Iredell, M.; Saha, S.; White, G.; Woollen, J.; Zhu, Y.; Leetmaa, A.; Reynolds, R.; Chelliah, M.; Ebisuzaki, W.; Higgins, W.; Janowiak, J.; Mo, K. C.; Ropelewski, C.; Wang, J.; Jenne, Roy and Joseph, Dennis. 1996. The NCEP/NCAR 40-Year Reanalysis Project. Bulletin of the American Meteorological Society, **77**(3), 437–471.

Kedzierski, Robin Pilch. 2013. Comparison of extratropical cyclone characteristics from atmospheric global climate model simulations at different resolutions. Master thesis, Christian-Albrechts-Universität Kiel.

Keeley, S. P. E.; Sutton, R. T. and Shaffrey, L. C. 2012. The impact of North Atlantic sea surface temperature errors on the simulation of North Atlantic European region climate. Quarterly Journal of the Royal Meteorological Society, **138**(668), 1774–1783.

Keenlyside, N. S.; Latif, M.; Jungclaus, J.; Kornblueh, L. and Roeckner, E. 2008. Advancing decadal-scale climate prediction in the North Atlantic sector. Nature, **453**(7191), 84–88. WOS:000255398800043.

Kushnir, Y.; Robinson, W. A.; Bladé, I.; Hall, N. M. J.; Peng, S. and Sutton, R. 2002. Atmospheric GCM Response to Extratropical SST Anomalies: Synthesis and Evaluation*. Journal of Climate, **15**(16), 2233–2256.

Lohmann, U. and Roeckner, E. 1996. Design and performance of a new cloud microphysics scheme developed for the ECHAM general circulation model. Climate Dynamics, **12**(8), 557–572.

Minobe, Shoshiro; Kuwano-Yoshida, Akira; Komori, Nobumasa; Xie, Shang-Ping and Small, Richard Justin. 2008. Influence of the Gulf Stream on the troposphere. Nature, **452**(7184), 206–U51. WOS:000253925600038.

Minobe, Shoshiro; Miyashita, Masato; Kuwano-Yoshida, Akira; Tokinaga, Hiroki and Xie, Shang-Ping. 2010. Atmospheric Response to the Gulf Stream: Seasonal Variations*. Journal of Climate, **23**(13), 3699–3719.

Nakamura, H.; Sampe, T.; Tanimoto, Y. and Shimpo, A. 2004. Observed associations among storm tracks, jet streams and midlatitude oceanic fronts. Geophysical Monograph Series, **147**, 329–345.

Nordeng, Thor Erik. 1994. Extended versions of the convective parametrization scheme at ECMWF and their impact on the mean and transient activity of the model in the tropics. Reading, Berks.: European Centre for Medium-Range Weather Forecasts].

Ogawa, Fumiaki; Nakamura, Hisashi; Nishii, Kazuaki; Miyasaka, Takafumi and Kuwano-Yoshida, Akira. 2012. Dependence of the climatological axial latitudes of the tropospheric westerlies and storm tracks on the latitude of an extratropical oceanic front. Geophysical Research Letters, **39**(5), n/a–n/a.

Omrani, N.-E.; Keenlyside, N. S.; Bader, Jürgen and Manzini, Elisa. 2014. Stratosphere key for wintertime atmospheric response to warm Atlantic decadal conditions. Climate Dynamics, **42**(3-4), 649–663.

Palmer, Tn and Zhaobo, S. 1985. A Modeling and Observational Study of the Relationship Between Sea-Surface Temperature in the Northwest Atlantic and the Atmospheric General-Circulation. Quarterly Journal of the Royal Meteorological Society, **111**(470), 947–975. WOS:A1985AYH1200002.

Peng, Shiling; Mysak, L. A.; Derome, J.; Ritchie, H. and Dugas, B. 1995. The Differences between Early and Midwinter Atmospheric Responses to Sea Surface Temperature Anomalies in the Northwest Atlantic. Journal of Climate, **8**(2), 137–157.

Piazza, M.; Terray, L.; Boe, J. and Sanchez-Gomez, E. to be submitted. High resolution modeling of small-scale air-sea interaction in the Gulf Stream region and impact on North Atlantic winter storm tracks.

Pohlmann, Holger; Jungclaus, Johann H.; Koehl, Armin; Stammer, Detlef and Marotzke, Jochem. 2009. Initializing Decadal Climate Predictions with the GECCO Oceanic Synthesis: Effects on the North Atlantic. Journal of Climate, **22**(14), 3926–3938. WOS:000268292300004.

Pope, V. D.; Pamment, J. A.; Jackson, D. R. and Slingo, A. 2001. The Representation of Water Vapor and Its Dependence on Vertical Resolution in the Hadley Centre Climate Model. Journal of Climate, **14**(14), 3065–3085.

Reynolds, Richard W.; Rayner, Nick A.; Smith, Thomas M.; Stokes, Diane C. and Wang, Wanqiu. 2002. An Improved In Situ and Satellite SST Analysis for Climate. Journal of Climate, **15**(13), 1609–1625.

Robson, Jon; Sutton, Rowan; Lohmann, Katja; Smith, Doug and Palmer, Matthew D. 2012. Causes of the Rapid Warming of the North Atlantic Ocean in the Mid-1990s. Journal of Climate, **25**(12), 4116–4134. WOS:000306043600009.

Röckner, E.; Bäuml, G.; Bonaventura, L.; Brokopf, R.; Esch, M.; Giorgetta, M.; Hagemann, S.; Kirchner, I.; Kornblueh, L.; Manzini, E.; Rhodin, A.; Schlese, U.; Schulzweida, U. and Tompkins, A. 2003. Technical report, No. 349, The Atmospheric general circulation modell ECHAM5. Tech. Rept. Max-Planck-Institut für Meteorologie, Hamburg.

Rodwell, M. J.; Rowell, D. P. and Folland, C. K. 1999. Oceanic forcing of the wintertime North Atlantic Oscillation and European climate. Nature, **398**(6725), 320–323. WOS:000079369600047.

Roeckner, E.; Brokopf, R.; Esch, M.; Giorgetta, M.; Hagemann, S.; Kornblueh, L.; Manzini, E.; Schlese, U. and Schulzweida, U. 2006. Sensitivity of Simulated Climate to Horizontal and Vertical Resolution in the ECHAM5 Atmosphere Model. Journal of Climate, **19**(16), 3771–3791.

Scaife, A. A.; Arribas, A.; Blockley, E.; Brookshaw, A.; Clark, R. T.; Dunstone, N.; Eade, R.; Fereday, D.; Folland, C. K.; Gordon, M.; Hermanson, L.; Knight, J. R.; Lea, D. J.; MacLachlan, C.; Maidens, A.; Martin, M.; Peterson, A. K.; Smith, D.; Vellinga, M.; Wallace, E.; Waters, J. and Williams, A. 2014. Skillful long-range prediction of European and North American winters. Geophysical Research Letters, **41**(7), 2014GL059637.

Scaife, Adam A.; Copsey, Dan; Gordon, Chris; Harris, Chris; Hinton, Tim; Keeley, Sarah; O'Neill, Alan; Roberts, Malcolm and Williams, Keith. 2011. Improved Atlantic winter blocking in a climate model. Geophysical Research Letters, **38**(23), L23703.

Stevens, Bjorn; Giorgetta, Marco; Esch, Monika; Mauritsen, Thorsten; Crueger, Traute; Rast, Sebastian; Salzmann, Marc; Schmidt, Hauke; Bader, Jürgen; Block, Karoline; Brokopf, Renate; Fast, Irina; Kinne, Stefan; Kornblueh, Luis; Lohmann, Ulrike; Pincus, Robert; Reichler, Thomas and Roeckner, Erich. 2013. Atmospheric component of the MPI-M Earth System Model: ECHAM6. Journal of Advances in Modeling Earth Systems, **5**(2), 146–172.

Storch, Hans. 2010. Statistical Analysis in Climate Research. Reprint Aufl. Cambridge University Press.

Taguchi, Bunmei; Nakamura, Hisashi; Nonaka, Masami; Komori, Nobumasa; Kuwano-Yoshida, Akira; Takaya, Koutarou and Goto, Atsushi. 2012. Seasonal Evolutions of Atmospheric Response to Decadal SST Anomalies in the North Pacific Subarctic Frontal Zone: Observations and a Coupled Model Simulation. Journal of Climate, **25**(1), 111–139. WOS:000299130000008.

Tiedtke, M. 1989. A Comprehensive Mass Flux Scheme for Cumulus Parameterization in Large-Scale Models. Monthly Weather Review, **117**(8), 1779–1800. WOS:A1989AL24800009.

Visbeck, M.; Cullen, H.; Krahmann, G. and Naik, N. 1998. An ocean model's response to North Atlantic Oscillation-like wind forcing. Geophysical Research Letters, **25**(24), 4521–4524. WOS:000077882600033.

Volosciuk, Claudia; Maraun, Douglas; Semenov, Vladimir A. and Park, Wonsun. 2015. Extreme Precipitation in an Atmosphere General Circulation Model: Impact of Horizontal and Vertical Model Resolutions. Journal of Climate, **28**(3), 1184–1205.

Woollings, T.; Gregory, J. M.; Pinto, J. G.; Reyers, M. and Brayshaw, D. J. 2012. Response of the North Atlantic storm track to climate change shaped by ocean-atmosphere coupling. Nature Geoscience, **5**(5), 313–317.

Xie, Pingping and Arkin, Phillip A. 1997. Global Precipitation: A 17-Year Monthly Analysis Based on Gauge Observations, Satellite Estimates, and Numerical Model Outputs. Bulletin of the American Meteorological Society, **78**(11), 2539–2558.

Xie, S. P. 2004. Satellite observations of cool ocean-atmosphere interaction. Bulletin of the American Meteorological Society, **85**(2), 195ff. WOS:000220121800015.

Xie, Shang-Ping; Deser, Clara; Vecchi, Gabriel A.; Ma, Jian; Teng, Haiyan and Wittenberg, Andrew T. 2010. Global Warming Pattern Formation: Sea Surface Temperature and Rainfall*. Journal of Climate, **23**(4), 966–986.

Yeager, Stephen; Karspeck, Alicia; Danabasoglu, Gokhan; Tribbia, Joe and Teng, Hayan. 2012. A Decadal Prediction Case Study: Late Twentieth-Century North Atlantic Ocean Heat Content. Journal of Climate, **25**(15), 5173–5189. WOS:000307089300002.

Yin, Jeffrey H. 2005. A consistent poleward shift of the storm tracks in simulations of 21st century climate. Geophysical Research Letters, **32**(18), L18701.

Acknowledgements

On this last pages I want to thank all those, who helped to let me finish this work. Namely I want to mention the following people:

Prof. Dr. Noel Keenlyside initiated the topic and supervised this work. Despite the complications of a remote supervision in the second half of my PhD time, I always was able to enjoy an extremely comfortable atmosphere and got furthering guidance through all obstacles of the PhD time. Thanks also for giving me plenty of great opportunities to make contacts with colleagues from all over the world. Furthermore, I cordially thank Prof. Dr. Richard Greatbatch for taking over ATMOS and being a helpful additional local supervisor after Noel's move to Bergen. Both, his expertise as well as the companionable atmosphere in his working group made important contributions to let this thesis grow.

Many thanks to Nour-Eddine Omrani for fruitful discussions about the secrets of the atmosphere's dynamics and all other aspects of academic and non-academic life. Claudia Volosciuk not only offered many opportunities for recreative and/or inspiring coffee breaks, but also helped a lot by doing the final proofreading. Guidi Zhou gave useful help with using ECHAM and provided his very useful eddy diagnostic software. Connie Schuster and Sabine Niewels sorted out all kinds of bureaucratic issues. Kai Grunau from GEOMAR's computing center provided extensive support with all imaginable advanced Linux problems. Also, thanks to him for motivating me learning bash scripting a few years ago, a thing that helped me a lot during my PhD time and probably beyond.

Thanks also to all other people who made work in Kiel and elsewhere enjoyable during the last years: Thanks to my friends and former PhDs from Noel's working group, namely Jenny, Wan-Ling, Jin and Hui, for being such awesome academic siblings and sharing a really good time before we got widely dispersed; also thanks to Richard's group for adopting me afterward. Thanks to Sasha and Hannes for always being really nice office mates and also to all other colleagues at GEOMAR for sharing a long time sweetened by plenty of really tasty cakes. Also thanks to all colleagues at Universitet i Bergen for giving me a really good time during several visits to the rainy North. In this context, special thanks to Steffi

for providing me a cosy home close to my remote desk in Bergen from time to time. Many thanks also go to Helene for being an inspiring conference roomie all the time. Ben offered some calming continuity, being the only one, sharing my whole time as a student here in Kiel - from the first common day at the university to the submission of this thesis. Many thanks also to Doreen, Henner, Steffen and Helene for plenty of reviving interdisciplinary discussions.

Coming to the end, I want to thank Katharina, Ezra and Fritz for providing me the best motivation ever to finally get to this next-to-last page and thus nearly have completed this work for submission. Looking forward to share the road with you guys during the next weeks!

Last but not least thanks to all friends and family members, who are too many to be namely mentioned, but who gave security and shared recreation time when accompanying me through my PhD time.

This work was funded by the German Federal Ministry of Education and Research (BMBF) through the MiKliP program.

Eidesstattliche Erklärung

Hiermit erkläre ich, dass die vorliegende Doktorarbeit selbständig unter Befolgung der Regeln guter wissenschaflicher Praxis der Deutschen Forschungsgemeinschaft (DFG) verfasst wurde und keine über die angegebenen Quellen hinausgehenden Hilfsmittel verwendet wurden. Ich versichere, dass diese Arbeit noch nicht zur Erlangung eines Doktorgrades an anderer Stelle vorgelegen hat.

Kiel im Februar 2015

(Ralf Hand)